# SCIENTIFIC NOTEBOOK 714E

## Flow Paths in the Unsaturated Zone

*by*

**Stuart A. Stothoff**

**Southwest Research Institute**
**Center for Nuclear Waste Regulatory Analyses**
**San Antonio, Texas**

**July 1, 2010**

# Initial Entries

Scientific NoteBook: # 714E

Issued to: S. A. Stothoff

Issue Date: May 10, 2005

Computerized Initials: SAS

This computerized Scientific NoteBook is intended to address the criteria of CNWRA QAP–001.

This scientific notebook is intended to document independent analyses related to flow in the unsaturated zone preparatory to receipt of the license application for Yucca Mountain.

The analyses are broken into chapters on flow paths, lateral diversion, and seepage workshop analyses.

RL 7/7/2010

## Contents

RL 7/7/2010

## List of Figures

## List of Tables

RL 7/7/2010

# 1 Flow paths in the unsaturated zone

### 05/12/05 Analyis of rubble heat-flow experiment.

SAS

Ron Green ran a dozen experiments with different temperature boundary conditions to examine thermal transfer through rubble. The experiments examined heat flux in the middle 15x15 cm patch of a 90x90 cm cell, with transfer occurring across 15 cm. The cell was filled with crushed Tptpll welded tuff, with chunks larger than 6 cm discarded.

Ron found that heat transfer is enhanced relative to pure conduction at higher temperatures. He looked at radiative transfer and convection as possible explanations, discarding radiative transfer and suggesting that convection cells would occur based on the Rayleigh number to explain the enhanced transfer. While critiquing the paper, I noticed that the radiative transfer calculations had an error and so I started looking at the issue in a little greater depth.

Ron concluded that radiative transfer was negligible based on a formula for radiative transfer as an equivalent thermal conductivity. The formula is in the form

$$q_{rad} = -4\chi d_p \sigma T^3 \nabla T \tag{1-1}$$

where $q_{rad}$ is radiative flux, $\chi$ is a porous-medium shape factor (0.29 to 1.3), $d_p$ is a characteristic particle diameter, $\sigma$ is the Stefan-Bolzmann constant ($5.67\times10^{-8}$ W/m$^2$-K$^4$), and $T$ is temperature.

A couple of simple thought experiments on radiative transfer might motivate the equation. Consider radiative transfer between two parallel planes labelled 0 and 1. Net flux from 0 to 1 is

$$q_{net} = \sigma(T_0^4 - T_1^4) = \sigma(P_0 - P_1) \tag{1-2}$$

where $P = T^4$. Inserting $N$ planes between these two boundaries,

$$q_N = \frac{\sigma}{N+1} q_{net} \tag{1-3}$$

and the temperature of intermediate planes can be obtained from

$$P_i = \frac{i}{N+1} P_1 + \left(1 - \frac{i}{N+1}\right) P_0 \tag{1-4}$$

Note that distance between the planes is immaterial.

As a sidelight for the case of a waste package in rubble, which can be considered a heat source at 0 with strength $q_{net}$ and fixed $P_1$,

$$\sigma(P_0 - P_1) = \frac{\sigma}{N+1}(P_0^* - P_1) \tag{1-5}$$

where $P_0^*$ is the temperature required for the source to radiate its heat. This expression can be rearranged to yield

$$\frac{P_0^*}{P_1} = 1 + (N+1)\left(\frac{P_0}{P_1} - 1\right) \tag{1-6}$$

Getting back to porous media. Let's characterize porous media as a series of intermediate planes separated by a characteristic distance $D$. Heat flux across a distance $L$ is roughly

$$q_{rad} = \sigma \frac{D}{L}(T_0^4 - T_1^4) \tag{1-7}$$

which can be cast into differential form

$$q_{rad} = -\sigma D \nabla T^4 = -4\sigma D T^3 \nabla T \tag{1-8}$$

which is exactly the form given before when $D = \chi d_p$.

Using Ron's paper for a reference, thermal flux due to conduction, $q_{cond}$ is given using Fourier's law,

$$q_{cond} = -\kappa \nabla T \tag{1-9}$$

and thermal flux due to convection, $q_{conv}$ is (not quite in the form given)

$$\begin{aligned} q_{conv} &= -c_{conv} Ra^{1/4} \nabla T \\ &= -c_{conv}^* \left[ (\nabla T)^{5/4} - |\nabla T|_c^{5/4} \right] \end{aligned} \tag{1-10}$$

where $c_{conv}$ is a convection fitting parameter, and subscript $c$ represents a critical value. The Rayleigh number $Ra$ is defined by

$$Ra = \frac{k \rho^2 g \beta \Delta T C_v L}{\mu \kappa_{eff}} \tag{1-11}$$

where $k$ is intrinsic permeability [L$^2$], $\rho$ is air density [M/L$^3$], $g$ is acceleration due to gravity [L/T$^2$], $\beta$ is the volumetric expansion factor [1/K], $\Delta T$ is temperature drop across the cell [K], $C_v$ is heat capacity at constant volume [E/MK], $\mu$ is air viscosity [M/LT], and $\kappa_{eff}$ is effective thermal conductivity [E/MT]. Ballpark reference figures for air parameters at sea level include: $\rho = 1.25$ kg/m$^3$; $g = 9.8$ m/s$^2$; $\beta = 0.0258$ 1/K; $C_v = 720$ J/kg-K; and $\mu = 1.7 \times 10^{-5}$ kg/m-s. These will vary somewhat with temperature and pressure.

The flux equation should be interpreted as $q_{conv} = 0$ when $|(\nabla T)^{5/4}| > |(\nabla T)^{5/4}|_c$. There is some ambiguity in the draft document, which incorrectly implies that the exponent should be on $T$ rather than on its gradient.

As a quick bounding analysis of how much gas flow is needed to handle the convective load, let's pick an extreme condition of a temperature difference of 150 °C and an unexplained thermal transfer rate of 75 W/m$^2$. Let's also assume that a one-dimensional (1D) gas flux moves from high to low temperature, which might represent one portion of a convection cell. Convective flux in this case is

$$q_{conv} = \rho C_v q_{gas} \Delta T \tag{1-12}$$

With an approximate heat capacity of 760 J/kg-K for dry air and air density of 1.25 kg/m$^3$, the necessary mass flux is

$$q_{gas} = \frac{q_{conv}}{\rho C_v \Delta T} \tag{1-13}$$

For the given numbers, $q_{gas} = 0.05$ cm/s; assuming a porosity of 0.4, the average pore-gas velocity is about 1.3 mm/s. The implied local pore-gas velocity may be as much as an order of magnitude greater, depending on convection-cell details. Neglecting density effects, gas mass flux is governed by

$$q_{gas} = -\frac{k}{\mu} \nabla P \tag{1-14}$$

If this mass flux was driven by a pressure gradient, rather than convection cell details, assuming $k = 10^{-7}$ m$^2$ and $\mu = 1.7 \times 10^{-5}$N-s/m$^2$, a flux of 1 cm/s requires a pressure difference across 0.15 m of about 0.25 N/m$^2$, which is a very small pressure difference. So the bounding analysis suggests that convection is not an unreasonable mechanism for heat transfer in the test cell.

I evaluated the potential for radiative and convective mechanisms for heat transfer by performing a least-squares analysis to compare observation and prediction, using the equation

$$1 = [-KeG - De(4\sigma)G - Ce(Gp - Gpc)]/q_{obs} \tag{1-15}$$

where $G$ represents the observed $T$ gradient across the cell, $Gp$ represents the observed $T^{5/4}$ gradient across the cell (both forms were evaluated since there was ambiguity), $Gpc$ represents $|\nabla T|_c^{5/4}$, and $Ke$, $De$, and $Ce$ are regression coefficients. Conduction was always included, while all combinations of mechanisms of radiative and convective transfer were considered in separate regressions.

It is not possible to directly evaluate $|\nabla T|_c^{5/4}$ in a regression, so ballpark values were used. As it turns out, using $Gpc = 2800$ gives a reasonable fit in both cases, based on perturbing the value up or down by 20 percent and rerunning. This implies that the critical $\Delta T$ is about 570°C, instead of the value suggested by Ron using $k = 10^{-7}$ m$^2$. This implies that the media's effective intrinsic permeability is actually about $0.6{\times}10^{-7}$ m$^2$ if convection is occurring, simply scaling the imposed $k$ so that $k\Delta T$ is held constant (*i.e.*, $k = k_0(\Delta T)_0/\Delta T$, where a subscript denotes the original value in Ron's analyis and the $\Delta T$ values denote critical values). It also implies that convection would not be occurring in any experiment if the media's effective $k$ is less than $0.35{\times}10^{-7}$ m$^2$ (*i.e.*, $(\Delta T)_0 = 350$°C and $\Delta T = 1000$°C).

Table 1-1: Regression results for thermal-loading experiment.

| Case | Ke | De | Ce | Mean | Max | LS | SDev |
|---|---|---|---|---|---|---|---|
| $q_{cond}$ | 0.406 | 0 | 0 | 0.0698 | 0.156 | 0.0871 | 0.0546 |
| $q_{cond} + q_{rad}$ | 0.277 | 0.0153 | 0 | 0.0185 | 0.0662 | 0.0288 | 0.023 |
| $q_{cond} + q_{conv}$ | 0.386 | 0 | 0.0325 | 0.0292 | 0.1 | 0.041 | 0.0303 |
| $q_{cond} + q_{rad} + q_{conv}$ | 0.277 | 0.0153 | 9e-005 | 0.0185 | 0.0663 | 0.0288 | 0.0231 |

The first test lies somewhat off the curve implied by the other tests. This offset implies that heat transfer was more efficient in that test, which would be consistent with an initially wetter media that dried after the measurements for the first test and before the second test. All of the regression analyses neglect the first test.

Regression results are summarized in Table 1 and shown in Figure 1-1. Quality of fit is summarized in Table 1 by mean, maximum, and least-squares estimates of relative error, as well as the standard deviation of relative error. Relative error is $R = (q_o - q_r)/q_o$, where $q_r$ is predicted flux from the regression and $q_o$ is observed flux. Although the regression with $Gp$ denoting $\nabla T^{5/4}$ is not shown, the two forms of $Gp$ give very similar results.

Simply using a single effective thermal conductivity is not outrageously bad at predicting thermal transfer, with a mean $R$ of about 7 percent. Adding just conductive flux to the predictive equation yields a mean $R$ of about 2.9 percent, while adding just radiative flux yields a mean $R$ of 1.9 percent. Combining radiative and conductive flux yields $R$ values very similar to the case without conductive flux, and the predicted $Ce$ value drops to about 0.3 percent of the value without radiative flux.

These regression results reflect the fairly subtle deviations from linearity that the data exhibits. The two models do not allow a strong discrimination between the different modes of non-conductive thermal transfer. Both models match the observations quite well and all predictions are well within the error bounds for the data. The conductive-radiative model does do a somewhat better job of explaining the observed data than the conductive-convective model, having roughly 2/3 of the discrepancy between observation and regression. The conductive-radiative model would be preferred for this data based on the improved fit to data with one less fitting coefficient (plus the additional fitting coefficient in the conductive-convective model does not lend itself to linear regression).

From physical grounds, however, it may be difficult to assume that radiative transfer is

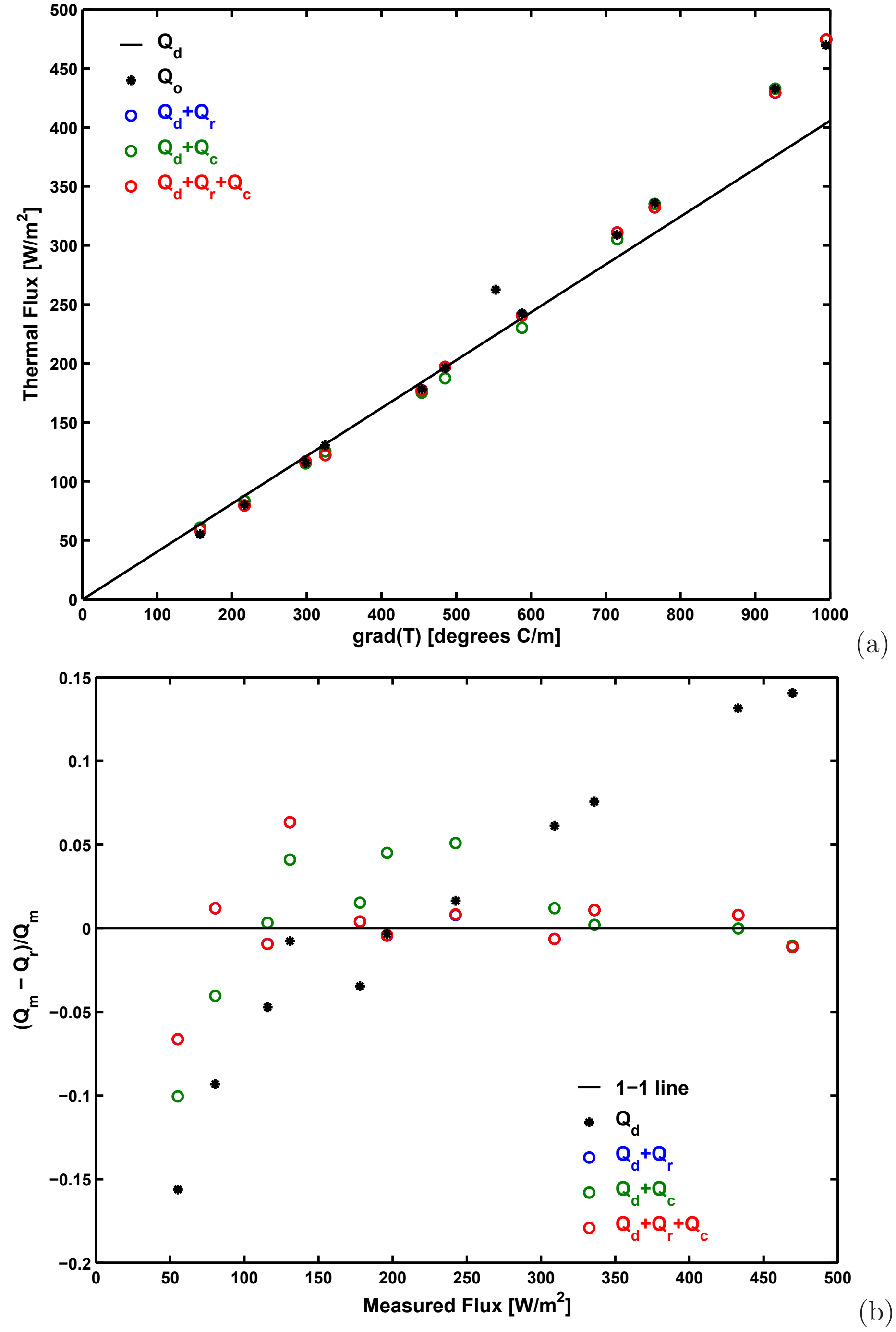

Figure 1-1: (a) Comparison of observed and regressed fluxes, and (b) deviation of regressed flux from observed flux for experimental results of thermal loading across Tptpll cuttings. The outlier at $\nabla T = 552$°C/m is not used in regressions. Labels $Q_d$, $Q_r$, and $Q_c$ refer to conductive, radiative, and convective transfer, respectively. Both pure-conduction and conduction/convection cases have systematic patterns of deviations from a fit, while the conduction/radiation case does not.

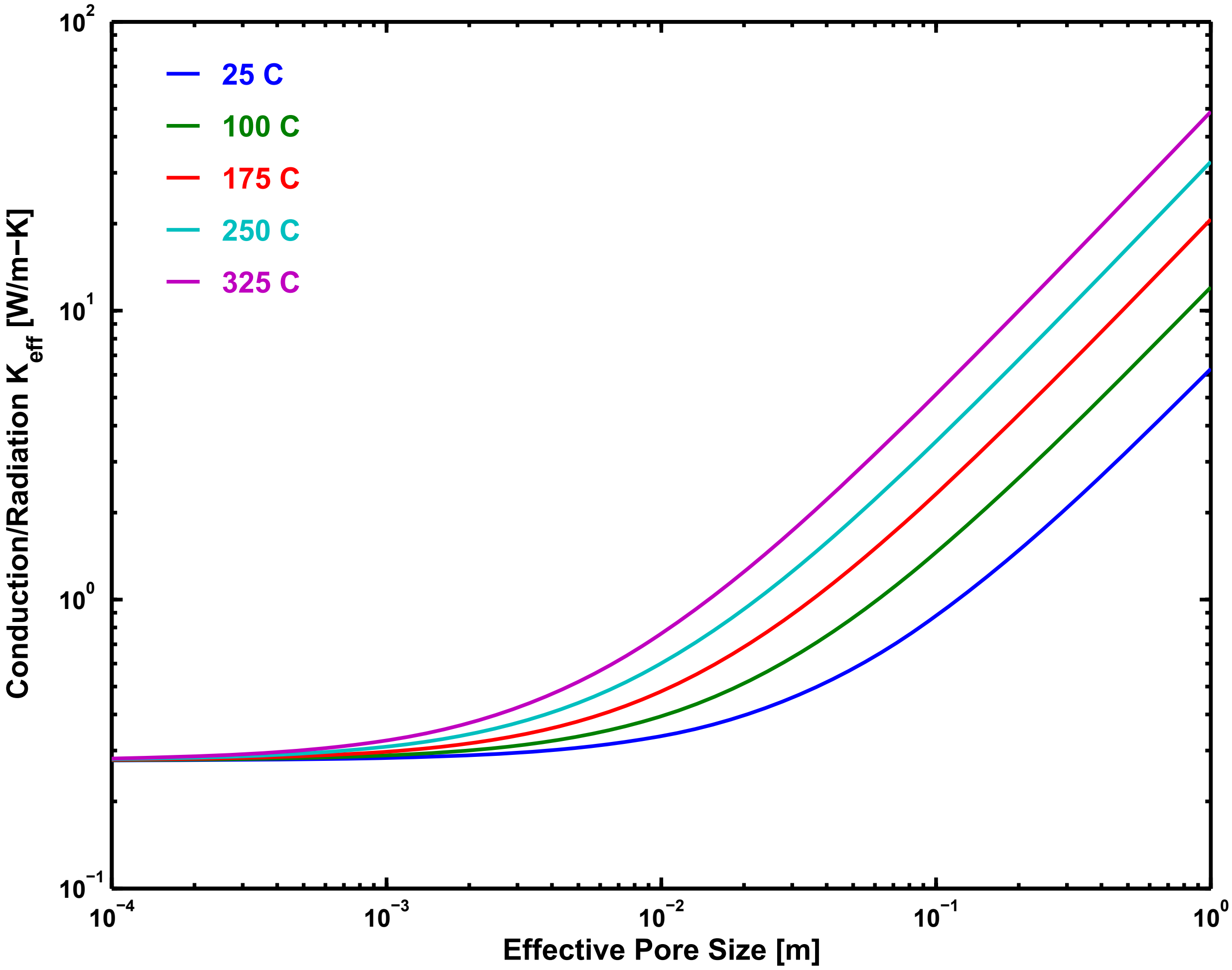

Figure 1-2: Influence of effective particle size and temperature on effective thermal conductivity.

significant, since radiative transfer is probably only very effective between big particles and there was reportedly a good amount of fines in the medium that would fill up the pore space.

### 05/13/05 Rubble-model consequences and thoughts.

SAS

One way to look at the different models is through simple examples.

The conduction/radiation model is considered in Figure 1-2, which demonstrates how effective thermal conductivity responds to both effective particle size and temperature. Figure curves were generated using the regressed properties, simply changing $D$. It appears from this figure that radiative transfer is minor when the effective distance $D$ is significantly less than 1 cm and significant regardless of temperature when $D$ is more than 10 cm. The situation at Yucca Mountain (YM) will depend on how the rockfall occurs, but likely rocks in some locations will be large enough to make thermal transfer significant.

The conduction/convection model can't be analyzed quite so conveniently, since convection is not a local process and it depends on geometry. Simply scaling up Ron's experiment is an extreme example, since it is essentially 1D while a waste-package/rubble example would be more radial, which will result in thermal flux per unit area dropping with distance from the waste package. Nevertheless, some illumination can be had. Let's consider the effect of rubble thickness for a fixed heat source, then vary the strength of the heat source. The temperature gradient is unknown and must be solved for, as is the value of $\kappa_{\mathit{eff}}$ matching the temperature gradient. Calculation is done by finding the value of $G = \Delta T/L$ where

$$q = KeG + CeRa_f^{1/4} L^{1/2} \max(0, G^{5/4} - G_c^{5/4}) \tag{1-16}$$

$$Ra_f = \frac{k\rho^2 g\beta C_v}{\mu\kappa_{\mathit{eff}}} \tag{1-17}$$

$$G_c = \frac{\Delta T_c}{L} \tag{1-18}$$

$$\Delta T_c = \frac{Ra_c}{Ra_f L} \tag{1-19}$$

$$\kappa_{\mathit{eff}} = \frac{q}{G} \tag{1-20}$$

where $Ra_f$ includes all factors in $Ra$ except $\Delta T$ and $L$, and $\Delta T_c$ is the temperature change at the critical $Ra$. This formula can be readily analyzed using the fzero routine from *Matlab*. Note that the analysis depends on $k$, which is problematic to estimate for large rubble chunks. As a first approximation, let's assume that $k$ is proportional to $d_p^2$, which is often done for porous media, and assume that $k = 10^{-7}$ m$^2$ for a particle size of 1 cm.

We can also consider the analogous effect with radiative transfer instead of convective transfer. Since thermal conductivity is dependent on temperature, the bulk properties cannot be determined directly. As an alternative, it is possible to solve the ordinary differential equation (ODE)

$$\frac{\partial T}{\partial x} = \frac{q}{\kappa_{\mathit{eff}}} \tag{1-21}$$

subject to a specified initial $T$ at a distance $L$ from the source. The *Matlab* routine ode45 readily evaluates this ODE. In this case $\kappa_{\mathit{eff}} = qL/\Delta T$, where $\Delta T$ is taken across the entire rubble thickness.

Comparisons were run for three representative heat fluxes (0.05, 5, and 500 W/m$^2$) and three representative particle sizes (0.1, 1, and 10 cm). Predicted effective thermal conductivities for the

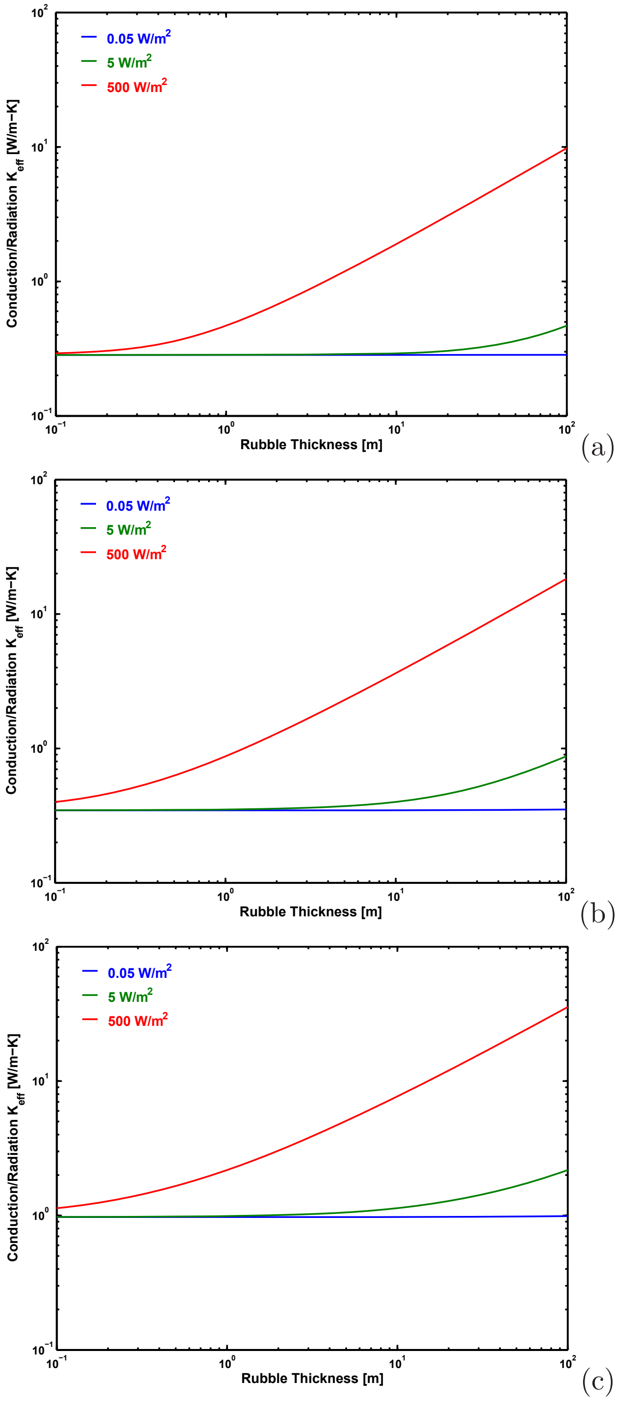

Figure 1-3: Effective thermal conductivity across various thicknesses of a rubble layer, using the conduction/radiation model. The coarse-fragment diameters from the lab experiment are multiplied by (a) 0.1, (b) 1, and (c) 10.

conduction/radiation model are shown in Figure 1-3, which can be compared with the conduction/convection model in Figure 1-4. The temperature drops across the rubble layer corresponding to these effective thermal conductivies are shown in Figure 1-5 and Figure 1-6, respectively.

### 05/16/05 Justification of transfer mechanisms in experiment.

SAS

Since the data does not unambiguously discriminate between radiative and convective transfer of heat in Ron's experiments, let's look at the plausibility of both mechanisms from a data standpoint.

As noted in the entry for 5/12/05, convection would not be expected in any of Ron's cases for intrinsic permeabilities less than about $3.5\times10^{-8}$ m$^2$. According to Freeze and Cherry (1979), the range of $k$ for gravel is $10^{-10}$ to $10^{-7}$ m$^2$, and the high end for clean sand is $10^{-9}$ m$^2$. This implies that convection is not expected in Ron's experiment, even if the coarse tuff particles are representative of the upper end of the gravel range, since a fine component blocking the pores should drag the overall permeability below the convection threshold.

Energy transport in a dry porous medium differs from mass transport. Energy transport is dominated by conduction within grains and is limited by grain-to-grain connections, while mass transport only occurs within pores and is limited by pore-to-pore connections. Large grains in energy transport are analogous to large pores in mass transport, as these are preferred pathways. The crevices between grains are negligible in mass transport, but play a critical role in energy transfer between grains. There must be some zone between touching coarse grains that is free of fine grains, simply because the fine grains are too large, and another zone that only has a thin layer of fine particles. These zones are prime candidates for radiative transfer.

A back-of-the-envelope calculation suggests that the effective exclusion zone may be about 40 percent of the grain's cross-sectional area. The regressed data give $\chi D \approx 1$ cm, and I identify $\chi$ as the effective area fraction for radiative transfer. In the experiment, chunks larger than about 6 cm were discarded. Assuming that the coarse matrix has chunks that are roughly 2 to 3 cm in diameter, say $D = 2.5$ cm, $\chi$ is about 0.4.

These considerations imply that radiative transfer is more plausible from a physical standpoint than convective transfer *for Ron's experiment.*

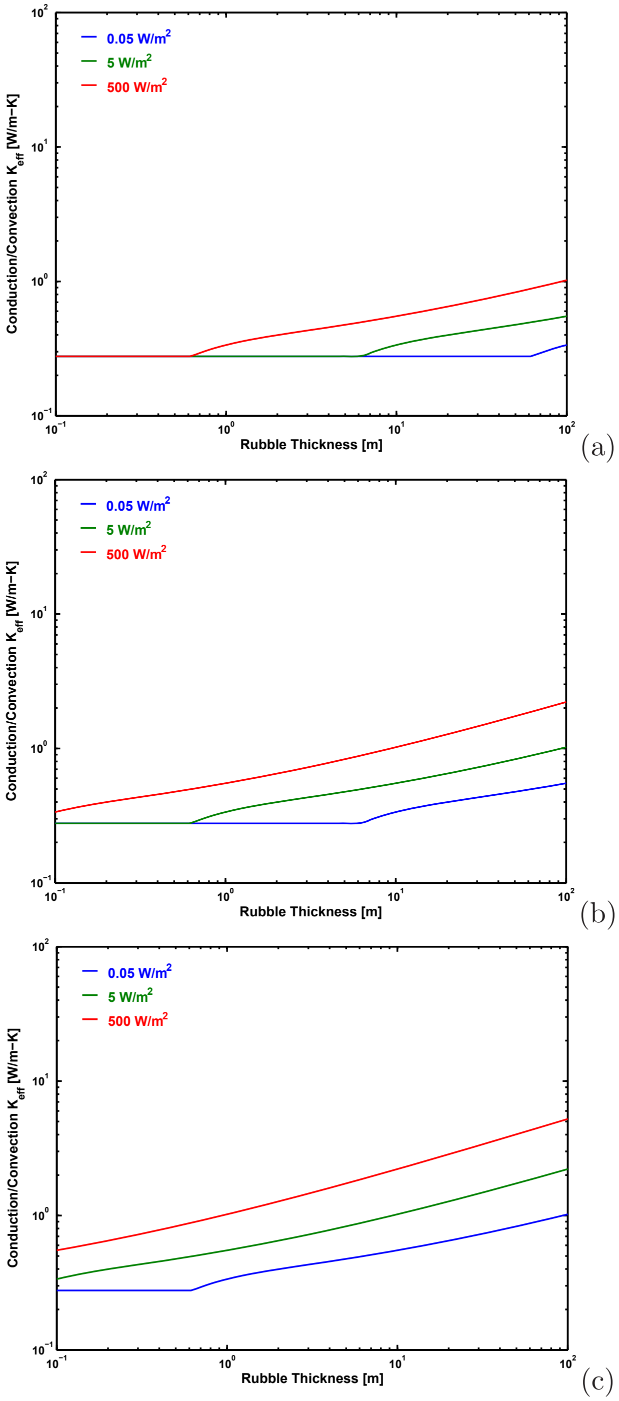

Figure 1-4: Effective thermal conductivity across various thicknesses of a rubble layer, using the conduction/convection model. The coarse-fragment diameters from the lab experiment are multiplied by (a) 0.1, (b) 1, and (c) 10.

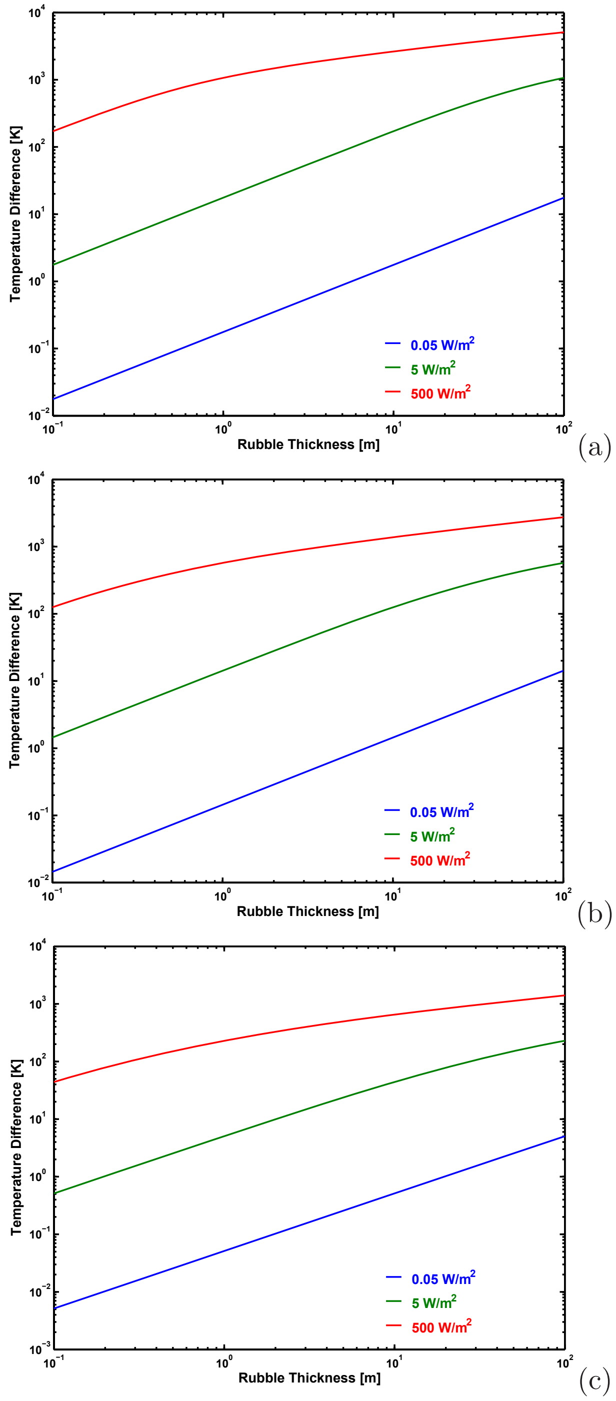

Figure 1-5: Predicted temperature drop across various thicknesses of a rubble layer, using the conduction/radiation model. The coarse-fragment diameters from the lab experiment are multiplied by (a) 0.1, (b) 1, and (c) 10.

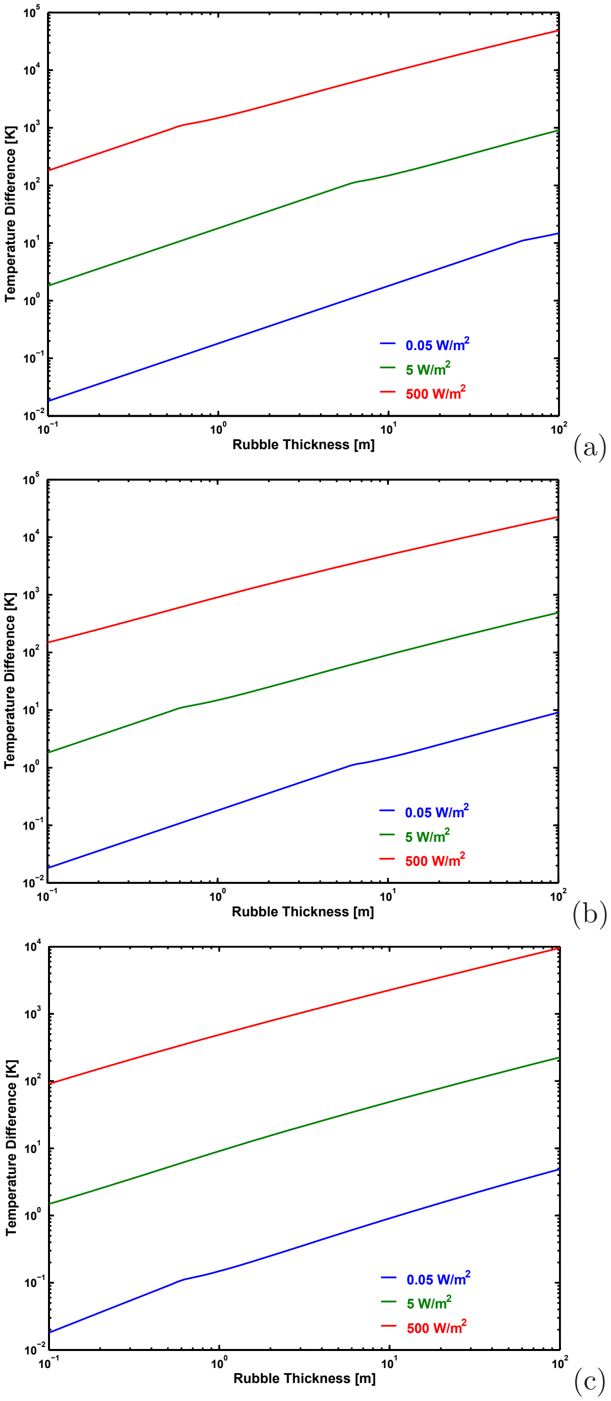

Figure 1-6: Predicted temperature drop across various thicknesses of a rubble layer, using the conduction/convection model. The coarse-fragment diameters from the lab experiment are multiplied by (a) 0.1, (b) 1, and (c) 10.

## 07/27/05 Calculations reviewing TPA 5.0 input document.

SAS

As part of my technical review for the document entitled “‘Updates to Hydrology-Related Abstractions and Inputs for Total-system Performance Assessment Version 5.1.1 Code” by Fedors and others, dated July, 2005, I performed some back-of-the-envelope calculations to verify that layer thicknesses were appropriately calculated for the vitric component of the Calico Hills unit. The original calculations were performed by Shannon Colton using input from Paul Landis and Randy Fedors.

I decided to check the calculations for subarea 3 in particular, since this was a large subarea and it has the thinnest vitric component. Vitric layers are the only layers with matrix permeability sufficiently large that all realizations of the TPA code have matrix flow, hence are important for retardation/sorption.

I obtained the spreadsheet that Shannon performed the calculations in, and modified it to independently calculate vitric layer thicknesses. The original approach used the Geologic Framework Model (GFM) to calculate all layer thicknesses for the TPA runs, with the Mineralogic Model (MM) only used to examine the Calico Hills unit because the GFM does not differentiate the Calico Hills into subunits. The MM was used to estimate percent of the Calico Hills that could be attributed to being vitric, and this percentage is applied to the GFM thickness for the Calico Hills.

Two types of checks were made: (i) calculation of areal averages, and (ii) uncertainty in determining the appropriate value of zeolite fraction that transitions between vitric and zeolite designations. All of these calculations are performed in a copy of the original spreadsheet developed by Shannon and documented in scientific notebook 432E, page XII–34, as “zeolite_tpa.xls”. My modified spreadsheet, called “zeolite_tpa3.xls”, is stored in the subdirectory “Spreadsheet” as part of the directory tree that this scientific notebook is located in. Documentation of the calculations is in the new worksheet “Information” in the spreadsheet.

I did the following checks

- Estimate vitric thickness by directly averaging calculated vitric-layer thicknesses from the MM points used to obtain properties
- Estimate vitric thickness by directly averaging calculated vitric-layer thicknesses from the MM points used to obtain properties, but weighting the four corner points as 1/2 of the weight of the center point (this is an exact integral of the areal average for a rectangle divided into triangles with properties linearly varying along the triangle edges)

- Estimate vitric thickness by directly averaging calculated vitric-layer thicknesses from the MM points used to obtain properties, but weighting the four corner points as 1/4 of the weight of the center point
- Estimate vitric thickness by independently averaging Calico Hills thickness and vitric fraction
- Calculate each of these quantities for transition values of 10, 15, and 25 percent zeolitic content

My best quick estimate would be the triangle estimate. Shannon subsequently calculated some estimates using the MM properties by subdividing each subarea into triangles and assuming that properties vary linearly between points. Shannon's calculations are not included in the spreadsheet.

In my checking, I found no place where Shannon performed a calculation incorrectly. Based on the checks, however, I question whether the most appropriate method for estimating the desired quantity was used.

Based on the calculations, the four different methods for estimating the areal average of vitric thickness can produce estimates that vary by slightly more than a factor of 2. In subarea 3, with zeolite cutoff of 15 percent, the estimates for average thickness range from 3.4 to 4.8 m using the four methods, with a value of 4.2 in the TPA document. The most preferred comparison, triangle to document, has a maximum ratio of 1.5 in subarea 2, between 1.2 and 1.4 in subareas 1, 6, and 7, and less than 1.04 in subareas 3, 4, 5, and 8. All subareas have values for the TPA 5.0 input file that are either within the spread of values from the MM input or are just outside an extreme value (in part because of different total layer thicknesses).

The zeolite cutoff value also is important for subarea 3. With a cutoff of 10 percent, the range of average vitric thickness from the MM is 1.2 to 2.8 m, while with a cutoff of 25 percent, the range of average vitric thickness from the MM is 5.7 to 6.3 m. As a comparison, the range of values sampled for TPA in subarea 3 is 0 to 9.1 m, which is considerably larger than the range It seems that for this thin layer, the cutoff is important. Other layers are not as sensitive.

I created a summary worksheet comparing the TPA document's calculated thicknesses with my best back-of-the-envelope calculation, using the triangle distribution scaled to the thickness used in the document. In the summary worksheet, I also plotted the resulting probability distributions for each subarea. The comparison is reproduced in Table 1.

What becomes clear from Table 1 and the figures is that in general the mean values for the document and my estimate are generally pretty close, and almost invariably my distribution

Table 1-2: Comparison of CHnv thicknesses from TPA document calculation and independently estimated values. All thicknesses are in m.

| | TPA Document | | | Independent Estimate | | |
|---|---|---|---|---|---|---|
| Subarea | Minimum | Mean | Maximum | Minimum | Mean | Maximum |
| 1 | 0 | 27.7 | 66.9 | 19.4 | 21.1 | 26.8 |
| 2 | 0 | 16.4 | 77.9 | 10.8 | 10.8 | 16.9 |
| 3 | 0 | 4.2 | 9.1 | 1.6 | 4.1 | 5.9 |
| 4 | 51.7 | 55.5 | 62.1 | 53.4 | 55.1 | 65.4 |
| 5 | 3.2 | 49.4 | 62.7 | 40.7 | 50.6 | 59.7 |
| 6 | 2.4 | 16.7 | 71.2 | 3.1 | 13.0 | 14.4 |
| 7 | 2.4 | 38.5 | 104 | 25.3 | 27.7 | 54.5 |
| 8 | 3.9 | 65.0 | 96.0 | 63.2 | 63.2 | 65.1 |

is entirely within the document's distribution. In Subarea 4, my upper bound is higher than the document's by 3.3 m. The uncertainty limits for the TPA document are generally much larger than the uncertainty limits calculated with my estimate.

The question arising from the analysis is what is an appropriate technique for assigning bounds. From a physical perspective, I'd think that you are trying to get at the average residence time in the matrix. If the flow were truly 1D, calculating the areal average thickness is needed and the cutoff between vitric and zeolitic is the key uncertainty. In the actual situation, flow may redistribute laterally towards high-permeability zones. If the zeolitic zones are at least as permeable as vitric layers due to fracturing, there should be little redistribution since the vitric units easily accept all flows. However, if the zeolitic units are much less permeable than the vitric units (as suggested by perching), redistribution would favor movement into the vitric units.

Assuming that the zeolitic units are flow barriers, it may be more appropriate to truncate the probability distribution at the lower end to reflect the uncertainty due to zeolite cutoff value but leave the upper end alone to account for lateral redistribution into the vitric.

Some more thought might be desirable on this topic over the next few months.

### 12/28/05 Calculations reviewing Mohanty et al. document.

SAS

As part of the technical review of "A model for estimating heat transfer through drift degradation-based natural backfill materials" by S. Mohanty, A. Ghosh, and G. Adams, being submitted to the International High Level Radioactive Waste Management Conference, I performed a pair of calculation checks.

One check consisted of verifying that Figure 3 of the paper was correctly calculated. I chose to reproduce the figure using just the information in the paper, and compare this to the figure in the paper. To do this, I used a short *Matlab* program to reproduce the relevant equations, plug in the relevant values from the paper, and plot it. The corresponding figure is shown in Figure 1-7, generated by a code labeled The code is reproduced in the code listing appendix for this review.

I was confused by the last paragraph in section 3.2.1 that purportedly compares mean and median rubble diameters to a two-parameter Schuhmann cumulative probability distribution in the form

$$P = \left(\frac{x}{F}\right)^{\alpha} \tag{1-22}$$

where $x$ is fragment size, $P$ is fraction less than $x$, $F$ is maximum fragment size, and $\alpha$ is a uniformity parameter. This translates the nomenclature and representation slightly from the paper but the idea is the same. The probability density distribution is

$$p = \frac{\mathrm{d}P}{\mathrm{d}x} = \frac{\alpha}{F}\left(\frac{x}{F}\right)^{\alpha-1} \tag{1-23}$$

It was asserted that it is difficult to match both mean and median of the parameter distribution with observed values. I disagree, since this is a 2-parameter distribution and two values are to be matched. Let's see how to do it.

The median value occurs where $y = 1/2$. Letting $\hat{x}$ be the measured median and rearranging the expression for $y$

$$\left(\frac{1}{2}\right)^{1/\alpha} = \frac{\hat{x}}{F} \tag{1-24}$$

or

$$F = \hat{x}2^{1/\alpha} \tag{1-25}$$

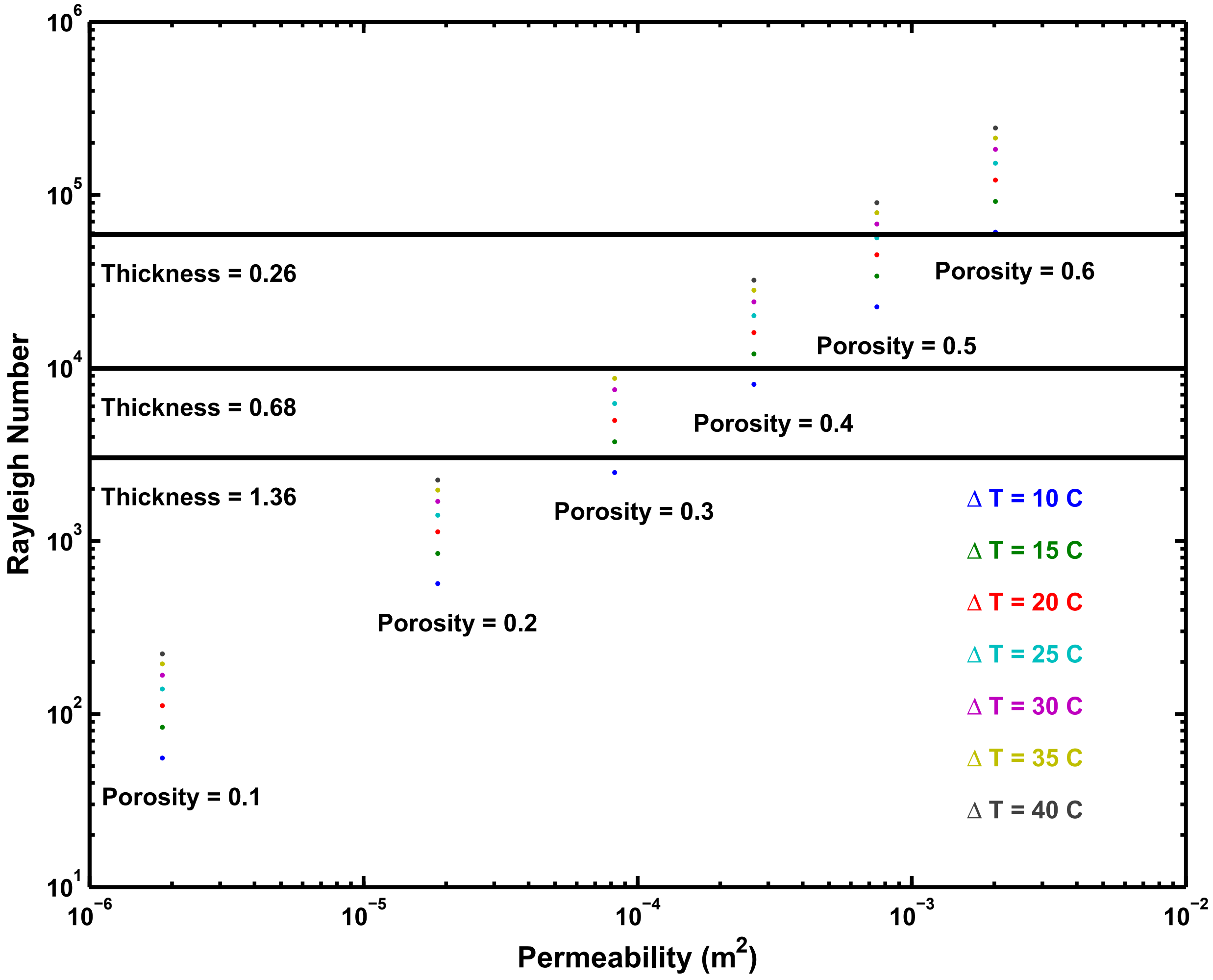

Figure 1-7: Rayleigh number as a function of permeability and porosity, with lines indicating where the Nusselt number is 10 (marking a lower bound of the convection-dominated heat transfer regime). This figure is essentially identical to Figure 3 by Mohanty et al..

The mean value occurs by integrating $x$ with the probability density distribution in the form

$$\begin{aligned}\bar{x} &= \int_0^F px \, \mathrm{d}x \\ &= \frac{\alpha}{F^\alpha}\int_0^F x^\alpha \, \mathrm{d}x \\ &= \left(\frac{\alpha}{\alpha+1}\right)\frac{F^{\alpha+1}}{F^\alpha} \\ &= \left(\frac{\alpha}{\alpha+1}\right)F \qquad (1\text{-}26)\end{aligned}$$

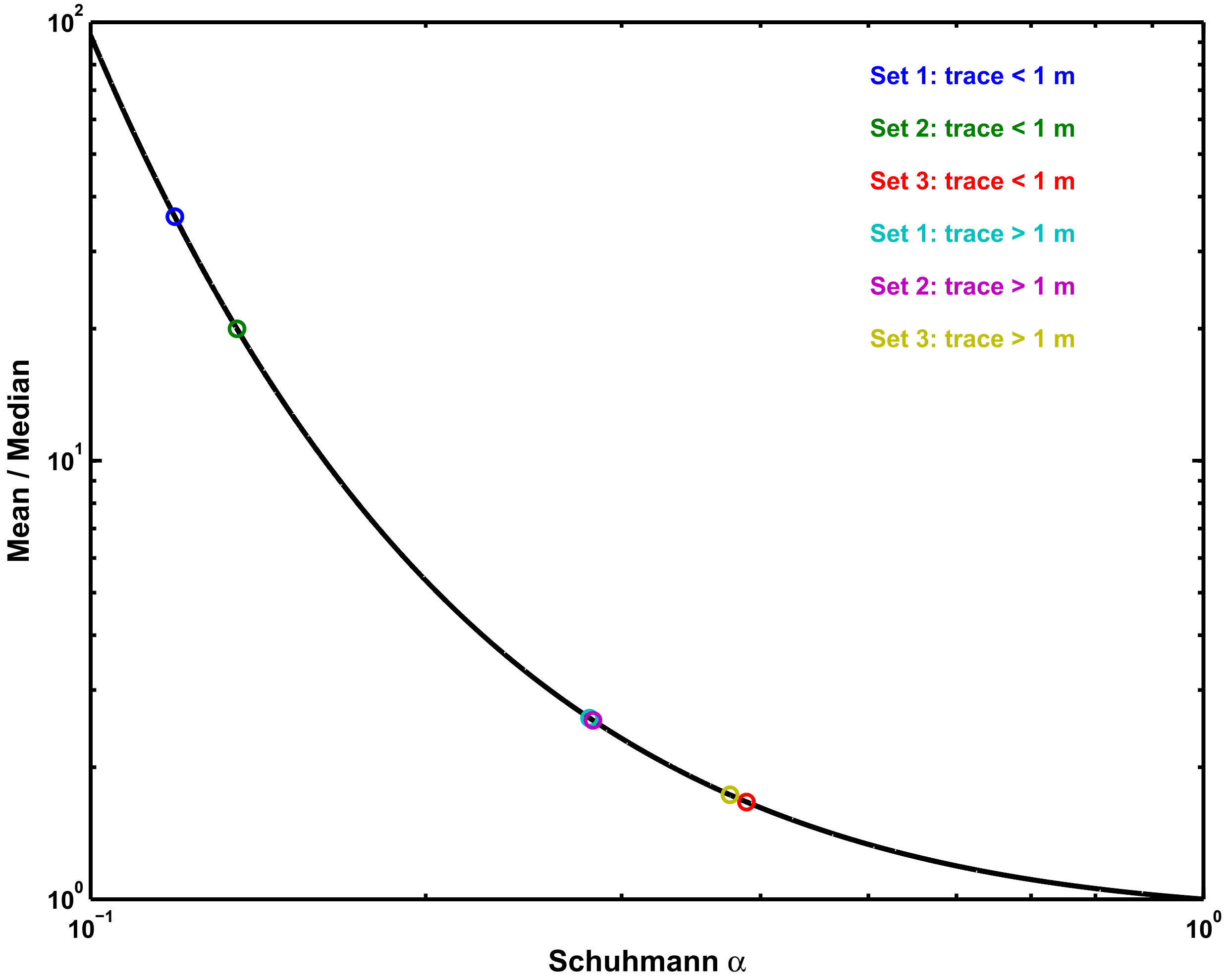

Figure 1-8: The analytic $\mu/\hat{x}$ function based on $\alpha$ with points marking where data sets 1 through 3 fall. Data are from Table 1 and 2 of the Mohanty et al. draft.

where $\bar{x}$ is the measured mean. Plugging in $F$

$$\frac{\bar{x}}{\hat{x}} = 2^{1/\alpha}\left(\frac{\alpha}{\alpha+1}\right) \tag{1-27}$$

Using these relationships, I created a small *Matlab* routine that finds match points between measured $\bar{x}/\hat{x}$ values and the function parameterized by $\alpha$. The function is shown in Figure 1-8. Given an $\alpha$ matching observed $\bar{x}$ and $\hat{x}$, $F$ is determined by plugging in the matching $\alpha$. The data sets from Tables 1 and 2 in the Mohanty et al. draft, together with fitted parameters, are listed in Table 1. Note that all of the data sets fall within an $\alpha$ range of 0.119 through 0.375, not greatly dissimilar to the assertion by Mohanty et al. that $\alpha$ lies approximately between 0.1 and 0.35 using

Table 1-3: Calculated Schuhmann parameters for the Tptpll fracture sets from Tables 1 and 2 in the Mohanty et al. draft.

| Case | Mean (mm) | Median (mm) | $\alpha$ | $F$ (mm) |
|---|---|---|---|---|
| Set 1: trace < 1 m | 1080 | 30 | 0.119 | 10200 |
| Set 2: trace < 1 m | 240 | 12 | 0.135 | 2010 |
| Set 3: trace < 1 m | 100 | 60 | 0.388 | 358 |
| Set 1: trace > 1 m | 1890 | 730 | 0.281 | 8620 |
| Set 2: trace > 1 m | 1790 | 700 | 0.283 | 8120 |
| Set 3: trace > 1 m | 2750 | 1590 | 0.375 | 10100 |

the median values. However, the assertion that considering the mean values expands the range of $\alpha$ to 0.1 to 0.6 does not seem justified. Also note that $F$ ranges from 360 to $10^4$ mm in the short-trace sets and $8\times10^3$ to $10^4$ mm in the long-trace sets, without strong justification for assuming the mean of 700 mm suggested by the Mohanty et al. draft.

### 12/30/05 Followup on Mohanty et al. document.

SAS

The approach outlined in the Mohanty et al. document describes a method for estimating fracture separations, but does not follow through to a desired end result of a particle size distribution. I decided to see what the implications of considering a joint distribution of blocks created from the statistics presented in the Mohanty et al. document.

The first step is to plot up the predicted relationships for each of the six fracture sets. The probability distribution implied by the statistics is shown in Figure 1-9, showing that the probability of occurrence decreases as the separation increases. The end of each curve at the large-separation end corresponds to the $F$ value calculated in the previous entry. The cumulative probability that a separation is less than a given value is shown in Figure 1-10 for each set. Note that all three of the fracture sets are quite similar in their large-trace statistics (Set 1 and Set 2 are almost identical). The Set-1 and Set-2 fine-trace statistics are more similar than either are to Set 3. It stands to reason that Set 3 (the subhorizontal set) may be quite different from the others, but it is not to me clear why Sets 1 and 2 should be substantially different.

After talking with Kevin Smart, it appears that "in theory" the statistics derived from the fine-scale fractures (trace length less than 1 m) should be consistent with the statistics generated from the large-scale fractures in the ECRB cross-drift line surveys. Accordingly, I considered just

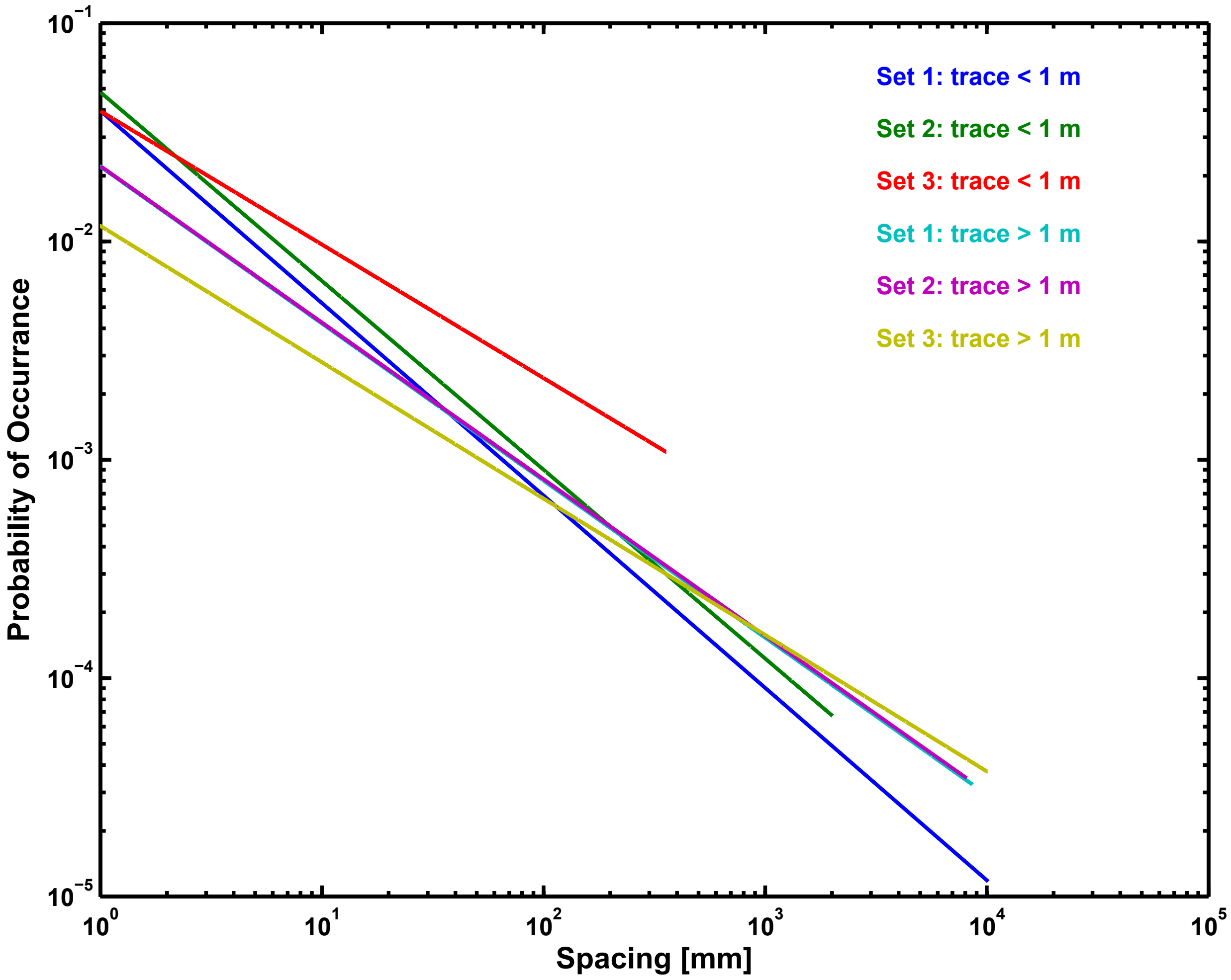

Figure 1-9: The probability density function for the fracture sets. Data are from Table 1 and 2 of the Mohanty et al. draft. The right-most termination point for each fracture set corresponds to $x = F$ for that set.

the fine-scale data in the following. I suspect that there may not be sufficient data to properly estimate the statistics for Set 3.

The idea is quite simple. Just use the statistics of fracture separations to estimate three dimensions of "bricks" that correspond to rubble particles. Several assumptions are made.

- Fractures are mutually orthogonal and planar.
- Fractures separations are independently distributed between sets (*i.e.*, each set can be sampled without considering the others).

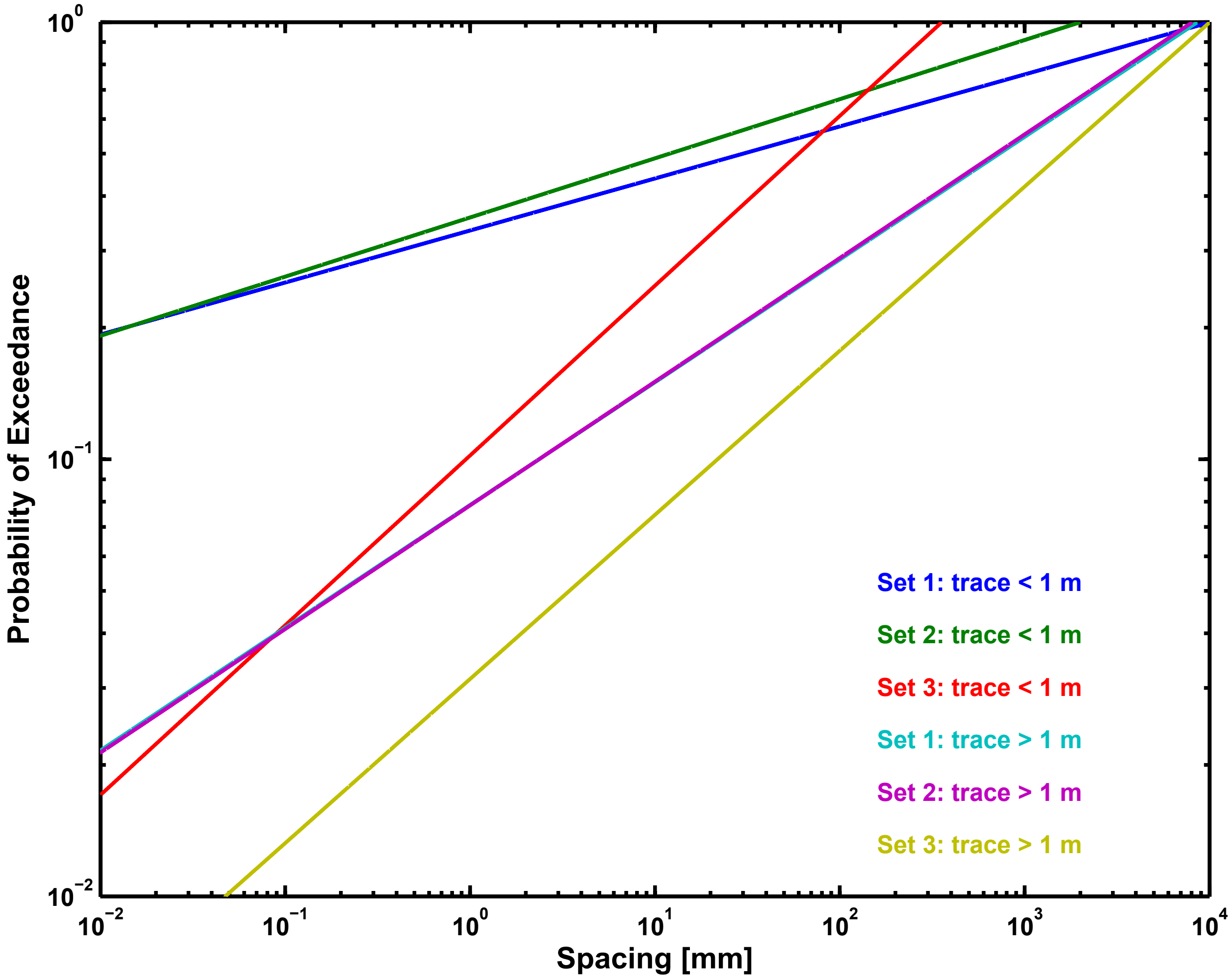

Figure 1-10: The cumulative probability density function for the fracture sets. Data are from Table 1 and 2 of the Mohanty et al. draft.

- The physics of the material, and deviations from fracture planarity, place a limit on the asperity ratio of a block. In other words, the ratio between longest and shortest block thickness is bounded. Cutoff ratios of 2, 5, 10, and 20 are considered, which should bound the actual situation.

The procedure is straightforward. A large ($10^6$) number of realizations are independently drawn from each set's separation distribution, forming a pool of potential blocks. The ratio of maximum to minimum separation for each block is calculated, and only blocks with ratios no greater than the cutoff ratio are retained for further analysis (other blocks are assumed to break up with the same asperity distribution).

The cumulative probability distribution of the aspect ratio for each subset of blocks matching the cutoff-ratio criteria is shown in Figure 1-11. Note that the distribution is fairly linear for the smallest cutoff value. As the cutoff value increases, the high end of the distribution becomes increasingly nonlinear.

The cumulative probability distribution for each of the cutoff ratios are shown in Figure 1-12. In the high end of the size distribution where neither Set 2 or 3 have any probability of contributing (*i.e.*, where $x$ is larger than their $F$), maximum block size is controlled by Set 1. The triplet curve is to the right of the Set-1 curve when either Set 1 and Set 2 can provide the upper bound, and the triplet curve changes slope yet again when all three sets can contribute. This provides distinct kinks in the triplet curve at the upper bounds for the size distributions for Sets 2 and 3.

The interesting information to be taken from these curves is that the block sizes implied by the fracture sets will predominantly be larger than 1 cm, with upper bounds (depending on ratio) ranging from 0.5 to perhaps 5 m.

Following a suggestion by Scott Painter, it is possible to calculate an equivalent block dimension that is simply the thickness of a cube with the same volume as the block. The radius of a sphere with the same volume is obtained by multiplying by $(4\pi/3)^{1/3} = 1.612$. Doing this calculation for the same set of cutoff ratios results in Figure 1-13, where the complement of the cumulative probability distribution is plotted. As a reference, the equivalent block dimension is fitted to an exponential distribution using the value at a complement of $10^{-2}$.

The results of the fitting process are summarized in Figure 1-14 for the four cutoff ratios considered. An exponential distribution is shown for comparison, fitting

$$P = P_0 \exp(-x/L) \tag{1-28}$$

where $P$ is the complementary cumulative probability distribution, $P_0$ is a scaling parameter, $x$ is the effective dimension [mm], and $L$ is the length-scaling parameter [mm]. The curves were fit using the value of $x$ at a ratio of $P/P_0 = 0.1$ to determine $L$, then using $x = 2$ mm to determine $P_0$. The values of $P_0$ and $L$ are different for each curve.

The curves in Figure 1-14 suggest that roughly 90 percent of the blocks will have an effective dimension ranging from 10 cm to between 0.5 m and 1 m, depending on the level used for the cutoff ratio. These values correspond to values for effective spheres of about 15, 80, and 160 cm, respectively.

The *Matlab* code doing the analysis and creating the figures is archived in the code listing

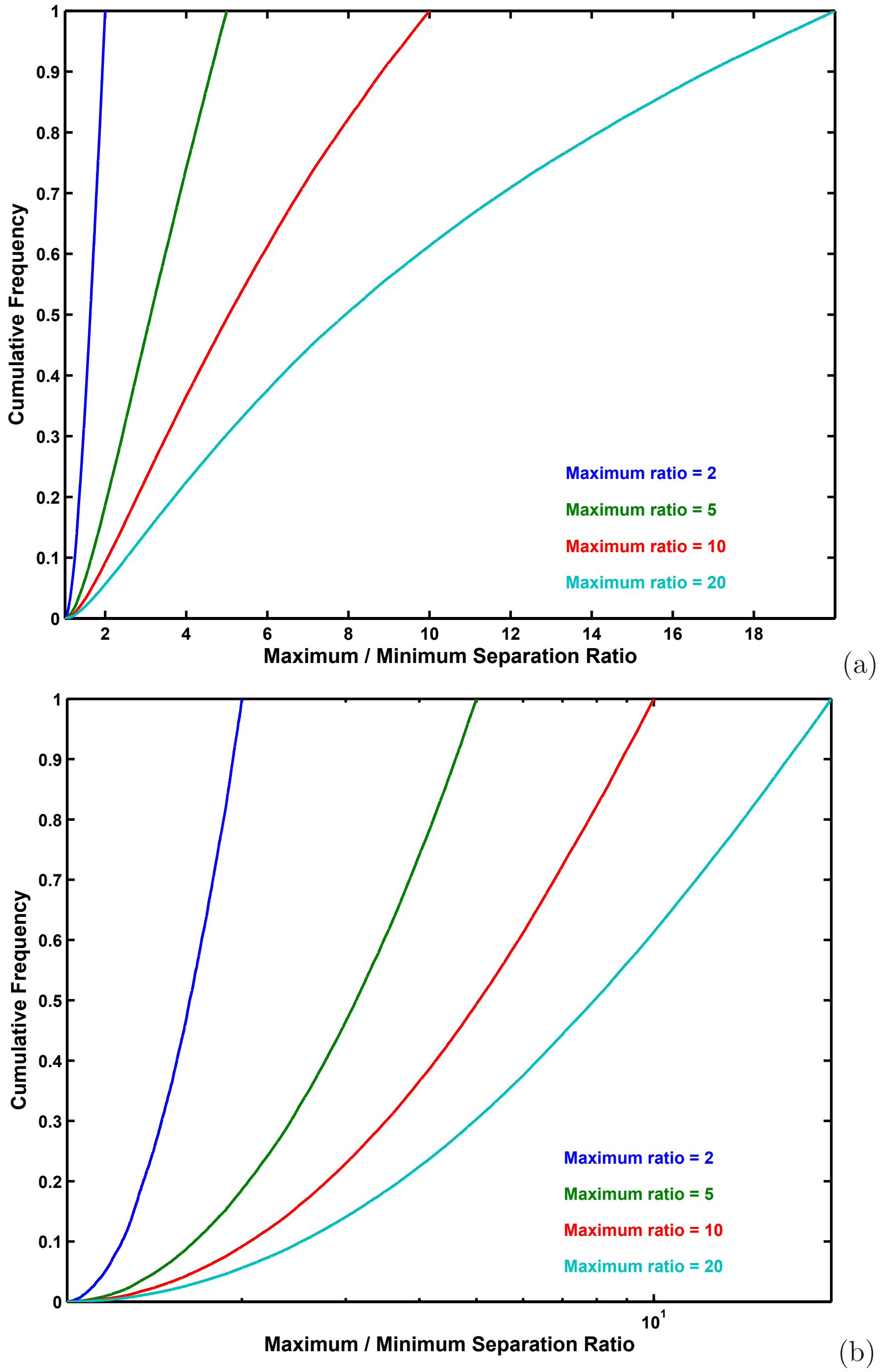

Figure 1-11: The cumulative probability density function for the maximum/minimum thickness ratio for blocks constructed from the fracture sets. The block sets are constrained to fall within cutoff ratios. The plots have (a) linear, and (b) logarithmic axes.

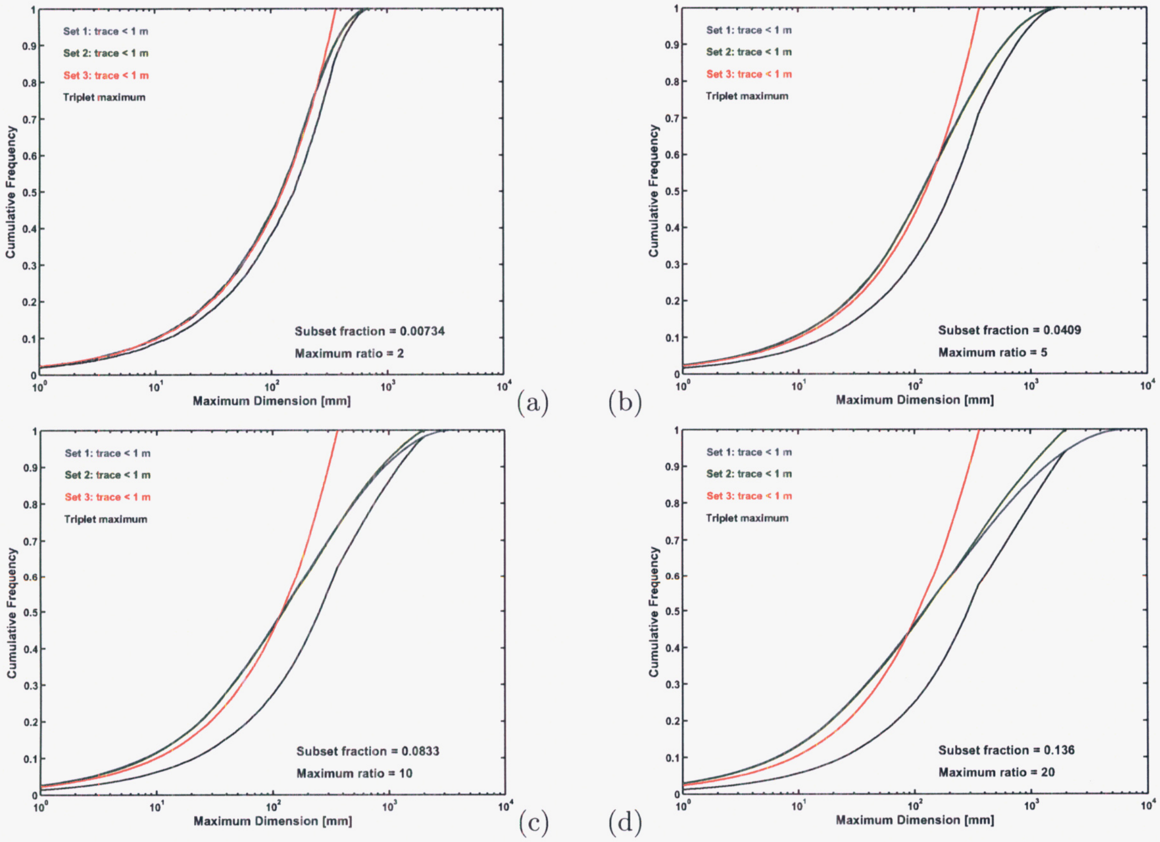

Figure 1-12: Cumulative probability density functions for censored fracture sets and maximum block thickness for the censored sets. Censoring occurs to restrain blocks to have aspect ratios less than (a) 2, (b) 5, (c) 10, and (d) 20, respectively.

appendix for the Mohanty et al. review.

RL 7/7/2010

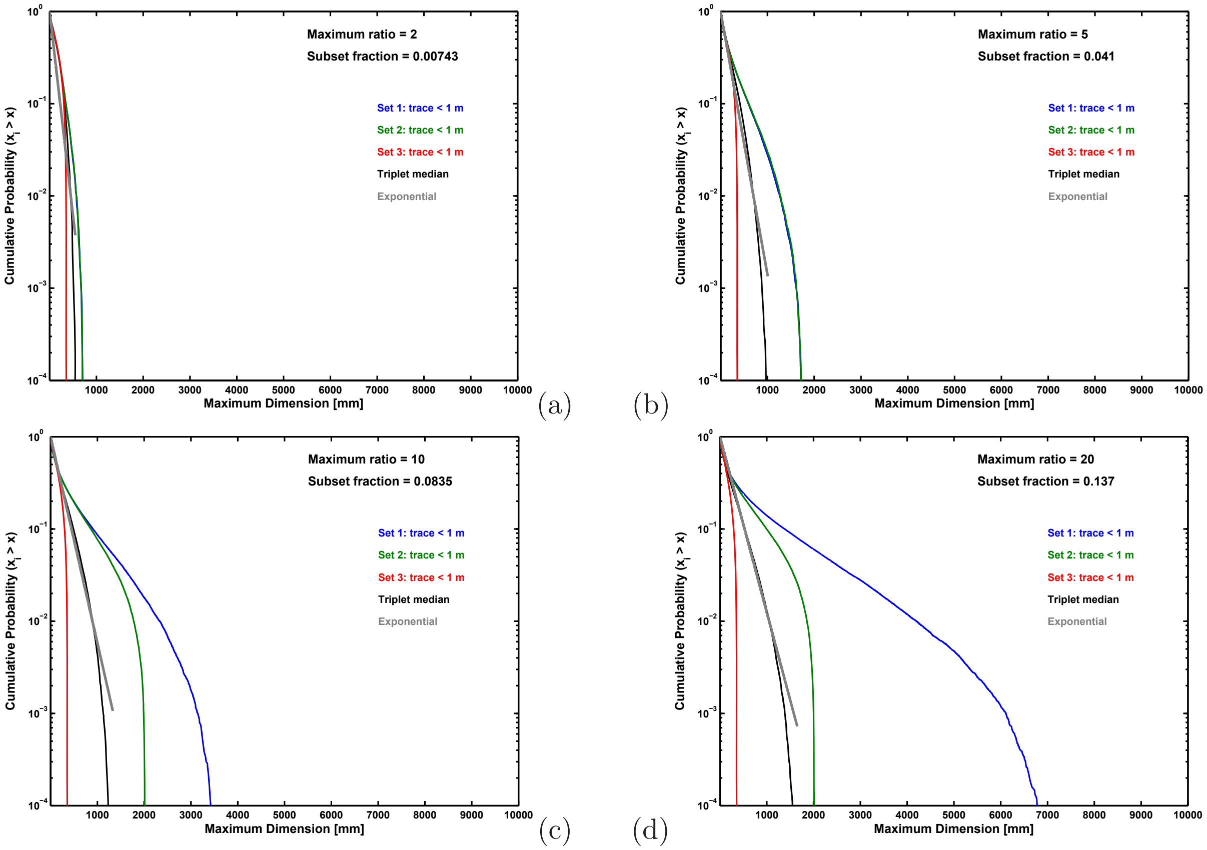

Figure 1-13: Complementary cumulative probability density functions for censored fracture sets and effective block thickness for the censored sets. Censoring occurs to restrain blocks to have aspect ratios less than (a) 2, (b) 5, (c) 10, and (d) 20, respectively.

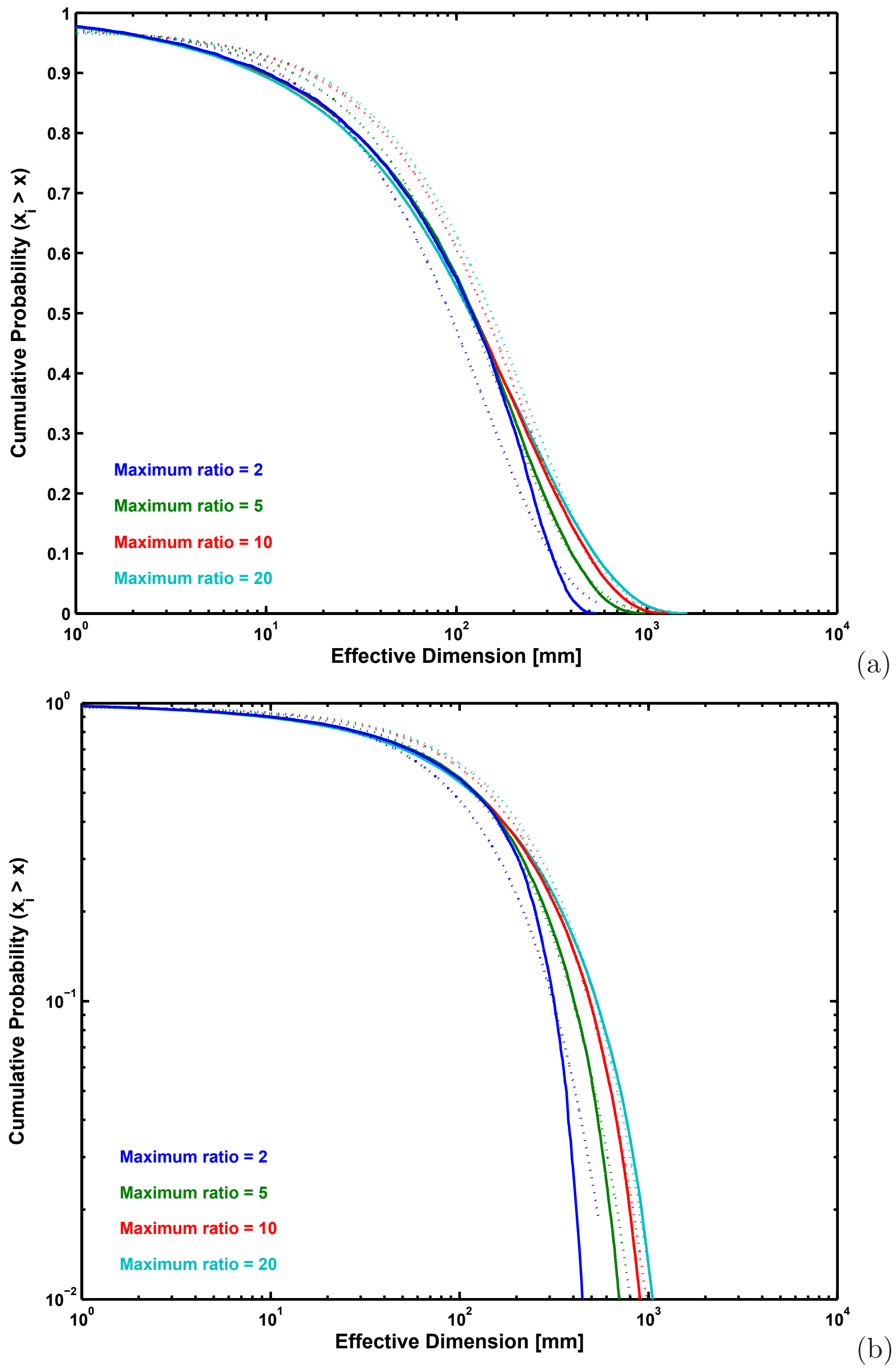

Figure 1-14: The complementary cumulative probability density function for the effective block dimension for blocks constructed from the fracture sets. The block sets are constrained to fall within cutoff ratios. The plots have (a) linear, and (b) logarithmic axes. Solid lines are assembled from randomly sampled sets, while dashed lines are exponential functions fit to the sampled sets.

## References

Freeze, R. A. and J. A. Cherry. 1979. *Groundwater*. Englewood Cliffs, NJ: Prentice-Hall, Inc.

RL 7/7/2010

# 2 Lateral diversion

### 08/19/05 Vegetative evidence for lateral diversion.

SAS

There has been a project ongoing since 2000 at a very low level of effort that was intended to provide a constraint on lateral flow due to the non-welded Paintbrush Tuff nonwelded (PTn) layer. The motivating concern is that Department of Energy (DOE) simulations with mountain-scale unsaturated zone (UZ) flow models consistently indicate significant lateral diversion occuring due to capillary effects at the PTn, while field evidence is not provided supporting model results. Lateral diversion occurs where the Tiva Canyon welded (TCw) unit contacts the PTn, as well as where the PTn contacts the Topopah Spring welded (TSw) unit. Lateral diversion in the calibrated UZ flow model is sufficient to limit seepage below the PTn to about 4 mm/yr in the north of the repository footprint, essentially funneling waters into faults. Diversion distances are on the order of 0.5 km and larger. On the other hand, expert elicitations (Geomatrix Consultants, Inc., 1997), fine-scale modeling (Flint et al., 2003), and analog-site investigations (Fedors et al., 2002) all support the interpretation that diversion due to lateral flow would be far smaller, perhaps on the order of tens of meters.

The contradiction between site-scale predictions and physical intuition regarding lateral diversion led Jim Winterle to suggest that perhaps there was a location where the PTn crops out at the surface that could be examined for evidence of lateral flow. He suggested that, since plants are responsive to available moisture, perhaps vegetation density could be examined to provide evidence regarding lateral redistribution.

A series of previously undocumented activities have occurred to examine this idea. The work was performed at such a low level of effort that documentation has not yet been captured in a scientific notebook. With the departure of Randy Fedors to the Nuclear Regulatory Commission (NRC) and preliminary image analysis complete, I am now documenting previous activity and will complete the analysis.

The summary of events, as I understand it:

- Randy Fedors acquired a set of four IKONOS images at a 1-m resolution in 2000 and 2001.
- Randy led some field work measuring spectral characteristics in and around YM in 2001, documented in Scientific Notebook 428.
- Preliminary multispectral analysis was performed by Mitchel Bell, documented in Scientific

Notebook 470; this work was terminated before usable analyses were completed.

- Randy also identified ridges north of the repository footprint that might provide the special characteristics needed to test whether lateral flow exists. He recognized that it is necessary to have both up-dip and down-dip exposures of the PTn in order to draw conclusions, and this does not occur within the footprint. Potentially suitable ridges are in the vicinity of Mile High Mesa.
- Lisa Harrell subsequently worked with the IKONOS data. She has georectified it into a consistent coordinate system with the geologic outcrop data. She has also created polygons representing PTn outcrops in the area of interest using ArcView. She has performed some preliminary analyses of the images to generate Normalized Difference Vegetation Index (NDVI) coverages. Overlapping the PTn polygons and the NDVI coverages, she has been able to create some simple statistics for NDVI within the polygons. And she is in the process of trying to account for features such as shadows with the guidance of Marius Necsiou.
- Lisa has also worked with the Geologic Framework Model to create contours of the top of the PTn. This work was intended to be a precursor to estimating lateral flow.
- Lisa also collected precipitation data from nearby gauges for the months prior to and during image acquisition.

Randy discussed some of his thoughts on the analysis before he left. He said that he did not see visual evidence of lateral flow from inspection of the NDVI coverages, but he was not comfortable without quantification of the coverages.

I have only looked at the potential for analyzing the problem to date, not the data itself. Based on this initial first look, I think it is going to be difficult to make definitive conclusions for several reasons, including

- There are few exposures of PTn, and the ones that exist tend not to be well exposed (diversion at the bottom of the PTn may be covered up by alluvium).
- There is going to be some confounding due to different solar radiation loads on the different sides of the ridges; lower potential evapotranspiration (PET) on north-facing slopes gives much greater vegetation density relative to south-facing slopes over the repository.
- It's possible that vegetation types are the not same on both sides of the ridges. South-facing sideslopes have Mojave vegetation and north-facing sideslopes have Great Basin vegetation

over the repository. The ridges being looked at are pointed to the southeast, so it would be necessary to verify in the field.

- Ridges are at an angle to the dipping direction, so lateral flow would be at an angle to the ridge orientation (I'm not sure if this is an advantage or a disadvantage).
- There is the potential for confounding due to different bedrock types (*e.g.*, PTn may be more or less suitable for vegetation than TCw).
- It's not even clear that the vegetation is dense enough to get reasonable indications of vegetation density from the spectral analysis.

It seems to me that there are enough potential confounding issues that the best approach may be to quantify the difference in vegetation index between the TCw unit and the PTn unit on both sides of the selected ridges. I'd guess that the ratio of NDVI above and below the TCw/PTn contact would be a reasonable index. Presumably lateral diversion would make this ratio different on the down-dip side of the ridge. Perhaps the index could be for all cells within a particular offset of the interface – some playing around will be necessary here. If possible the same thing could be done for the PTn/TSw contact.

Note to self: first new coverage to extract is elevation above the TCw/PTn interface for each pixel. If it seems reasonable, another coverage for elevation above the PTn/TSw interface.

### 09/01/05 Update on vegetative evidence for lateral diversion.

SAS

I sat down with Lisa Harrell for some time this week to look at the available data. My impression after looking at the data is that the lateral diversion determination would be even harder than I originally thought for several reasons. These include

- The only area where lateral diversion might work is on opposing faces to a wash, and alluvium is mapped over the bottom of the PTn in significant stretches.
- There are numerous small drainage channels cutting through the sideslopes, and these drainage channels have an extremely noticable NDVI signature that may be much larger than the background.
- Shadow is a noticable feature.

- Apparently only two scenes exist that completely cover the area of interest (although Lisa was not sure of this).

It seems to me that a followup with Marius Necsiou would be useful to determine what he thinks can come out of this exercise. My thought is pessimistic at best that a useful analysis can be done.

With that said, I am more optimistic for looking at the possibility of using the image data to estimate vegetation cover nearer to the repository. I am inclined to use the large amount of spectral data collected in the field to estimate properties. It will be interesting to see if the high resolution of the image coverage will allow a good estimate with the field data collected at a similar scale.

### 09/07/05 Update on vegetative evidence for lateral diversion.

SAS

I discussed the project with Marius. He had previously looked at the IKONOS satellite images that Lisa is using, and came to the conclusion that the images would be difficult to use for thematic classification, especially with regards to vegetation classification and land cover. Apparently the image processing algorithms result in color smearing, and the algorithms used by the vendor were not released. There are also apparently issues with the timing of the images.

As a result, Lisa is being redirected to create a GIS catalog of the field-derived information gathered by Randy Fedors, Dave Farrell, and Mike Smith in several field campaigns. This data was collected to provide ground-truthing of the images, with usable data from roughly 150 locations. Each location may have numerous spectrometer readings. The catalog work will be performed under the UZ1 (climate and infiltration) umbrella.

### 09/08/05 Lateral diversion estimates using modeling.

SAS

Apparently excessive lateral diversion is a nagging concern regarding the modeling work performed by DOE using the calibrated properties in the unsaturated-zone flow model.

One hypothesis is that the calibrated properties are tied closely to the vertical discretization in the flow model. Flint et al. (2003) found that lateral diversion was large when the PTn was discretized into just a few layers, but was greatly reduced when the gradation of layer properties was accounted for. I suspect that it may be simply that vertical resolution was increased with additional layers, although it is not clear from the document whether the same number of vertical grid blocks were used in all cases or whether the number of layers determined the number of grid blocks.

Flint et al. (2003) bound the predictions of lateral diversion using the work of Ross (1990) and Steenhuis et al. (1991). These approaches are semi-analytic, and apply to a single interface.

A 1D approach can be taken for estimating lateral diversion, which is somewhat more complex but still quite straightforward. Under conditions where a "long" profile exists in the direction of the dip and are uniform laterally perpendicular to the dip direction, moisture content reaches an equilibrium configuration in the vertical relative to the interfaces. Sufficiently far downslope, two conditions must hold

$$\frac{\mathrm{d}\theta}{\mathrm{d}y} = 0 \tag{2-1}$$

$$\frac{\mathrm{d}\theta}{\mathrm{d}\tau} = 0 \tag{2-2}$$

where $\theta$ is saturation, $\tau$ is the coordinate pointing directly down-dip, and $y$ is the lateral coordinate direction perpendicular to $\tau$. Under these conditions, lateral flow down-dip does not enter the vertical mass balance equation and, under steady conditions, vertical flux $q_z$ is a constant throughout the column. Note that when a monotonic relationship exists between $\theta$ and $P_c$, where $P_c$ is capillary pressure, the conditions are equivalent to

$$\frac{\mathrm{d}P_c}{\mathrm{d}y} = 0 \tag{2-3}$$

$$\frac{\mathrm{d}P_c}{\mathrm{d}\tau} = 0 \tag{2-4}$$

Using the Richards approximation with Darcy flow, flux is expressed as

$$\mathbf{q} = -K(P_c)[\nabla(-P_c) + \rho g \nabla z] \tag{2-5}$$

where $\mathbf{q}$ is the flux vector, $K$ is unsaturated hydraulic conductivity [L/T], $P_c$ is unsaturated hydraulic conductivity [L/T], $\rho$ is water density [M/L$^3$], $g$ is acceleration due to gravity [L/T$^2$], and $z$ is elevation above a datum [L]. In the vertical direction ($z$ is positive upwards), $\nabla z = 1$, leaving

$$q_z = -K(P_c)\left(-\frac{\partial P_c}{\partial z} + \rho g\right) \tag{2-6}$$

In the direction down-dip, $\nabla P_c = 0$, leaving

$$q_\tau = -K(P_c)\rho g \frac{\mathrm{d}z}{\mathrm{d}\tau} \tag{2-7}$$

A series of equivalent ratios allows the rate of down-dip offset to be calculated for the steady profile.

$$\frac{q_\tau}{q_z} = \frac{q_\tau/\epsilon}{q_z/\epsilon} = \frac{v_\tau}{v_z} = \frac{\mathrm{d}x/\mathrm{d}t}{\mathrm{d}z/\mathrm{d}t} = \frac{\mathrm{d}x}{\mathrm{d}z} \tag{2-8}$$

where $x$ is travel distance in the $\tau$ direction, $\epsilon$ is volumetric water content, and $v$ is water velocity. Plugging in for $q_\tau$,

$$\frac{\mathrm{d}x}{\mathrm{d}z} = -\frac{K(P_c)\rho g}{q_z}\frac{\mathrm{d}z}{\mathrm{d}\tau} \tag{2-9}$$

which is an ordinary differential equation for along-dip travel distance. Another ordinary differential equation for capillary pressure is obtained by rearranging the expression for $q_z$

$$\frac{\mathrm{d}P_c}{\mathrm{d}z} = \frac{q_z}{K(P_c)} + \rho g \tag{2-10}$$

Now there are two equations, one for $P_c$ and one for cumulative offset $x$, both as a function of $z$. An ODE solver can be used to integrate both equations simultaneously, given a constant value for $q_z$ and initial conditions for $P_c$ and $\tau$. The two obvious initial conditions for $P_c$ are

$$P_c = \begin{cases} P_c = 0 & \text{at a water table} \\ P_c = K^{-1}(-q_z/\rho g) & \text{at a drainage condition} \end{cases} \tag{2-11}$$

while $\tau = 0$ is the obvious initial condition for $\tau$.

Note that I got the idea for integrating the flux equation from Gordon Wittmeyer, who used a similar approach to integrate vertical flux for YM back when infiltration fluxes were thought to be extremely small in the 1990's. I'm not aware of other work using this approach for estimating lateral diversion.

### 02/20/06 Lateral diversion – fracture at a cavity.

SAS

I have been trying to quantify lateral diversion at the interface between a fracture and a cavity (*e.g.*, drift). The easiest way to quantify this is if the cavity is a sloping plane, which might represent the gradient between the crown of a drift and the outside radius of a waste package. Different angles of the fracture with the axis of the drift would yield different angles of the sloping plane with respect to horizontal.

My idea is to calculate the lateral diversion in the saturated fringe above the cavity assuming that there are a series of identical parallel fractures that carry all of the flux. This calculation only makes sense if the flux in the fracture above the saturated fringe is through gravity drainage, hence is not fully saturated. The lateral diversion would represent the maximum length of dry drift ceiling.

Assume that the background flux of water in the fracture is uniformly distributed,

$$q_v = q_i(B/b) \tag{2-12}$$

where $q_i$ is areal average flux [L/T] (*i.e.*, infiltration), $B$ is separation between parallel fractures [L], and $b$ is fracture aperture [L].

Using the parallel-plate assumption to represent fracture flow, maximum aperture-averaged gravity velocity in a vertical fracture is

$$v_{max} = K = \frac{\rho g b^2}{12\mu} \tag{2-13}$$

where $v_{max}$ is aperture-averaged velocity [L/T], $\rho$ is density [M/L$^3$], $g$ is acceleration due to gravity [L/T$^2$], and $\mu$ is viscosity [M/L-T]. Maximum volumetric flux per unit length of fracture is

$$Q_{vmax} = bK \tag{2-14}$$

Maximum separation of fractures with gravity drainage occuring is when $Q_{vmax}$ occurs, hence

$$B_{max} = \frac{Q_{vmax}}{q_i} = \frac{bK}{q_i} \tag{2-15}$$

Note that when $B < B_{max}$, probably the assumption of uniform flow should be modified into the assumption of rivulets that are saturated separated by essentially dry zones.

What I'll call a saturated fringe is the zone in the fracture with positive pressure above the cavity. The height of this positive-pressure saturated fringe is

$$H = \frac{2\sigma\cos(\alpha)}{b\rho g} \tag{2-16}$$

where $H$ is thickness of the positive-pressure zone [L], $\sigma$ is surface tension [M/T$^2$], and $\alpha$ is wetting angle [–].

The key to the analysis lies in a slippery assumption, that we have laterally uniform conditions in the saturated fringe of the fracture. The slipperiness arises from an inconsistency, in that capillary forces are not so important downgradient of the first seepage location so the capillary rise is not necessarily correct, but the slope of the top of the fringe is assumed parallel with the cavity implying that lateral gradients are negligible. Granting this assumption, the width-averaged velocity in the fringe is

$$v_\tau = -K\frac{\partial \tau}{\partial x} = -KS_x \tag{2-17}$$

where $\tau$ is the direction of the gradient in the fracture. Average flux in the direction of the gradient, $Q_\tau$, is

$$Q_\tau = bv_\tau = \frac{\rho g b^3}{12\mu} S_x \tag{2-18}$$

Lateral diversion, $L$, is determined by the ratio of fluxes

$$L = \frac{Q_\tau}{q_i B} H = \frac{bKS_x}{q_i B} H = A\frac{b^2 S_x}{q_i B} \tag{2-19}$$

$$A = \frac{\sigma \cos(\alpha)}{6\mu} \tag{2-20}$$

Note that lateral diversion is small if slope is small or downward fracture flow is large. The expression for $L$ is counter-intuitive at first, since $L$ is proportional to $b^2$ (*i.e.*, larger fractures have greater diversion). The explanation for this arises from the different scaling of lateral flux and capillary rise, since $Q_\tau$ is proportional to $b^3$ while $H$ is inversely proportional to $b$. This result breaks down if water does not bridge the fracture aperture, in which case capillarity rise does not occur.

Representative values for these parameters in an air/water system are: (i) $\sigma = 72$ dyne/cm, (ii) $\alpha = 0$ (in a fully wetting system) (iii) $\rho = 1$ gm/cm$^3$, and (iv) $\mu = 0.0114$ gm/cm-s. Plugging in these values, $A = 1050$ cm/s. With these values, diversion lengths are calculated for typical active-fracture separations and infiltration fluxes in Table 2. The corresponding fraction of maximum gravity-drainage fracture capacity, assuming film flow without crevices, is shown in Table 2. The corresponding fraction of the fracture occupied by films, assuming two-side flows, is shown in Table 2.

The analysis suggests that fractures with relatively fine apertures (10 and 20 $\mu$m) will have seepage with reasonably small separations at plausible infiltration fluxes, while 100-$\mu$m fractures will have seepage only for flux rates and separations that are relatively large.

The analysis also shows that large diversions only occur when the fluxes in the fracture are far below capacity. Dani Or (verbal communication) suggests that bridging occurs spontaneously when the films occupy about two-thirds of the volume, due to unavoidable oscillations. Notice that there is a relatively fine combination of fluxes and apertures in Table 2 that would promote bridging according to this criterion. Without bridging, one would expect film flow processes to dominate, which naturally leads to drop formation at the cavity instead of lateral flow.

In the tabulated combinations of fracture aperture, fracture spacing, and input flux, only the 1-micron fracture has lateral diversion more than 33 cm when the fracture is more than about two-thirds full.

Table 2-1: Diversion length for a combination of fracture aperture, fracture spacing, and infiltration flux assuming the fracture intersects a cavity with $S_x = 0.1$. Missing entries are inconsistent with gravity drainage in the fracture. All diversion lengths are in cm.

| $B$ | $q_i$ | Aperture ($\mu$m) | | | | | |
|---|---|---|---|---|---|---|---|
| m | mm/yr | 1 | 10 | 20 | 50 | 100 | 1000 |
| 0.01 | 1 | $3.32{\times}10^2$ | $3.32{\times}10^4$ | $1.33{\times}10^5$ | $8.30{\times}10^5$ | $3.32{\times}10^6$ | $3.32{\times}10^8$ |
| | 10 | | $3.32{\times}10^3$ | $1.33{\times}10^4$ | $8.30{\times}10^4$ | $3.32{\times}10^5$ | $3.32{\times}10^7$ |
| | 100 | | $3.32{\times}10^2$ | $1.33{\times}10^3$ | $8.30{\times}10^3$ | $3.32{\times}10^4$ | $3.32{\times}10^6$ |
| 0.1 | 1 | | $3.32{\times}10^3$ | $1.33{\times}10^4$ | $8.30{\times}10^4$ | $3.32{\times}10^5$ | $3.32{\times}10^7$ |
| | 10 | | $3.32{\times}10^2$ | $1.33{\times}10^3$ | $8.30{\times}10^3$ | $3.32{\times}10^4$ | $3.32{\times}10^6$ |
| | 100 | | $3.32{\times}10^1$ | $1.33{\times}10^2$ | $8.30{\times}10^2$ | $3.32{\times}10^3$ | $3.32{\times}10^5$ |
| 1 | 1 | | $3.32{\times}10^2$ | $1.33{\times}10^3$ | $8.30{\times}10^3$ | $3.32{\times}10^4$ | $3.32{\times}10^6$ |
| | 10 | | $3.32{\times}10^1$ | $1.33{\times}10^2$ | $8.30{\times}10^2$ | $3.32{\times}10^3$ | $3.32{\times}10^5$ |
| | 100 | | | $1.33{\times}10^1$ | $8.30{\times}10^1$ | $3.32{\times}10^2$ | $3.32{\times}10^4$ |
| 10 | 1 | | $3.32{\times}10^1$ | $1.33{\times}10^2$ | $8.30{\times}10^2$ | $3.32{\times}10^3$ | $3.32{\times}10^5$ |
| | 10 | | | $1.33{\times}10^1$ | $8.30{\times}10^1$ | $3.32{\times}10^2$ | $3.32{\times}10^4$ |
| | 100 | | | | $8.30{\times}10^0$ | $3.32{\times}10^1$ | $3.32{\times}10^3$ |
| 100 | 1 | | | $1.33{\times}10^1$ | $8.30{\times}10^1$ | $3.32{\times}10^2$ | $3.32{\times}10^4$ |
| | 10 | | | | $8.30{\times}10^0$ | $3.32{\times}10^1$ | $3.32{\times}10^3$ |
| | 100 | | | | | $3.32{\times}10^0$ | $3.32{\times}10^2$ |

So one would expect that as a fracture experiences fluxes that increase from infinitesmal to full capacity for gravity drainage, the regimes would change from (i) no dripping (evaporation-dominated); to (ii) dripping (film-flow dominated, with perhaps some drop diversion inside the cavity); to (iii) maximum (but moderate) capillary diversion into a zone of dripping (bridging occurs near fracture capacity); and finally to (iv) decreasing capillary diversion as fracture capacity is reached. Roughly speaking, when the fracture is at or above about 44 percent of its flux capacity capillarity dominates and moderate diversion occurs, while below 44 percent flux capacity capillarity is rare and minimal diversion occurs.

Table 2-2: Fraction of fracture flux capacity for a combination of fracture aperture, fracture spacing, and infiltration flux assuming the fracture intersects a cavity with $S_x = 0.1$. Missing entries are inconsistent with gravity drainage in the fracture. Fraction of flux capacity is dimensionless.

| $B$ | $q_i$ | Aperture ($\mu$m) | | | | | |
|---|---|---|---|---|---|---|---|
| m | mm/yr | 1 | 10 | 20 | 50 | 100 | 1000 |
| 0.01 | 1 | $4.42\times10^{-1}$ | $4.42\times10^{-4}$ | $5.53\times10^{-5}$ | $3.54\times10^{-6}$ | $4.42\times10^{-7}$ | $4.42\times10^{-10}$ |
| | 10 | | $4.42\times10^{-3}$ | $5.53\times10^{-4}$ | $3.54\times10^{-5}$ | $4.42\times10^{-6}$ | $4.42\times10^{-9}$ |
| | 100 | | $4.42\times10^{-2}$ | $5.53\times10^{-3}$ | $3.54\times10^{-4}$ | $4.42\times10^{-5}$ | $4.42\times10^{-8}$ |
| 0.1 | 1 | | $4.42\times10^{-3}$ | $5.53\times10^{-4}$ | $3.54\times10^{-5}$ | $4.42\times10^{-6}$ | $4.42\times10^{-9}$ |
| | 10 | | $4.42\times10^{-2}$ | $5.53\times10^{-3}$ | $3.54\times10^{-4}$ | $4.42\times10^{-5}$ | $4.42\times10^{-8}$ |
| | 100 | | $4.42\times10^{-1}$ | $5.53\times10^{-2}$ | $3.54\times10^{-3}$ | $4.42\times10^{-4}$ | $4.42\times10^{-7}$ |
| 1 | 1 | | $4.42\times10^{-2}$ | $5.53\times10^{-3}$ | $3.54\times10^{-4}$ | $4.42\times10^{-5}$ | $4.42\times10^{-8}$ |
| | 10 | | $4.42\times10^{-1}$ | $5.53\times10^{-2}$ | $3.54\times10^{-3}$ | $4.42\times10^{-4}$ | $4.42\times10^{-7}$ |
| | 100 | | | $5.53\times10^{-1}$ | $3.54\times10^{-2}$ | $4.42\times10^{-3}$ | $4.42\times10^{-6}$ |
| 10 | 1 | | $4.42\times10^{-1}$ | $5.53\times10^{-2}$ | $3.54\times10^{-3}$ | $4.42\times10^{-4}$ | $4.42\times10^{-7}$ |
| | 10 | | | $5.53\times10^{-1}$ | $3.54\times10^{-2}$ | $4.42\times10^{-3}$ | $4.42\times10^{-6}$ |
| | 100 | | | | $3.54\times10^{-1}$ | $4.42\times10^{-2}$ | $4.42\times10^{-5}$ |
| 100 | 1 | | | $5.53\times10^{-1}$ | $3.54\times10^{-2}$ | $4.42\times10^{-3}$ | $4.42\times10^{-6}$ |
| | 10 | | | | $3.54\times10^{-1}$ | $4.42\times10^{-2}$ | $4.42\times10^{-5}$ |
| | 100 | | | | | $4.42\times10^{-1}$ | $4.42\times10^{-4}$ |

Table 2-3: Fraction of fracture volume occupied with water for two-sided film flow for a combination of fracture aperture, fracture spacing, and infiltration flux assuming the fracture intersects a cavity with $S_x = 0.1$. Missing entries are inconsistent with gravity drainage in the fracture. Fraction of fracture volume is dimensionless.

| $B$ | $q_i$ | Aperture ($\mu$m) | | | | | |
|---|---|---|---|---|---|---|---|
| m | mm/yr | 1 | 10 | 20 | 50 | 100 | 1000 |
| 0.01 | 1 | $6.65\times10^{-1}$ | $2.10\times10^{-2}$ | $7.44\times10^{-3}$ | $1.88\times10^{-3}$ | $6.65\times10^{-4}$ | $2.10\times10^{-5}$ |
| | 10 | | $6.65\times10^{-2}$ | $2.35\times10^{-2}$ | $5.95\times10^{-3}$ | $2.10\times10^{-3}$ | $6.65\times10^{-5}$ |
| | 100 | | $2.10\times10^{-1}$ | $7.44\times10^{-2}$ | $1.88\times10^{-2}$ | $6.65\times10^{-3}$ | $2.10\times10^{-4}$ |
| 0.1 | 1 | | $6.65\times10^{-2}$ | $2.35\times10^{-2}$ | $5.95\times10^{-3}$ | $2.10\times10^{-3}$ | $6.65\times10^{-5}$ |
| | 10 | | $2.10\times10^{-1}$ | $7.44\times10^{-2}$ | $1.88\times10^{-2}$ | $6.65\times10^{-3}$ | $2.10\times10^{-4}$ |
| | 100 | | $6.65\times10^{-1}$ | $2.35\times10^{-1}$ | $5.95\times10^{-2}$ | $2.10\times10^{-2}$ | $6.65\times10^{-4}$ |
| 1 | 1 | | $2.10\times10^{-1}$ | $7.44\times10^{-2}$ | $1.88\times10^{-2}$ | $6.65\times10^{-3}$ | $2.10\times10^{-4}$ |
| | 10 | | $6.65\times10^{-1}$ | $2.35\times10^{-1}$ | $5.95\times10^{-2}$ | $2.10\times10^{-2}$ | $6.65\times10^{-4}$ |
| | 100 | | | $7.44\times10^{-1}$ | $1.88\times10^{-1}$ | $6.65\times10^{-2}$ | $2.10\times10^{-3}$ |
| 10 | 1 | | $6.65\times10^{-1}$ | $2.35\times10^{-1}$ | $5.95\times10^{-2}$ | $2.10\times10^{-2}$ | $6.65\times10^{-4}$ |
| | 10 | | | $7.44\times10^{-1}$ | $1.88\times10^{-1}$ | $6.65\times10^{-2}$ | $2.10\times10^{-3}$ |
| | 100 | | | | $5.95\times10^{-1}$ | $2.10\times10^{-1}$ | $6.65\times10^{-3}$ |
| 100 | 1 | | | $7.44\times10^{-1}$ | $1.88\times10^{-1}$ | $6.65\times10^{-2}$ | $2.10\times10^{-3}$ |
| | 10 | | | | $5.95\times10^{-1}$ | $2.10\times10^{-1}$ | $6.65\times10^{-3}$ |
| | 100 | | | | | $6.65\times10^{-1}$ | $2.10\times10^{-2}$ |

## References

Fedors, R. W., J. R. Winterle, W. A. Illman, C. L. Dinwiddie, and D. L. Hughson. 2002. *Unsaturated Zone Flow at Yucca Mountain, Nevada: Effects of Heterogeneity and Flow in the Nonwelded Paintbrush Tuff Unit.* , Center for Nuclear Waste Regulatory Analyses, San Antonio, TX.

Flint, L. E., A. L. Flint, and J. S. Selker. 2003. Influence of transitional volcanic strata on lateral diversion at Yucca Mountain, Nevada. *Water Resources Research 39*(4), SBH 4-1-4-17.

Geomatrix Consultants, Inc. 1997. *Unsaturated Zone Flow Model Expert Elicitation Project.* , Geomatrix Consultants, Inc., San Francisco, CA.

Ross, B. 1990. The diversion capacity of capillary barriers. *Water Resources Research 26*(10), 2625-2629.

Steenhuis, T. S., J.-Y. Parlange, and K.-J. S. Kung. 1991. Comment on "The Diversion Capacity of Capillary Barriers". *Water Resources Research 27*(9), 2155-2156.

RL 7/7/2010

# 3 Seepage Workshop Report

## 07/25/07 Seepage workshop analyses.

SAS

A series of meetings were held in 2007 related to updating parameters for Total-System Performance Assessment (TPA) version 5.1. These meetings were collectively called the Seepage Workshop. This project entry documents analyses for the workshop report.

One section of the report discusses the subarea wet fraction and waste package flow multiplication factor in TPA. The basis for these calculations is provided in the following. The text closely follows the original draft of section 3.1 of the report.

Any flow entering drifts at YM will likely almost completely arise from flow in fractures, with only a negligible contribution from the welded tuff matrix because of the strong capillary forces where the drift wall intersects the welded tuffs. Accordingly, the conceptual model for the seepage process neglects the water in the matrix and focuses on the contribution of the fractures. From the standpoint of characterizing seepage, it is convenient to break down the process into factors arising outside the influence of the drift, in the near-field of the drift, and within the drift. The subarea wet fraction and waste package flow multiplication factor parameters are used to describe flow processes in the fractures in the mountain above the influence of the drift itself, although the geometry of the drift and waste packages is considered in estimating the parameter values.

The welded units at YM have far more capacity in the fracture system to carry flow than is likely to occur under natural infiltration. Accordingly, most fractures must be at least partially dry, or unsaturated, although some fractures may be completely saturated. Under this over-capacity situation, the interplay between fracture network geometry, capillary forces, and the supply of water to the system will mediate between those fractures carrying liquid water and those fractures remaining dry. Capillary forces are inversely proportional to the radius of curvature of the water/air interface, which is largely determined by the fracture aperture, thus capillary forces preferentially draw water into the smallest apertures first if water is available, and the importance of capillary forces relative to gravity rapidly decreases with increasing fracture aperture. On the other hand, the volume of flow is proportional to the cube of the aperture for a given gradient in potential. In gravity-dominated flow within a fracture, flow moves in the steepest direction without a tendency to move laterally unless flow is restricted by some barrier.

Only seepage occurring above the waste package itself can drip on the waste package. The geometry of this potential-drip zone is extremely long and narrow, because the waste packages will be laid end-to-end in the drift. The essentially 1D long-and-narrow geometry of the potential-drip zone suggests that a 1D analysis reasonably describes seepage locations, with seepage occurring at discrete intervals along the drift. This assumption is appropriate because the waste packages are long relative to the length of most fracture traces in the drift dimension above the waste package footprint, thus few seeping fractures will be expected to drip on more than one waste package.

Fractures carrying water outside of the influence of the drift are somewhat loosely called seeps in the following because these fractures would provide potential drip locations in the absence of the near-drift processes such as capillary diversion and evaporation that are captured in the $F_{mult}$ factor in TPA version 5.1. With the assumption of a 1D analysis, two factors are important in describing seeps: (i) the separation between seep locations, and (ii) the amount of water flowing in each seep. These factors are strongly inversely related when there is a fixed total flow rate of water. For example, consider two situations where the average separation between seeps differs by a factor of 10. If the same total flow is moving through the system, on average the flow in the seeps with the large separation will be 10 times greater than the flow in the seeps with the small separation.

The TPA code uses the related concepts of a subarea wet fraction and a waste package flow multiplication factor to describe seeps. The subarea wet fraction characterizes the fraction of waste packages that are contacted by seeps, and the waste package flow multiplication factor characterizes the relative increase in the quantity of water contacting waste packages due to convergence and divergence above the drift horizon. To date, there is no reported direct observation of drips in the TSw tuff within the Exploratory Studies Facility (ESF) and the Enhanced Characterization of the Repository Block (ECRB) cross drift at YM. Bulkheads have been emplaced in the ECRB cross drift; anecdotal evidence of moisture in the ECRB cross drift has been been observed after extended periods with closed bulkheads and no ventilation. The anecdotal evidence, in the form of scattered discolored spots and corrosion, may be due to condensation or due to dripping from fractures and anchor bolt cavities. Because direct evidence of dripping is lacking, estimates for these TPA parameters are derived from indirect evidence and interpretive models.

Detailed line surveys in the ESF and ECRB collected intersections of long fractures with the 1D scanline located 0.9 m below the left wall spring line (Albin et al., 1997; Barr et al., 1997; Beason et al., 1997; Eatman et al., 1997; Mongano et al., 1999). Only fractures at least 1 m in length were recorded, and fracture apertures were not determined. Approximately 15 percent of the total length of emplacement drifts is anticipated to occur within the Tptpmn horizon, with the remainder in the Tptpll horizon. For the purposes of an illustrative analysis, the intersection data from station 1015.04 to station 1442.28 in the ECRB cross drift was used to describe the Tptpmn

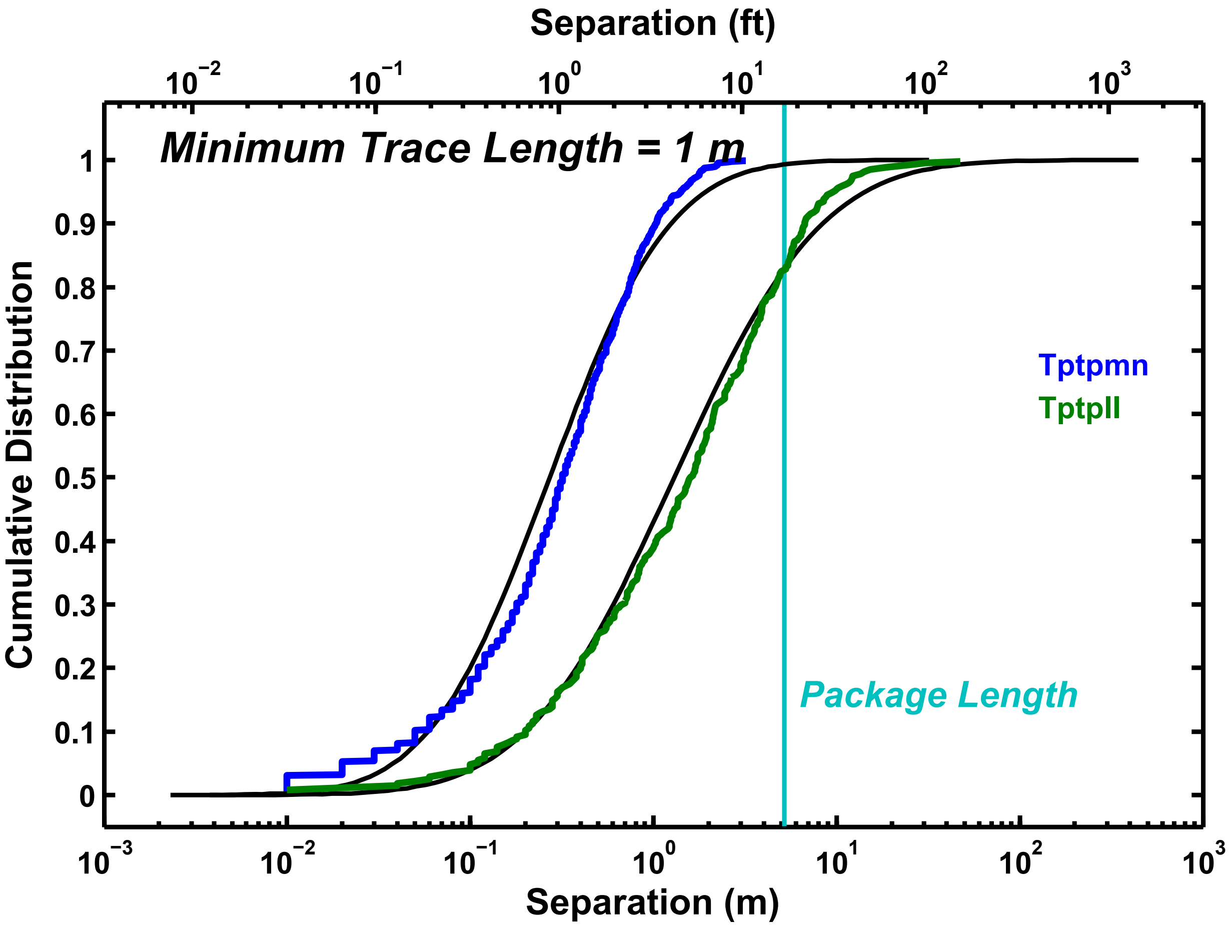

Figure 3-1: Cumulative distribution of fracture separations in the Tptpmn and Tptpll horizons determined using detailed line surveys. Lognormal distributions with the same mean and standard deviation of the log-transformed separations are shown for reference.

horizon and the intersection data from station 1445.49 to station 2324.48 was used to describe the Tptpll horizon. Features identified as fractures, shears, faults, vapor phase partings and cooling joints were considered in calculating intersection separation. The mean, median, and standard deviation of the intersection separations are 0.46, 0.32, and 0.45 m, respectively, for the Tptpmn and are 2.9, 1.6, and 4.4 m, respectively, for the Tptpll. These statistics are likely to vary somewhat across the repository footprint due to differences in ashflow cooling histories, layer thicknesses, etc.

The cumulative distribution of intersection separation is shown for both segments in Figure 3-1, with the length of a waste package indicated for reference. A lognormal distribution for each horizon is indicated for reference, calculated using the mean and standard deviation of the log-transformed separations. Figure 3-1 suggests that at least one long fracture would be expected above essentially every waste package in the Tptpmn horizon and approximately 80 percent of waste packages in the Tptpll horizon.

There are known biases in measuring fracture trace length and orientation using the detailed line survey methodology (Smart et al., 2006). For example, the numerous fractures with traces less than 1 m in length are not considered. In addition, the ECRB is a near-horizontal tunnel oriented at 229°, therefore shallowly dipping (*i.e.*, subhorizontal) fractures or fractures nearly parallel to the ECRB (*i.e.*, northeast-southwest striking fractures) are undersampled in this data set. Because seepage is expected to occur primarily in subvertical fractures, the undersampling of subhorizontal fractures in these analyses was considered to be insignificant in determining the subarea wet fraction and waste package flow multiplication factor. Smart et al. (2006) considered biases in the line survey methodology, finding that the major fracture set orientations in the Tptpll do not include a significant proportion of northeast-southwest striking fractures. Further, the ECRB is expected to be nearly parallel to the drift orientations, thus the orientation biases in the ECRB may be similar to the biases in the actual drifts. Accordingly, the intersection data is used directly in the following analysis, with the caveat that the many smaller fractures are not considered.

Not all fractures described in the line survey are expected to seep. Based on field and experimental observations, only a fraction of the connected fractures transmit water in a partially saturated and fractured host rock (Liu and Bodvarsson, 2001; Liu et al., 2003; Liu et al., 2004; Seol et al., 2003; Zhou et al., 2006). These fractures are often termed active fractures. Liu et al. (1998) used the concept of active fractures to describe the fraction of connected fractures in an unsaturated fractured domain that contribute to fracture flows, and used inverse modeling to estimate that approximately 18 to 27 percent of the connected fractures in the TSw unit are active. The potential repository would be located in the TSw unit. The fracture connectedness in the line survey was not evaluated, and the fraction of surveyed fractures that are disconnected is a significant source of uncertainty. Because the line survey only considered fractures with long traces, it is reasonable to expect that many or most of the surveyed fractures are connected to some extent, if only through myriad unmapped small fractures, but some fraction of the fractures may be disconnected. Accordingly, it is reasonable to expect that the methods of Liu et al. (1998) would suggest that less than 18 to 27 percent of the mapped fractures would carry water.

A straightforward analysis illustrates the interplay between fracture spacings, the active fracture concept, the subarea wet fraction, and the waste package multiplication factor. The two lognormal distributions shown in Figure 3-1 are used to describe the fracture spacing statistics along a hypothetical drift. The distributions were used to generate a set of 105 hypothetical fracture spacings for the Tptpmn horizon and another for the Tptpll horizon, assuming for the purposes of illustration that adjacent fracture spacings are uncorrelated. The spacings provided a sequence of fracture locations. A line of waste packages was placed under the fracture sequence, each package 5.2 m long and with the packages separated by 0.1 m.

The subarea wet fraction is straightforwardly determined by simply counting the number of waste packages with an overlying fracture. Randomly discarding a fraction of the fractures before counting the intersections accounts for the active fracture concept. Figure 3-2a demonstrates the subarea wet fraction determined as a function of the seeping fracture fraction, which is the fraction of mapped fractures that seep. The seeping fracture fraction and the active fracture fraction are the same if all mapped fractures are connected. The 18 and 27 percent limits suggested by Liu et al. (1998) are provided in Figure 3-2a for visual reference. At these limits, the subarea wet fraction is approximately 0.75 to 0.9 for the Tptpmn horizon and approximately 0.3 to 0.4 for the Tptpll horizon.

The waste package flow multiplication factor is estimated using the same fracture sets. Each flowing fracture carries all of the water flowing within a ”capture zone” or localization zone, with the remainder of the capture zone either matrix or dry fractures. In the analysis, each seeping fracture is assigned half of the distance to the next seeping fracture on either side. The waste package flow multiplication factor is calculated by summing the total capture zone length over all seeping fractures that intersect a waste package, and dividing by the total length of the waste packages that have a seep above it.

Figure 3-2b demonstrates the waste package flow multiplication factor determined as a function of the seeping fracture fraction. Again the 18 and 27 percent limits suggested by Liu et al. (1998) are provided for visual reference. At these limits, the waste package flow multiplication factor is approximately 1.15 to 1.3 for the Tptpmn horizon and approximately 2.4 to 3.5 for the Tptpll horizon.

Figure 3-2 suggests that, for a given seeping fracture fraction, waste packages in the Tptpmn are more likely to have seeps intersecting them but the amount of water focused onto the waste packages is likely to be smaller relative to waste packages in the Tptpll. Figure 3-3 shows the subarea wet fraction and waste package flow multiplication factor for each seeping fracture fraction, confirming that the subarea wet fraction and waste package flow multiplication factor are inversely related for both horizons. Note that this inverse relationship implies that the fewer packages contacted by water, the greater the amount of water (on average) contacting each of the wetted waste packages.

The actual distribution of flow in fractures remains speculative at YM. Niche and alcove

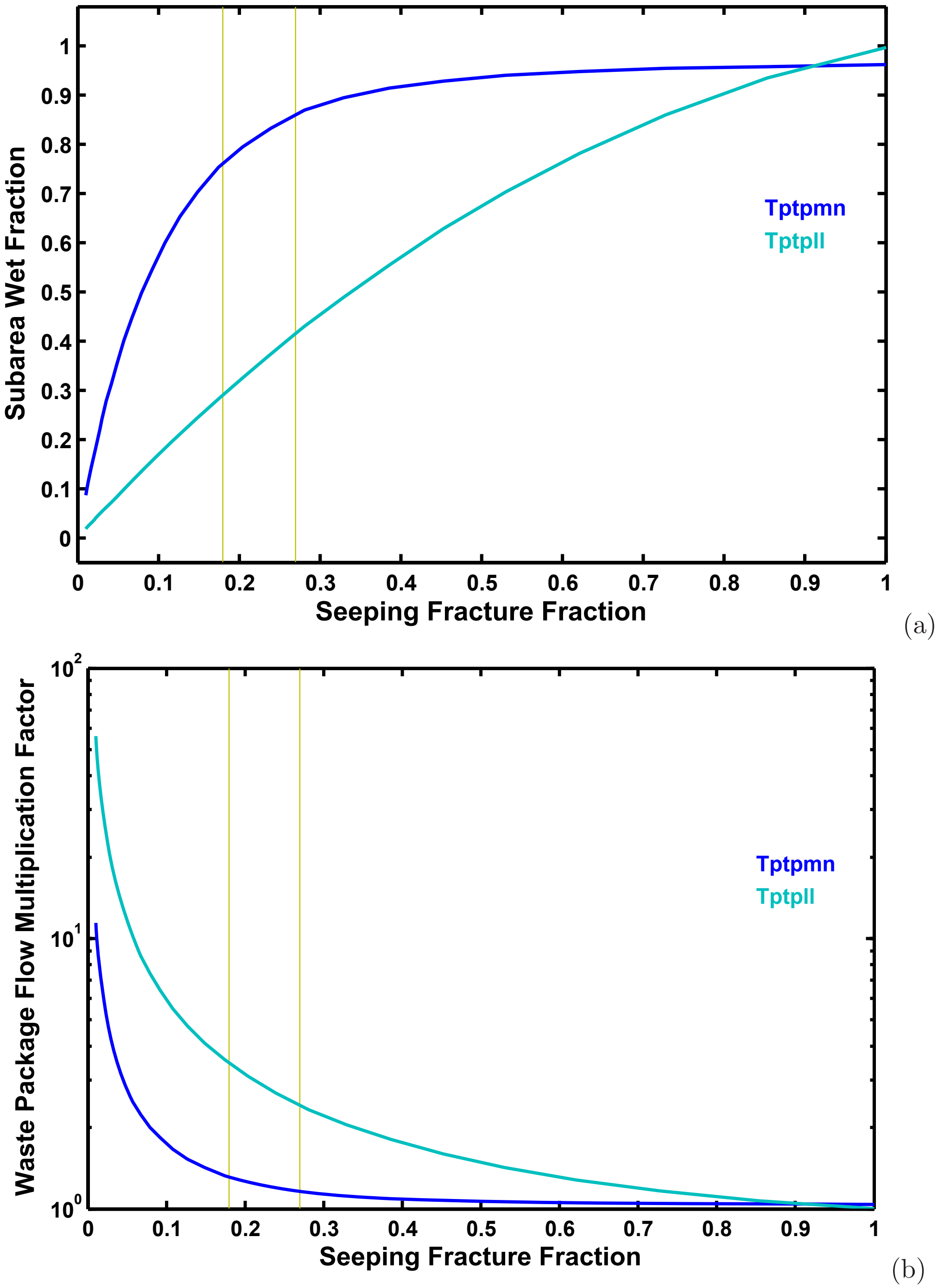

Figure 3-2: (a) Subarea wet fraction and (b) waste package flow multiplication factor for the Tptpmn and Tptpll horizons as a function of seeping fracture fraction. The range of active fracture fractions estimated by Liu et al. (1998) is shown for reference.

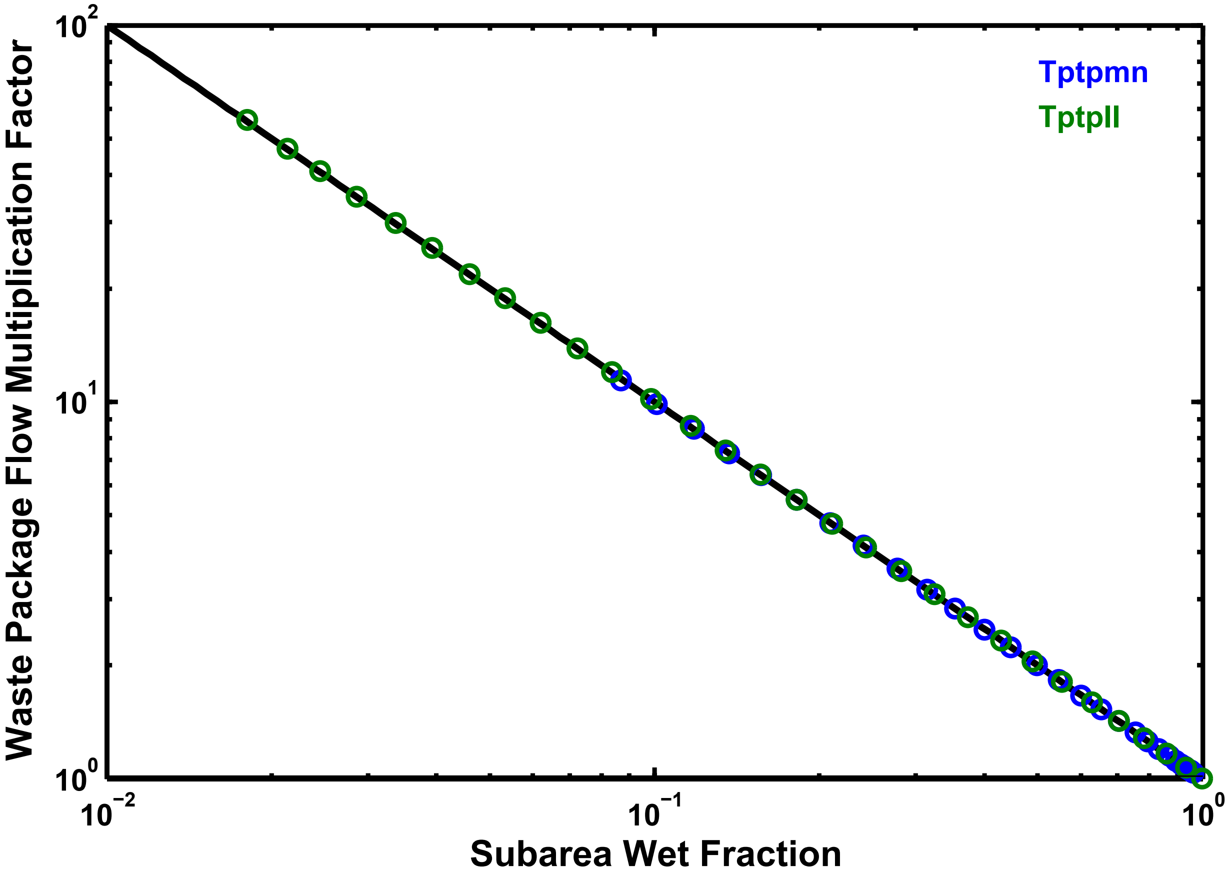

Figure 3-3: Subarea wet fraction and waste package flow multiplication factor pairs in the Tptpmn and Tptpll horizons given a seeping fracture fraction. The two parameters are inversely related.

experiments have rapidly introduced large volumes of water into the unsaturated zone, with flow characteristics examined for these cases, but it is not clear that these experiments are representative of the low-magnitude long-duration flows more likely to be typical of YM. These tests exhibited minimal flow entering the cavities, but successive injection tests along horizontal boreholes suggest that seepage patterns may be more closely linked to the character of fractures intersected in the borehole than to diversion by capillarity in the fracture network approaching the niche and alcove ceilings. In the extreme of fully saturated conditions, fracture network characteristics throughout the network determine the flow pathways. As the network becomes more unsaturated, it is reasonable to expect that the link between fracture network characteristics and flow pathways is increasingly governed by local fracture and intersection characteristics, thus the spatial distribution of the water entering the layer becomes increasingly important. With this reasoning, the spatial distribution of water-carrying fractures in a highly transmissive gravity-dominated layer may be largely determined at the upstream end by the spatial patterns of water moving through low-transmissivity upstream layers, with these inherited patterns gradually coalescing into a new characteristic distribution given contact with sufficient numbers of fracture intersections.

The PTn unit represents the most significant low-fracture-transmissivity layer at YM, because the matrix is permeable, relatively few discontinuities exist, and capillary forces tend to draw water into the matrix. Data on discontinuity separation is sparse because of the relatively short intervals exposed in the ESF, but it is reasonable to expect that the cumulative distribution of fracture separations would lie to the right of the Tptpll distribution in Figure 3-1. It is likely that the transitions between the overlying TCw unit, the PTn unit, and the underlying TSw unit provide a strong patterning to flow at the top of the TSw unit, and this patterning may not be fully muted at the proposed repository horizon. If the relatively widely separated discontinuities in the PTn control patterning at the repository horizon, then the representative seepage fraction at the horizon may be smaller than the characteristic seepage fraction at the repository horizon and the seeps would tend to be relatively widely separated. On the other hand, the densely fractured horizons between the PTn and the Tptpmn may overcome the patterning imposed at the top of the TSw unit. This would imply that the Tptpll unit would have a spatial patterning of seeps at the top of the horizon that is characteristic of the Tptpmn unit. Because there is a relatively short vertical distance from the base of the Tptpmn horizon to drifts in the Tptpll horizon, the characteristic seep separation for the Tptpll may not be achieved and the seep pattern for the Tptpmn horizon may be a more appropriate description for seeps at the drift horizon in the Tptpll horizon.

Speculation regarding the range of seepage patterns at the repository horizon implies that the subarea wet fraction is a fairly uncertain parameter. The upper bound of the range must be close to 1, reflecting the possibility that the characteristic Tptpmn seep characteristics apply in both horizons. The lower bound of the range is less well defined. Staff judgement sets the lower bound of the range to 0.25 for the purposes of TPA analyses, reasonably representing the range of alternatives arising from (i) imprinting from the nonwelded unit, (ii) the low end of the active fracture fraction distribution for the Tptpll horizon, and (iii) an estimate of 0.26 to 0.29 arising from a Monte Carlo analysis considering faults, fracture zones, and shear zones (CNWRA Scientific Notebook #382). A uniform distribution is the minimum entropy distribution for an uncertain parameter with known bounds and without known central tendencies. The seeping fracture fraction is used as the key uncertain parameter, and it is assumed that this parameter is uniformly distributed. In the Tptpll horizon, the subarea wet fraction is approximately proportional to the logarithm of the seeping fracture fraction when the seeping fracture fraction is greater than 0.2. Accordingly, a uniform distribution for the seeping fracture fraction implies that the subarea wet fraction is loguniformly distributed. With this rationale, the SubareaWetFraction parameter in TPA version

5.1 is described as loguniformly distributed between 0.25 and 1. This parameter is assumed to be held fixed throughout the simulation.

Under the extreme case where the subarea wet fraction is 1, the waste package flow multiplication factor must also be 1 to achieve a flow balance. Given this extreme case, the perfect negative correlation between the subarea wet fraction and the waste package flow multiplication factor seen in Figure 3-3 requires that the waste package flow multiplication factor must be loguniformly distributed between 1 and 4. With this rationale, the TPA version 5.1 parameter WastePackageFlowMultiplicationFactor is described as loguniformly distributed between 0.25 and 1, and the two parameters are correlated using the most negative correlation allowed by the TPA code.

Temporal variability of the waste package flow multiplication factor can be introduced by specifying a time-varying flow multiplication factor, $F_{ow}$, in the auxiliary input file wpflow.def. For the TPA reference case, $F_{ow} = 1$. Hence, the maximum potential flow rate approaching waste packages is scaled by WastePackageFlowMultiplicationFactor × $F_{ow}$.

The *Matlab* code doing the analysis and creating the figures is archived in the code listing appendix for the seepage workshop report.

### 07/26/07 Reflux formulation.

SAS

Phillips (1996) developed a formulation estimating the penetration distance of water flowing in a fracture into superheated rock based on the ability of the rock to supply heat. The penetration length, $L$, is defined in TPA version 5.1 as

$$L = \left( \frac{q_w h_w \rho_w}{\kappa \nabla T} \right) \tag{3-1}$$

where $q_w$ is liquid water flux [L/T], $h_w$ is liquid water enthalpy [J/M], $\rho_w$ is liquid water density [M/L$^3$], $\kappa$ is effective thermal conductivity [J/LTK], and $T$ is temperature [K].

The Phillips (1996) equation was developed assuming that the energy flow field is 1D. The difficulty in applying the equation to the TPA code is that the heat flow is essentially radial around a drift. A possible reformulation that addresses this limitation recognizes that $\kappa \nabla T$ is simply the heat flux, $q_e$. Steady radial flow in cylindrical space, assuming constant $\kappa$, is given by the Thiem solution,

$$T - T_0 = \Delta T = \frac{q_e}{2\pi\kappa} \ln(r/R) \tag{3-2}$$

where $r$ is radial distance [L] and $R$ is the distance where $T = T_0$ [L]. This solution requires that temperature is fixed at $R$, which is approximately correct due to the large thermal inertia at the boiling front. It follows that

$$\frac{\partial T}{\partial r} = \frac{q_e}{2\pi\kappa r} \tag{3-3}$$

Replacing $\nabla T$ with $q_e/2\pi\kappa r$ in the Phillips (1996) equation yields

$$L = \left(\frac{2\pi r^* q_w h_w \rho_w}{q_e}\right) \tag{3-4}$$

where $r^*$ is an effective radius [L]. It makes sense that $r^*$ is tied to the dryout zone thickness, which is the vertical distance between the drift wall and the boiling isotherm, which leads to the equation

$$r^* = f_b(R_d + D) + (1 - f_b)R_d = f_b D + R_d \tag{3-5}$$

where $R_d$ is the radius of the drift [L], $D$ is the dryout thickness [L], and $f_b$ is the fraction of the distance between drift wall and boiling isotherm that the evaluation will take place. Note that $R_d$ is on the order of 2.75 m, whereas calculated values for $D$ range up to approximately 12 m. This suggests that the maximum range in $L$ due to different values of $D$ is approximately $(15/2.75)^{1/2} = 2.33$. The value of $f_b$ that balances uncertainty, in the sense that there is a symmetric difference between $L$ evaluated with $f_b = 0$, $f_b^*$, and 1, varies with $D$ and can be evaluated using

$$(r^*)^{1/2} = \tfrac{1}{2}\left[(R_d + D)^{1/2} + R_d^{1/2}\right] \tag{3-6}$$

For $D = 0.1$, 1, and 10 m, $f_b = 0.5$, 0.48, and 0.41, respectively.

The formula for $L$ does not provide guidance on $q_w$. Under ambient conditions, $q_w$ is approximately equal to net infiltration, but under thermally perturbed conditions additional water is mobilized due to boiling. The actual fracture flux may be much larger than net infiltration flux in this situation. The saturated hydraulic conductivity for the fracture system provides an upper bound estimate for the fracture flux. Liu et al. (2004) provide fracture permeability estimates for the tsw33 and tsw34 units of $5.5{\times}10^{-13}$ and $3.5{\times}10^{-14}$, respectively, which correspond to hydraulic conductivities of $1.7{\times}10^{5}$ and $1.1{\times}10^{4}$ mm/yr, respectively. These estimates provide a ballpark upper-bound value for reflux where the fracture system is locally saturated. However, typical numerical simulations suggest that the fracture system is generally not saturated, fracture saturations may peak at 5 percent, and shedding tends to reduce fracture saturations relatively quickly (Scott Painter, personal communication, July 26, 2007). The relative permeability of the fracture system drops precipitously with decreasing saturation. Figure 3-4 shows the van Genuchten relative permeability for van Genuchten $m$ values of 0.633 (Liu et al., 2003) and 0.608 (Liu et al., 2004), typical of fracture models. Both curves suggest that relative permeability is 0.01

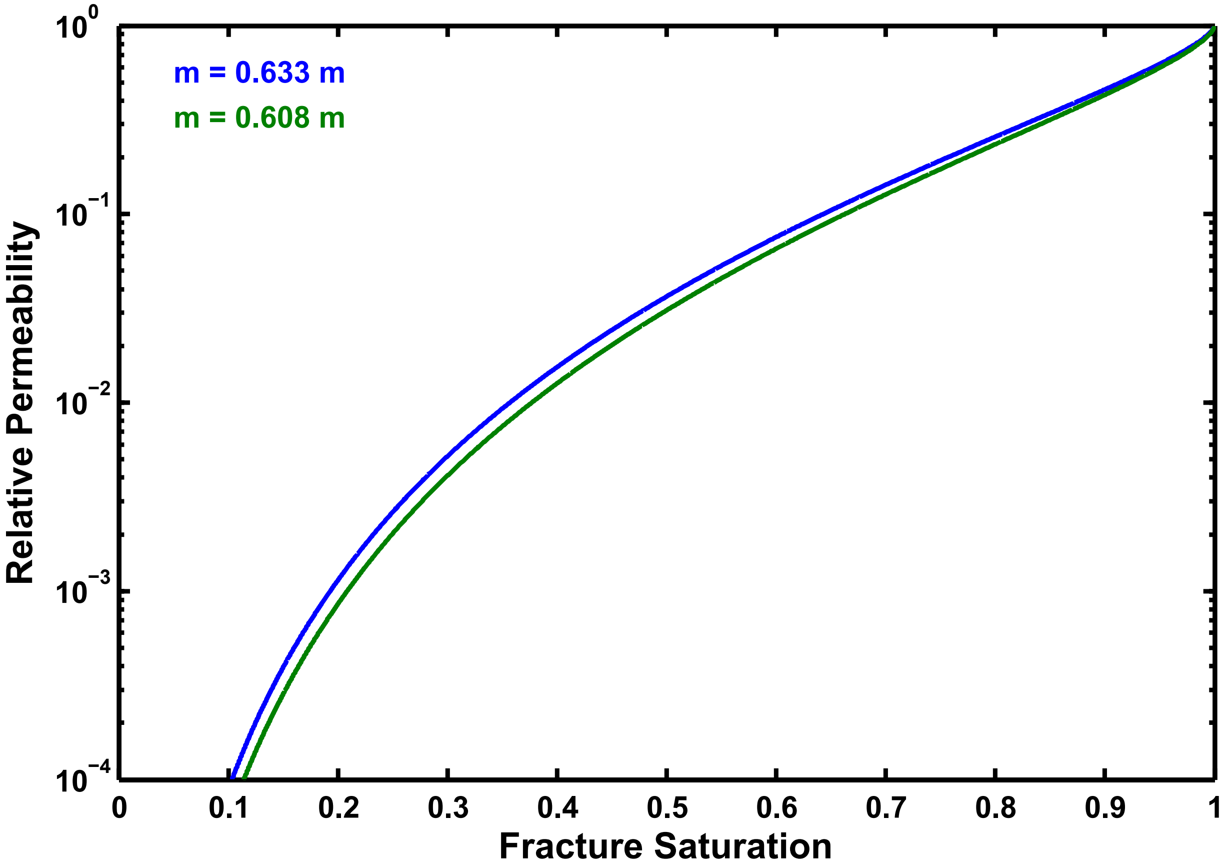

Figure 3-4: Wetting relative permeability as a function of saturation using the van Genuchten model.

at approximately 35 percent saturation. Assuming that approximately 20 percent of the fractures are active fractures implies that the saturations in the active fractures are about 5 times greater than the overall fracture continuum. With these bounding estimates, it is reasonable to consider an average upper bound fracture flux of approximately 1000 mm/yr, representing a reduction in tsw33 fracture permeability by approximately two orders of magnitude.

Figure 3-5 shows the cylindrical penetration length as a function of percolation flux, dryout zone thickness, and heat flux. The plotted $L$ is the average of the values calculated for the gradient at the drift wall and the gradient at the boiling isotherm. Figure 3-5(a) shows $L$ itself, and Figure 3-5(b) shows the fraction of the dryout zone that is penetrated. Figure 3-5(b) suggests that some dripping may be expected with shallow dryout zones, even with high heat fluxes, but a thick dryout zone precludes dripping even at relatively low heat fluxes.

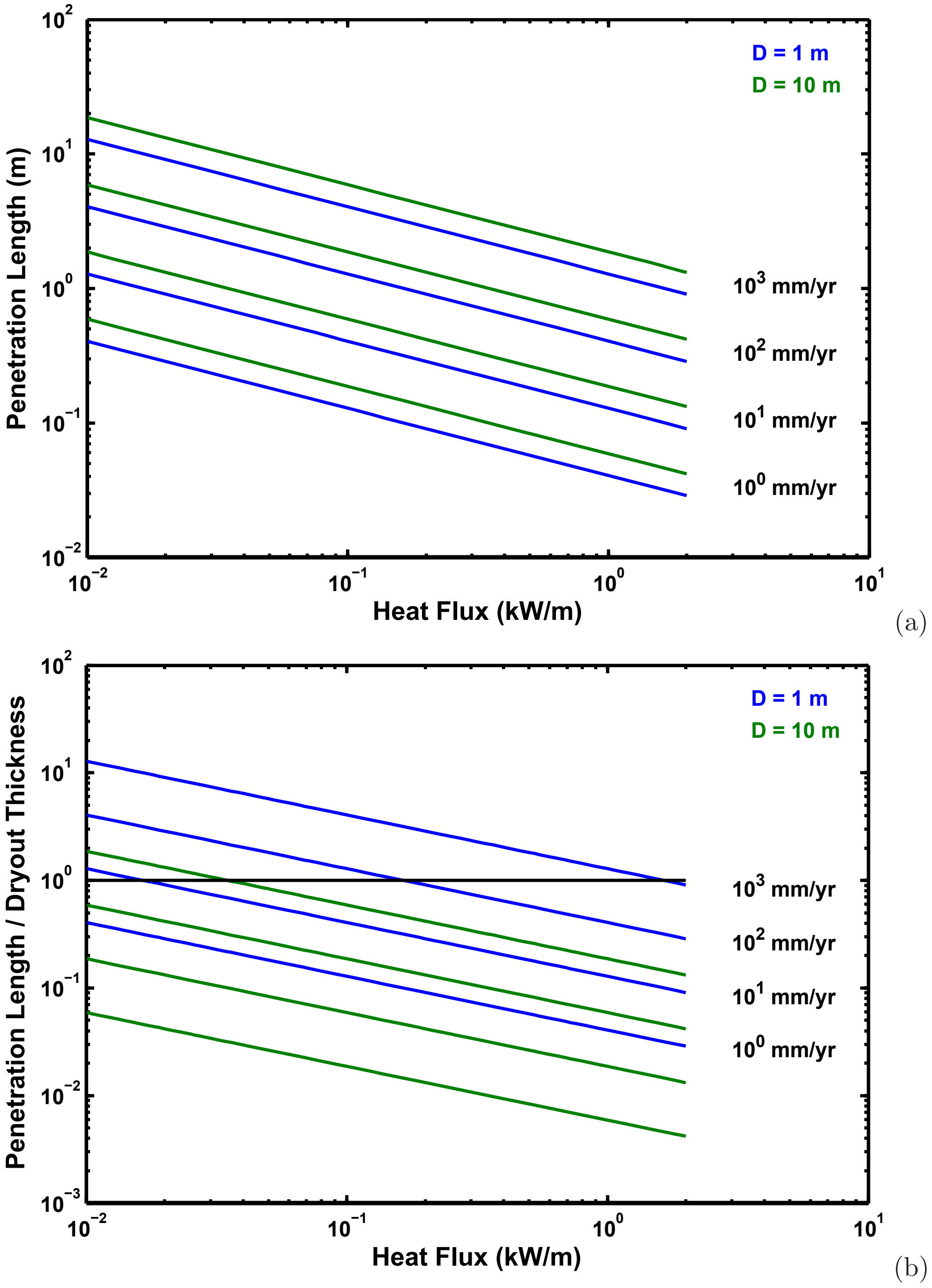

Figure 3-5: (a) Penetration length and (b) fraction of the dryout zone penetrated for various combinations of dryout zone thickness and flux in the penetrating finger.

## References

Albin, A. L., W. L. Singleton, T. C. Moyer, A. C. Lee, R. C. Lung, G. L. W. Eatman, and D. L. Barr. 1997. *Geology of the Main Drift–Station 28+00 to 55+00, Exploratory Studies Facility, Yucca Mountain Project, Yucca Mountain, Nevada*. Milestone Report SPG42AM3, Bureau of Reclamation and United States Geological Survey, Denver, CO. DOE Report DTN GS970208314224.005.

Barr, D. L., T. C. Moyer, W. L. Singleton, A. L. Albin, R. C. Lung, A. Lee, S. C. Beason, and G. Eatman. 1997. *Geology of the North Ramp–Station 4+00 to 28+00, Exploratory Studies Facility, Yucca Mountain Project, Yucca Mountain, Nevada*. DOE Report DTN GS960908314224.020, Bureau of Reclamation and United States Geological Survey, Denver, CO.

Beason, S. C., G. A. Turlington, R. C. Lung, G. L. W. Eatman, D. Ryter, and D. Barr. 1997. *Geology of the North Ramp–Station 0+60 to 4+00, Exploratory Studies Facility, Yucca Mountain Project, Yucca Mountain, Nevada*. , Bureau of Reclamation and United States Geological Survey, Denver, CO.

Eatman, G. L. W., W. L. Singleton, T. C. Moyer, D. L. Barr, A. L. Albin, R. C. Lung, and S. C. Beason. 1997. *Geology of the South Ramp–Station 55+00 to 78+77, Exploratory Studies Facility, Yucca Mountain Project, Yucca Mountain, Nevada*. , Bureau of Reclamation and United States Geological Survey, Denver, CO.

Liu, H.-H. and G. S. Bodvarsson. 2001. Constitutive relations for unsaturated flow in a fracture network. *Journal of Hydrology 252*, 116–125.

Liu, H. H., C. Doughty, and G. S. Bodvarsson. 1998. An active fracture model for unsaturated flow and transport in fractured rocks. *Water Resources Research 34*(10), 2633–2646.

Liu, H.-H., C. Haukwa, C. F. Ahlers, G. S. Bodvarsson, A. L. Flint, and W. B. Guertal. 2003. Modeling flow and transport in unsaturated fractured rock: an evaluation of the continuum approach. *62–63*, 173–188.

Liu, H. H., R. Salve, J. S. Wang, G. S. Bodvarsson, and D. Hudson. 2004. Field investigation into unsaturated flow and transport in a fault: model analyses. *74*, 39–59.

Mongano, G. S., W. L. Singleton, T. Moyer, S. C. Beason, G. L. W. Eatman, A. L. Albin, and R. C. Lung. 1999. *Geology of the ECRB Cross-Drift–Exploratory Studies Facility, Yucca Mountain Project, Yucca Mountain, Nevada*. Milestone Number SPG42GM3, United States Geological Survey, Denver, CO.

Phillips, O. M. 1996. Infiltration of a liquid finger down a fracture into superheated rock. *Water*

*Resources Research 32*(6), 1665–1670.

Seol, Y., H. H. Liu, and G. S. Bodvarsson. 2003. Effects of dry fractures on matrix diffusion in unsaturated fractured rocks. *Geophysical Research Letters.*

Smart, K., D. Y. Wyrick, P. S. Landis, and D. Waiting. 2006. *Summary and Analysis of Subsurface Fracture Data from the Topopah Spring Tuff Upper Lithophysal, Middle Nonlithophysal, Lower Lithophysal, and Lower Nonlithophysal Zones at Yucca Mountain, Nevada.* CNWRA 2005–04, Center for Nuclear Waste Regulatory Analyses, San Antonio, TX.

Zhou, Q., R. Salve, H.-H. Liu, J. S. Y. Wang, and D. Hudson. 2006. Analysis of a mesoscale infiltration and water seepage test in unsaturated fractured rock: Spatial variabilities and discrete fracture patterns. *87*, 96–122.

RL 7/7/2010

# Code listing appendix for thermal regression

## 05/17/05 regress_thermal_test.m.

SAS

The following *Matlab* program is used to regress properties for the analyses reported 5/12/05. Regression results are summarized in Table 1 and shown in Figure 1-1.

RL 7/7/2010

```
function regress_thermal_test(clist)
% regression of laboratory test of crushed tuff thermal observations
% to determine effective properties
%
% tests performed by Ron Green
%
% S. Stothoff   05/11/05        One-off analysis script developed

if (nargin < 1) clist   = 'g54';        end
if (~iscell(clist))     clist   = {clist};      end

ypr     = 0;                            % 1/0 to print figures
zdev    = 'abs';                        % absolute error reported
zdev    = 'rel';                        % relative error reported

% observed quantities from the thermal tests on rubble

%       T1(C)   T2(C)   Q(W/m2)
vT      = [
        95.5    12.6    262.5
        55.7    7       130.7
        37.6    5.1     80.4
        76.9    8.8     178.
        101.4   13.2    242.5
        131.3   16.5    335.9
        160.7   21.7    432.8
        67.8    23      115.7
        41.6    18      55.2
        92.9    20.1    196.2
        129.3   22      309.1
        173.4   24.2    469.5
];
Qo      = vT(:,3);
vT(:,3) = [];

% average temperature and relevant powers

Tbar    = mean(vT,2);
aTbar   = Tbar + 273.15;
aTbar3  = mean((273.15 + vT).^3, 2);
aTbarq  = mean((273.15 + vT).^0.25, 2);
```

```

% temperature gradient

gT      = -diff(vT,1,2) ./ 0.15;

% temperature^{5/4} gradient

vT54    = (273.15 + vT).^(5/4);
gT54    = -diff(vT54, 1, 2) ./ 0.15;

gT54c1  = (5/5)*2800;           % critical value for (grad T)^1.25
gT54c2  = (5/5)*2800;           % critical value for grad(T^1.25)

sig     = 5.67e-8;              % Stefan-Boltzmann constant [W/m2-K4]

b       = Qo;                   % total flux is right-hand side
b1      = ones(size(b));
va      = [];

% loop over list of options to evaluate

for it0 = 1:length(clist)

switch (clist{it0})

% calculate critical convection gradient for [grad(T)]^(5/4)

case 'T54+c'
        fprintf('evaluating [grad(T)]^(5/4)\n');
        Aall    = [gT (4*sig).*aTbar3.*gT gT.^1.25 ones(size(gT54)) ];

        ccoef   = {'Ke' 'De' 'ce' 'cegc'};
        ccase   = {
                '0'     [1]
                'r'     [1 2]
                'c'     [1 3 4]
                'a'     [1 2 3 4]
        };

% calculate critical convection gradient for grad[T^(5/4)]

```

```
case ’g54+c’
    fprintf(’evaluating grad[T^(5/4)]\n’);
    Aall    = [gT (4*sig).*aTbar3.*gT gT54 ones(size(gT54)) ];

    ccoef   = {’Ke’ ’De’ ’ce’ ’cegc’};
    ccase   = {
        ’0’     [1]
        ’r’     [1 2]
        ’c’     [1 3 4]
        ’a’     [1 2 3 4]
    };

% impose critical convection gradient for [grad(T)]^(5/4)

case ’g54’
    fprintf(’evaluating [grad(T)]^(5/4)\n’);
    Aall    = [gT (4*sig).*aTbar3.*gT (gT.^1.25 - gT54c1) ];
    Aall(Aall(:,3) < 0, 3)  = 0;

    ccoef   = {’Ke’ ’De’ ’ce’};
    ccase   = {
        ’0’     [1]
        ’r’     [1 2]
        ’c’     [1 3]
        ’a’     [1 2 3]
    };

% impose critical convection gradient for grad[T^(5/4)]

case ’T54’
    fprintf(’evaluating grad[T^(5/4)]\n’);
    Aall    = [gT (4*sig).*aTbar3.*gT (gT54 - gT54c2) ];
    Aall(Aall(:,3) < 0, 3)  = 0;

    ccoef   = {’Ke’ ’De’ ’ce’};
    ccase   = {
        ’0’     [1]
        ’r’     [1 2]
        ’c’     [1 3]
        ’a’     [1 2 3]
    };
```

```
end

Qp      = [];
i1      = 2:length(gT);

for it1 = 1:size(ccase,1)
        A       = Aall(i1,ccase{it1,2});

        A       = A ./ b(i1,ones([1 length(ccase{it1,2})]));
        a       = A \ b1(i1);
        Qp(:,it1)       = (A * a) .* b(i1);
%       a       = A \ b(i1);
%       Qp(:,it1)       = A * a;

        vpr(['acoef' ccase{it1,1}], a, ccoef(ccase{it1,2}));

        switch (zdev)
        case 'abs'
                Qdev(:,it1)     = (abs(Qp(:,it1) - Qo(i1)));
        case 'rel'
                Qdev(:,it1)     = (abs(Qp(:,it1) - Qo(i1)))./Qo(i1);
        end

        s       = [
                mean(Qdev(:,it1))
                max(Qdev(:,it1))
                sqrt(mean(Qdev(:,it1).^2))
                std(Qdev(:,it1))
        ];

        fprintf('\tmean err = %.3g\n', s(1));
        fprintf('\tmax err = %.3g\n', s(2));
        fprintf('\tLS err = %.3g\n', s(3));
        fprintf('\tsdev err = %.3g\n', s(4));

        eval(['acoef' ccase{it1,1} ' = a;']);

        v(it1,:)        = 0;
        v(it1,[1:4 4+ccase{it1,2}])     = [s' a'];
end
va      = [va; v];
```

```

% create labels

clab    = {
        'Q_d'           4
        'Q_o'           5
        'Q_d+Q_r'       1
        'Q_d+Q_c'       2
        'Q_d+Q_r+Q_c'   3
};

clabd   = {
        '1-1 line'      5
        'Q_d'           4
        'Q_d+Q_r'       1
        'Q_d+Q_c'       2
        'Q_d+Q_r+Q_c'   3
};

% plot grad(T) versus Q for predicted and observed

figure(1)
xlim    = [0 1000];
hp      = plot(gT(i1), Qp(:,[2 3 4]), 'o', ...
                xlim, xlim*acoef0, 'k', ...
                gT, Qo, 'k*');

set(hp, 'linew', 1.5);
label_it(hp, clab, 'tl');

pretty_plot('grad(T) [degrees C/m]', 'Thermal Flux [W/m^2]');
if (ypr)
        pr_or_pause(['therm_g-Q_' clist{it0}], ypr, 0, 1, 'epsc');
        pr_or_pause(['therm_g-Q_' clist{it0}], ypr, 0, 1, 'jpeg90');
end

figure(2)
hp      = plot(Qo(i1), 1 - Qp(:,[2 3 4])./Qo(i1,[1 1 1]), 'o', ...
                Qo(i1), 1 - Qp(:,1)./Qo(i1), 'k*', ...
                [0 500], [0 0], 'k');
set(hp, 'linew', 1.5);  axis square
```

```
label_it(hp, clabd, ’br’);

pretty_plot(’Measured Flux [W/m^2]’, ’(Q_m - Q_r)/Q_m’);
if (ypr)
        pr_or_pause([’therm_Qdev_’ clist{it0}], ypr, 0, 1, ’epsc’);
        pr_or_pause([’therm_Qdev_’ clist{it0}], ypr, 0, 1, ’jpeg90’);
end

figure(3)
hp      = plot(Qo(i1), Qp(:,[2 3 4]), ’o’, ...
                Qo(i1), Qp(:,1), ’k*’, ...
                [0 500], [0 500],’k’);
set(hp, ’linew’, 1.5);  axis square
label_it(hp, clabd, ’tl’);

pretty_plot(’Measured Flux [W/m^2]’, ’Regressed Flux [W/m^2]’);
if (ypr)
        pr_or_pause([’therm_Q-Q_’ clist{it0}], ypr, 0, 1, ’epsc’);
        pr_or_pause([’therm_Q-Q_’ clist{it0}], ypr, 0, 1, ’jpeg90’);
end

end

% output table in LaTeX format

fp      = fopen([’ThermRegr_’ zdev ’.out’], ’w’);
fprintf(fp, ’Case\t&Mean\t&Max\t&LS\t&SDev\t&Ke\t&De\t&Ce\\HLD\n’);

mlist   = 0;
nva     = size(va,1);
for it1 = 1:nva
        if (~mod(it1-1,size(v,1)))
                mlist   = mlist + 1;
                ci      = clist{mlist};
        end
        fprintf(fp, ’%s’,ci);
        fprintf(fp, ’\t&%.3g’,va(it1,:));
        if (it1 == nva) fprintf(fp, ’\t\\HLB\n’);
        else            fprintf(fp, ’\t\\HLS\n’);
        end
        ci      = ’’;
```

```
end
fclose(fp);


%>>>>>>>
function label_it(hp, clab, zpos)
% label the symbols

dy      = -0.06;
switch (zpos)
case 'tl'
        xl      = [0.05 0.08 0.1];
        yl      = 0.94;
case 'br'
        xl      = [0.05 0.08 0.1] + 0.6;
        yl      = -0.00 - dy*size(clab,1);
end
for it1 = 1:size(clab,1)
        zlab    = clab{it1,1};
        mhp     = clab{it1,2};

        zmark   = get(hp(mhp), 'marker');

        text(xl(3), yl, zlab, ...
                        'units', 'norm', ...
                        'fontw', 'bold', ...
                        'color', get(hp(mhp), 'color'), ...
                        'fonts', 12);

        xlim    = get(gca,'xlim');
        ylim    = get(gca,'ylim');
        xli     = xl .* xlim(2) + (1 - xl) .* xlim(1);
        yli     = yl .* ylim(2) + (1 - yl) .* ylim(1);

        switch (zmark)
        case 'none'
                hpi     = line(xli(1:2), yli([1 1]), ...
                                'linew', get(hp(mhp), 'linew'), ...
                                'color', get(hp(mhp), 'color'));
        otherwise
                hold on
                hpi     = plot(mean(xli(1:2)), yli, zmark);
                set(hpi, 'linew', get(hp(mhp), 'linew'), ...
                        'color', get(hp(mhp), 'color'));
                hold off
        end

        yl      = yl + dy;
end


%>>>>>>>
function vpr(zpr, v, cpr)
% print a vector

fprintf('%s:', zpr);
for it1 = 1:length(v)
        fprintf('\t%s = %.3g', cpr{it1}, v(it1));
end
fprintf('\n');

```

RL 7/7/2010

### 05/17/05 test_1D_rubble_Keff_conv.m.

SAS

The following *Matlab* program is used to create Figure 1-4 and Figure 1-6 for the conduction/convection model. The analysis using this program is reported 5/13/05.

RL 7/7/2010

```
function test_1D_rubble_Keff_conv
% test the implications of a 1D rubble

ypr      = 1;

D        = logspace(-4,0,50);

Ke       = 0.277;               % effective thermal conductivity [W/m-K4]
sig      = 5.67e-8;             % Stefan-Boltzmann constant [W/m2-K4]

%Ke      = 2;

% reference values

D0       = 0.01;
D        = 0.001;
Kmul     = (D/D0)^2;

kintr    = 1e-7;                % intrinsic permeability [m2]
densa    = 1.25;                % air density [kg/m3]
grav     = 9.8;                 % gravitational acceleration [m/s2]
beta     = 0.026;               % volumetric expansion coef [--]
Cv       = 720;                 % heat capacity at const volume [J/kg-K]
visca    = 1.7e-5;              % air viscosity [kg/m-s]

kintr    = kintr * Kmul;

dT       = 50;
Keff     = 0.3;
L        = 0.15;
Racomp   = (kintr * densa^2 * grav * beta * Cv) / (visca * Keff);
Ra       = Racomp * dT * L;
Rafq     = Racomp^(1/4);

Ce       = 0.0325;              % fitting from regression
cconv    = Ce / (Rafq * L^(0.5));

%Llist   = [0.1 0.2 0.5 1 2 5 10 20];
Llist    = logspace(-1,2,100);
dTlist   = dT .* (40 ./ Llist);
Ra_v     = Racomp .* dTlist(1) .* Llist(1);
```

```
Kec     = (cconv * Rafq) .* Llist.^(0.5) .* (dTlist ./ Llist).^(5/4);

Q       = [0.05 0.5 5 50 500];
Q       = [0.05 5 500];

dTfran  = [0 500e6];
%dTfran = 100;

%q      = -(Ke + Ce Ra^0.25) DT/L
%       = -(Ke + Ce Rac^0.25 (DT L)^0.25) DT/L

Racrit  = 4 * pi^2;
for it1 = 1:length(Q)
        qi      = Q(it1);
        for it2 = 1:length(Llist)
                Li      = Llist(it2);
                C1      = Ke;
                C2      = Ce * (Racomp * Li^2)^(1/4);
                C3      = qi;

                dTcrit  = Racrit / (Racomp * Li);
                Gcrit   = dTcrit / Li;
                C4      = Gcrit^(5/4);

                f       = @(x) C1 .* x + C2 .* max(0,x.^(5/4)-C4) - C3;

                dTf(it1,it2)    = fzero(f, dTfran) * Li;
                Kef(it1,it2)    = qi * Li / dTf(it1,it2);
        end
end

%loglog(Llist, Ralist);

clab    = {};
for it1 = 1:length(Q)
        clab{it1,1}     = [num2str(Q(it1)) ’ W/m^2’];
        clab{it1,2}     = it1;
end

% plot grad(T) versus Q for predicted and observed

```

```
figure(1)
hp      = loglog(Llist, dTf);

set(hp, 'linew', 1.5);
%set(gca, 'ylim', [1e-2 1e4]);
label_it(hp, clab, 'br');

pretty_plot('Rubble Thickness [m]', ...
        'Temperature Difference [K]');
if (ypr)
        pr_or_pause(['tconvT_Dq_D' num2str(D)], ypr, 0, 1, 'epsc');
        pr_or_pause(['tconvT_Dq_D' num2str(D)], ypr, 0, 1, 'jpeg90');
end

% plot grad(T) versus Q for predicted and observed

figure(2)
hp      = loglog(Llist, Kef);

set(hp, 'linew', 1.5);
set(gca,'ylim',[1e-1 1e2]);

label_it(hp, clab, 'tl');

pretty_plot('Rubble Thickness [m]', ...
        'Conduction/Convection K_e_f_f [W/m-K]');
if (ypr)
        pr_or_pause(['tconvK_Dq_D' num2str(D)], ypr, 0, 1, 'epsc');
        pr_or_pause(['tconvK_Dq_D' num2str(D)], ypr, 0, 1, 'jpeg90');
end


%>>>>>>>
function label_it(hp, clab, zpos)
% label the symbols

dy      = -0.06;
switch (zpos)
case 'tl'
        xl      = [0.05 0.08 0.1];
        yl      = 0.94;
```

```
case 'br'
        xl      = [0.05 0.08 0.1] + 0.6;
        yl      = -0.00 - dy*size(clab,1);
end
for it1 = 1:size(clab,1)
        zlab    = clab{it1,1};
        mhp     = clab{it1,2};

        zmark   = get(hp(mhp), 'marker');

        text(xl(3), yl, zlab, ...
                        'units', 'norm', ...
                        'fontw', 'bold', ...
                        'color', get(hp(mhp), 'color'), ...
                        'fonts', 12);

        xlim    = log10(get(gca,'xlim'));
        ylim    = log10(get(gca,'ylim'));
        xli     = 10.^(xl .* xlim(2) + (1 - xl) .* xlim(1));
        yli     = 10.^(yl .* ylim(2) + (1 - yl) .* ylim(1));

        switch (zmark)
        case 'none'
                hpi     = line(xli(1:2), yli([1 1]), ...
                                'linew', get(hp(mhp), 'linew'), ...
                                'color', get(hp(mhp), 'color'));
        otherwise
                hold on
                hpi     = plot(mean(xli(1:2)), yli, zmark);
                set(hpi, 'linew', get(hp(mhp), 'linew'), ...
                        'color', get(hp(mhp), 'color'));
                hold off
        end

        yl      = yl + dy;
end
```

## 05/17/05 test_1D_rubble_Keff_prof.m.

SAS

The following *Matlab* program is used to create Figure 1-3 and Figure 1-5 for the conduction/radiation model. The analysis using this program is reported 5/13/05.

RL 7/7/2010

```
function test_1D_rubble_Keff_prof
% test the implications of a 1D rubble

ypr     = 1;

D       = logspace(-4,0,50);

D       = 0.001;

Ke      = 0.277;                % effective thermal conductivity [W/m-K4]
sig     = 5.67e-8;              % Stefan-Boltzmann constant [W/m2-K4]

SKeff_prof.sig  = sig;

Tc      = [25 : 75 : 325];

Tabs    = 273.15 + Tc;

Llist   = logspace(-1,2,100);
Q       = [0.05 5 500];
for it1 = 1:length(Q)
        qi      = Q(it1);
        SKeff_prof.qi   = qi;
        for it2 = 1:length(Llist)
                Li      = Llist(it2);
%               SKeff_prof.Ke   = Ke;

                f       = @(x,T) qi / (Ke + 4*sig*T^3*D);

                sol     = ode45(f, [0 Li], 273.15+40);
                dTf(it1,it2)    = diff(sol.y([1 end]));
                Kef(it1,it2)    = qi * Li / dTf(it1,it2);
        end
end

clab    = {};
for it1 = 1:length(Q)
        clab{it1,1}     = [num2str(Q(it1)) ' W/m^2'];
        clab{it1,2}     = it1;
end

```

```
% plot grad(T) versus Q for predicted and observed

figure(1)
hp      = loglog(Llist, dTf);

set(hp, 'linew', 1.5);
%set(gca, 'ylim', [1e-2 1e4]);
label_it(hp, clab, 'br');

pretty_plot('Rubble Thickness [m]', ...
        'Temperature Difference [K]');
if (ypr)
        pr_or_pause(['tradT_Lq_D' num2str(D)], ypr, 0, 1, 'epsc');
        pr_or_pause(['tradT_Lq_D' num2str(D)], ypr, 0, 1, 'jpeg90');
end

% plot grad(T) versus Q for predicted and observed

figure(2)
hp      = loglog(Llist, Kef);

set(hp, 'linew', 1.5);
set(gca, 'ylim', [1e-1 1e2]);
label_it(hp, clab, 'tl');

pretty_plot('Rubble Thickness [m]', ...
        'Conduction/Radiation K_e_f_f [W/m-K]');
if (ypr)
        pr_or_pause(['tradK_Lq_D' num2str(D)], ypr, 0, 1, 'epsc');
        pr_or_pause(['tradK_Lq_D' num2str(D)], ypr, 0, 1, 'jpeg90');
end


%>>>>>>>
function label_it(hp, clab, zpos)
% label the symbols

dy      = -0.06;
switch (zpos)
case 'tl'
        xl      = [0.05 0.08 0.1];
        yl      = 0.94;
case 'br'
        xl      = [0.05 0.08 0.1] + 0.6;
        yl      = -0.00 - dy*size(clab,1);
end
for it1 = 1:size(clab,1)
        zlab    = clab{it1,1};
        mhp     = clab{it1,2};

        zmark   = get(hp(mhp), 'marker');

        text(xl(3), yl, zlab, ...
                        'units', 'norm', ...
                        'fontw', 'bold', ...
                        'color', get(hp(mhp), 'color'), ...
                        'fonts', 12);

        xlim    = log10(get(gca,'xlim'));
        ylim    = log10(get(gca,'ylim'));
        xli     = 10.^(xl .* xlim(2) + (1 - xl) .* xlim(1));
        yli     = 10.^(yl .* ylim(2) + (1 - yl) .* ylim(1));

        switch (zmark)
        case 'none'
                hpi     = line(xli(1:2), yli([1 1]), ...
                                'linew', get(hp(mhp), 'linew'), ...
                                'color', get(hp(mhp), 'color'));
        otherwise
                hold on
                hpi     = plot(mean(xli(1:2)), yli, zmark);
                set(hpi, 'linew', get(hp(mhp), 'linew'), ...
                        'color', get(hp(mhp), 'color'));
                hold off
        end

        yl      = yl + dy;
end
```

# Code listing appendix for review of Mohanty paper

## 12/28/05 test_K_Ra.m.

SAS

The following *Matlab* program is used to create Figure 1-7 as a QA check on Figure 3 by Mohanty et al. in a paper to be submitted to a conference. The analysis using this program is reported in the entry dated 12/28/05.

RL 7/7/2010

```
function test_K_Ra
% recreate figure 3 in Mohanty et al. (2005) from the specified information
%
% S. Stothoff   12/28/05

path(fullfile(fileparts(fileparts(pwd)), 'Util'), path);

% parameters

beta    = 0.00228;
visc    = 3.1e-5;
grav    = 9.81;
tort    = 2.125;
ri      = 1.39;
tdiff   = 3.32e-4;

Dp      = 0.13;
Cdp     = 0.18 / Dp;
skew    = 1.5;

poros   = [0.1 : 0.1 : 0.6];
dT      = 10 : 5 : 40;
dr      = [0.26 0.68 1.36];
ro      = ri + dr;

% calculate permeabilities

K       = fperm(Dp, poros, tort, Cdp, skew);

% calculate Rayleigh numbers

for it1 = 1:length(dT)
        Ra(it1,:)       = fRayleigh(grav, beta, K, ri, dT(it1), visc, tdiff);
end

% calculate Nusselt numbers

Rat     = logspace(3, 6, 1000);
for it1 = 1:length(ro)
        Nu(it1,:)       = fNusselt(ri, ro(it1), Rat);

```

```
% get value close to Nu = 10

        i1      = find(Nu(it1,:) <= 10);
        Rat10(it1)      = Rat(i1(end));
end

figure(1)
clf

% get colors for each dT

cord    = get_pap(’cord’);

% plot K/Ra points for the selected porosities

loglog(K, Ra, ’.’)
hold on

xlim    = get(gca, ’xlim’);

% plot and label Ra points corresponding to the selected thicknesses

for it1 = 1:length(Rat10)
        hp      = plot(xlim, Rat10([it1 it1]), ’k’);
        set(hp, ’linew’, 2);
        hp      = text(xlim(1)*1.1, Rat10(it1)*0.6, ...
                        sprintf(’Thickness = %g’, dr(it1)));
        set(hp, ’fontw’, ’bo’, ’fonts’, 10);
end

% add labels for porosity

for it1 = 1:length(poros)

        xi      = K(it1) * 0.6;
        yi      = min(Ra(:,it1)) * 0.6;

        hp      = text(xi, yi, sprintf(’Porosity = %g’, poros(it1)));
        set(hp, ’fontw’, ’bo’, ’fonts’, 10);
end

```

```
% add labels for temperature difference

xi      = 0.8;
yi      = 0.45;
dy      = -0.06;
for it1 = 1:length(dT)

        text(xi, yi, sprintf('\\Delta T = %g C', dT(it1)), ...
                        'fontw', 'bo', 'fonts', 10, 'units', 'norm', ...
                        'color', cord(it1,:));
        yi      = yi + dy;
end

% make the plot pretty

pretty_plot('Permeability (m^2)', 'Rayleigh Number');

%loglog(Rat, Nu)

% print it out

pr_or_pause('Rayleigh_K_Fig3', 1, 0, 1, 'epsc');

return


%>>>>>>>
function K      = fperm(Dp, poros, tort, Cdp, skew)
% permeability (Eq 2)

K       = Dp.^2 .* poros.^3 ./ (72 .* tort .* (1 - poros).^2) ...
                .* ((skew .* Cdp.^3 + 3 .* Cdp.^2 + 1) ...
                        ./ (1 + Cdp.^2)).^2;


%>>>>>>>
function Ra     = fRayleigh(grav, beta, K, ri, dT, visc, tdiff)
% Rayleigh number (Eq 1)

Ra      = (grav * beta * ri / (visc * tdiff)) .* K .* dT;
```

```

%>>>>>>>
function Nu     = fNusselt(ri, ro, Ra)
% Nusselt number (Eq 3)

Nu      = 0.44 .* sqrt(Ra) .* log(ro / ri) ./ (1 + 0.916 * (ri / ro)^(0.5));
```

RL 7/7/2010

### 12/28/05 test_rubble_stat.m.

SAS

The following *Matlab* program is used to create Figure 1-8 as a QA check on assertions in section 3.2.1 by Mohanty et al. in a paper to be submitted to a conference. The analysis using this program is reported in the entry dated 12/28/05.

RL 7/7/2010

```
function test_rubble_stat
% find Schuhmann parameters from rubble statistics
% Schuhmann cdf: P = (x/F)^a
% Schuhmann pdf: p = (a/F) (x/F)^(a - 1)

xmean   = [1080 240 100 1890 1790 2750]’;
xmed    = [30 12 60 730 700 1590]’;
zlab    = {
        ’Set 1: trace < 1 m’    ’o’
        ’Set 2: trace < 1 m’    ’o’
        ’Set 3: trace < 1 m’    ’o’
        ’Set 1: trace > 1 m’    ’d’
        ’Set 2: trace > 1 m’    ’d’
        ’Set 3: trace > 1 m’    ’d’
};

xnd     = xmean ./ xmed;

a       = logspace(-1, 0, 10000);

% create function of alpha

fa      = func_of_alpha(a);

% tabulate parameters

fprintf(’xmean\txmed\ta\tF\n’);

ai      = interp1(fa, a, xnd);
fi      = xmed .* 2.^(1./ai);
fai     = func_of_alpha(ai);

fprintf(’%g\t%g\t%.3g\t%.1f\n’, [xmean xmed ai fi]’);

figure(1)
clf

% get colors for each dT

cord    = get_pap(’cord’);

```

```
% plot function of alpha

hp      = loglog(a, fa, 'k');
set(hp, 'linew', 2);
hold on;

% plot calculated points

xi      = 0.7;
yi      = 0.94;
dy      = -0.06;
for it1 = 1:length(ai)

% point

        hp      = plot(ai(it1), fai(it1), 'o');
        set(hp, 'linew', 1.5, 'color', cord(it1,:));

% text

        hp      = text(xi, yi, zlab{it1,1}, 'units', 'norm');
        set(hp, 'fontw', 'bo', 'fonts', 10, 'color', cord(it1,:));
        yi      = yi + dy;
end

pretty_plot('Schuhmann \alpha', 'Mean / Median');
pr_or_pause('Schuhmann_fit', 1, 0, 1, 'epsc');


return;


%>>>>>>>>
function fa     = func_of_alpha(a)
% fitting function for alpha

fa      = 2.^(1./a) .* (a ./ (a + 1));
```

### 12/30/05 gen_rubble_stat.m.

SAS

The following *Matlab* program is used to create statistics on fracture separations and implied statistics on blocks bounded by triplets of fracture sets. The analysis using this program is reported in the entry dated 12/30/05.

RL 7/7/2010

```
function gen_rubble_stat
% find Schuhmann parameters from rubble statistics
%
% Schuhmann cdf: P = (x/F)^a
% Schuhmann pdf: p = (a/F) (x/F)^(a - 1)
%
% and display some implied statistics regarding the fracture spacings
% and blocks generated from fracture triplets
%
% S. Stothoff   12/30/05

ypr     = 1;

xmean   = [1080 240 100 1890 1790 2750]’;
xmed    = [30 12 60 730 700 1590]’;
zlab    = {
        ’Set 1: trace < 1 m’    ’o’
        ’Set 2: trace < 1 m’    ’o’
        ’Set 3: trace < 1 m’    ’o’
        ’Set 1: trace > 1 m’    ’d’
        ’Set 2: trace > 1 m’    ’d’
        ’Set 3: trace > 1 m’    ’d’
};

% get the model parameters fitting the data

[a,fa,ai,Fi,fai]        = fit_data_stats(xmean, xmed);

% print out parameters

if (0)
        fprintf(’xmean\txmed\ta\tF\n’);
        fprintf(’%g\t%g\t%.3g\t%.1f\n’, [xmean xmed ai Fi]’);
end

% plot fit

if (0)
        plot_data_fit(a, fa, ai, Fi, fai, zlab, ypr);
end

```

```
% calculate pdf and cdf of each distribution

if (0)
        show_stat_distr(ai, Fi, zlab, ypr);
end

% independently sample from the short-scale distributions

iset1   = [1 2 3];
iset2   = [4 5 6];

iset    = iset1;
nset    = length(iset);
N0      = 1e6;
R       = rand([nset N0]);

xsamp   = zeros([nset N0]);
for it1 = 1:length(iset)
        mset    = iset(it1);
        xsamp(it1,:)    = icdf_func(R(it1,:), ai(mset), Fi(mset));
end

% accumulate statistics from samples

xmax    = max(xsamp,[],1);
xmin    = min(xsamp,[],1);
xrat    = xmax ./ xmin;

% maximum thickness as CDF

if (0)
        lxrcut  = [2 5 10 20];
        for it1 = 1:length(lxrcut)
                xrcut   = lxrcut(it1);
                ztext   = sprintf('Maximum ratio = %g', xrcut);
                yuse    = xrat <= xrcut;
                zname   = sprintf('setDim_cdf_R%g', xrcut);

                show_maxdim_cdf(yuse, xmax, xsamp, iset, zlab, ...
                                        ztext, zname, ypr);
        end
```

```
end

% maximum thickness as CCDF

if (0)
        lxrcut  = [2 5 10 20];
        for it1 = 1:length(lxrcut)
                xrcut   = lxrcut(it1);
                ztext   = sprintf('Maximum ratio = %g', xrcut);
                yuse    = xrat <= xrcut;
                zname   = sprintf('setDim_ccdf_R%g', xrcut);

                show_maxdim_ccdf(yuse, xmax, xsamp, iset, zlab, ...
                                        ztext, zname, ypr);
        end
end

% effective thickness as CCDF

if (1)
        lxrcut  = [2 5 10 20];
        for it1 = 1:length(lxrcut)
                xrcut   = lxrcut(it1);
                ztext   = sprintf('Maximum ratio = %g', xrcut);
                yuse    = xrat <= xrcut;
                zname   = sprintf('setEffx_ccdf_R%g', xrcut);

                show_effdim_ccdf(yuse, xsamp, iset, zlab, ...
                                        ztext, zname, ypr);
        end
end

% set of effective thickness as CCDF

if (0)
        lxrcut  = [2 5 10 20];
        zname   = 'setEffx_ccdf_set';

        show_effdimset_ccdf(xsamp, iset, lxrcut, zlab, zname, ypr);
end

```

```
% maximum ratio of lengths

if (0)
        lxrcut  = [2 5 10 20];
        for it1 = 1:length(lxrcut)
                xrcut   = lxrcut(it1);
                i1      = find(xrat <= xrcut);
                N       = length(i1);

                c{it1,1}        = sort(xrat(i1));
                c{it1,2}        = [1 : N] ./ N;
                c{it1,3}        = sprintf('Maximum ratio = %g', xrcut);
                zname   = 'dxRat_cdf';

        end
        show_maxrat_cdf(c, zname, ypr);
end
return;


%>>>>>>>>
function fa     = func_of_alpha(a)
% fitting function for alpha

fa      = 2.^(1./a) .* (a ./ (a + 1));


%>>>>>>>>
function p      = pdf_func(x, a, F)
% probability distribution for x
% Schuhmann pdf: p = (a/F) (x/F)^(a - 1)

p       = (a ./ F) .* (x ./ F).^(a - 1);


%>>>>>>>>
function P      = cdf_func(x, a, F)
% cumulative probability distribution for x
% Schuhmann cdf: P = (x/F)^a

P       = (x ./ F).^a;
```

```


%>>>>>>>>
function x      = icdf_func(P, a, F)
% cumulative probability distribution for x
% Schuhmann cdf: P = (x/F)^a

x       = P.^(1/a) .* F;


%>>>>>>>>
function [a,fa,ai,Fi,fai]       = fit_data_stats(xmean, xmed)
% fit data to the model

a       = logspace(-1, 0, 10000);

% create function of alpha

fa      = func_of_alpha(a);

% tabulate parameters

ai      = interp1(fa, a, xmean ./ xmed);
Fi      = xmed .* 2.^(1./ai);
fai     = func_of_alpha(ai);


%>>>>>>>>
function plot_data_fit(a, fa, ai, Fi, fai, zlab, ypr)
% generate a figure summarizing data fit to alpha curve

figure(1)
clf

% get colors for each dT

cord    = get_pap('cord');

% plot function of alpha

hp      = loglog(a, fa, 'k');
```

```
set(hp, 'linew', 2);
hold on;

% plot calculated points

xi      = 0.7;
yi      = 0.94;
dy      = -0.06;
for it1 = 1:length(ai)

% point

        hp      = plot(ai(it1), fai(it1), 'o');
        set(hp, 'linew', 1.5, 'color', cord(it1,:));

% text

        hp      = text(xi, yi, zlab{it1,1}, 'units', 'norm');
        set(hp, 'fontw', 'bo', 'fonts', 10, 'color', cord(it1,:));
        yi      = yi + dy;
end

pretty_plot('Schuhmann \alpha', 'Mean / Median');

if (ypr)        pr_or_pause('Schuhmann_fit', 1, 0, 1, 'epsc');  end


%>>>>>>>
function show_stat_distr(ai, Fi, zlab, ypr)
% show statistical distributions implied by data

%x      = linspace(0, 1, 1e5);
x       = logspace(-6, 0, 1e5);
for it1 = 1:length(ai)
        xd(it1,:)       = x .* Fi(it1);
        p(it1,:)        = pdf_func(xd(it1,:), ai(it1), Fi(it1));
        P(it1,:)        = cdf_func(xd(it1,:), ai(it1), Fi(it1));
end

figure(1)
clf
```

```

% get colors for each dT

cord    = get_pap('cord');

% plot cumulative probability distribution

hp      = loglog(xd', P');
set(hp, 'linew', 1.5);

% label curves

xi      = 0.7;  yi      = 0.06; dy      = 0.06;
for it1 = length(ai):-1:1
        hp      = text(xi, yi, zlab{it1,1}, 'units', 'norm');
        set(hp, 'fontw', 'bo', 'fonts', 10, 'color', cord(it1,:));
        yi      = yi + dy;
end

set(gca,'xlim',[1e-2 1e4],'ylim',[1e-2 1]);
pretty_plot('Spacing [mm]', 'Probability of Exceedance');

if (ypr)        pr_or_pause('fracSet_cdf', 1, 0, 1, 'epsc');    end

% plot probability distribution

hp      = loglog(xd', p');
set(hp, 'linew', 1.5);

% label curves

xi      = 0.7;  yi      = 0.94; dy      = -0.06;
for it1 = 1:length(ai)
        hp      = text(xi, yi, zlab{it1,1}, 'units', 'norm');
        set(hp, 'fontw', 'bo', 'fonts', 10, 'color', cord(it1,:));
        yi      = yi + dy;
end

set(gca,'xlim',[1e-0 1e5]);
pretty_plot('Spacing [mm]', 'Probability of Occurrance');

```

```
if (ypr)        pr_or_pause(’fracSet_pdf’, 1, 0, 1, ’epsc’);    end
return


%>>>>>>>
function show_maxdim_cdf(yuse, xmax, xsamp, iset, zlab, ztext, zname, ypr)
% show the maximum dimension cdf for a given set

figure(1)
clf

% get colors for each set

cord    = get_pap(’cord’);

% make restricted set

i1      = find(yuse);

sxs     = sort(xsamp(:,i1),2);

% descriptive properties

N       = length(i1);
N0      = length(xmax);
frac    = N / N0;
nset    = length(iset);

lN      = [1 : N] .* (1/N);

hp      = semilogx(sort(xmax(i1)), lN, ’k’, sxs’, lN);
set(hp, ’linew’, 1.5);
%set(gca,’xlim’,[1e-4 1e4], ’ylim’, [1e-3 1]);
%set(gca,’xlim’,[1e-2 1e4], ’ylim’, [1e-3 1]);
set(gca,’xlim’,[1e-0 1e4]);

% label curves

xi      = 0.05; yi      = 0.94; dy      = -0.06;
for it1 = 1:nset
        hp      = text(xi, yi, zlab{iset(it1),1}, ’units’, ’norm’);
        set(hp, ’fontw’, ’bo’, ’fonts’, 10, ’color’, cord(it1,:));
        yi      = yi + dy;
end
hp      = text(xi, yi, ’Triplet maximum’, ’units’, ’norm’);
set(hp, ’fontw’, ’bo’, ’fonts’, 10, ’color’, ’k’);

% label set

ctext   = {
        ztext
        sprintf(’Subset fraction = %.3g’, N / N0);
};
xi      = 0.55; yi      = 0.06; dy      = 0.06;
for it1 = 1:length(ctext)
        hp      = text(xi, yi, ctext{it1}, ’units’, ’norm’);
        set(hp, ’fontw’, ’bo’, ’fonts’, 12);
        yi      = yi + dy;
end

pretty_plot(’Maximum Dimension [mm]’, ’Cumulative Frequency’);
if (ypr)        pr_or_pause(zname, 1, 0, 1, ’epsc’);    end


%>>>>>>>
function show_effdim_ccdf(yuse, xsamp, iset, zlab, ztext, zname, ypr)
% show the effective dimension ccdf for a given set

figure(1)
clf

% get colors for each set

cord    = get_pap(’cord’);

% make restricted set

i1      = find(yuse);

sxs     = sort(xsamp(:,i1),2);

% descriptive properties
```

```

N       = length(i1);
N0      = size(xsamp,2);
frac    = N / N0;
nset    = length(iset);

effx    = prod(xsamp(:,i1),1).^(1/nset);

lN      = 1 - [1 : N] .* (1/N);
seffx   = sort(effx);

Cfit    = 1e-2;
xfit    = interp1(lN, seffx, Cfit);
L       = -xfit / log(Cfit);

%hp     = loglog(seffx, lN, 'k', sxs', lN);
hp      = semilogy(seffx, lN, 'k', sxs', lN, seffx, exp(-seffx./L));
set(hp, 'linew', 1.5);
set(hp(end), 'color', [0.5 0.5 0.5], 'linew', 2.5);
%set(gca,'xlim',[1e-4 1e4], 'ylim', [1e-3 1]);
set(gca,'xlim',[1e-0 1e4], 'ylim', [1e-4 1]);
%set(gca,'xlim',[1e-0 1e4]);

% label curves

xi      = 0.70; yi      = 0.74; dy      = -0.06;
for it1 = 1:nset
        hp      = text(xi, yi, zlab{iset(it1),1}, 'units', 'norm');
        set(hp, 'fontw', 'bo', 'fonts', 10, 'color', cord(it1,:));
        yi      = yi + dy;
end
hp      = text(xi, yi, 'Triplet median', 'units', 'norm');
set(hp, 'fontw', 'bo', 'fonts', 10, 'color', 'k');
yi      = yi + dy;
hp      = text(xi, yi, 'Exponential', 'units', 'norm');
set(hp, 'fontw', 'bo', 'fonts', 10, 'color', [0.5 0.5 0.5]);

% label set

ctext   = {
        ztext
        sprintf('Subset fraction = %.3g', N / N0);
};
xi      = 0.55; yi      = 0.94; dy      = -0.06;
for it1 = 1:length(ctext)
        hp      = text(xi, yi, ctext{it1}, 'units', 'norm');
        set(hp, 'fontw', 'bo', 'fonts', 12);
        yi      = yi + dy;
end

pretty_plot('Maximum Dimension [mm]', 'Cumulative Probability (x_i > x)');
if (ypr)        pr_or_pause(zname, 1, 0, 1, 'epsc');    end


%>>>>>>>
function show_effdimset_ccdf(xsamp, iset, lxrcut, zlab, zname, ypr)
% show the effective dimension ccdf for all xcut sets

% statistics

xmax    = max(xsamp,[],1);
xmin    = min(xsamp,[],1);
xrat    = xmax ./ xmin;

figure(1)
clf

% get colors for each set

cord    = get_pap('cord');

% make restricted set

c       = cell([length(lxrcut) 4]);
xi      = 0.05; yi      = 0.06; dy      = 0.06;
for it1 = length(lxrcut):-1:1
        xrcut   = lxrcut(it1);
        ztext   = sprintf('Maximum ratio = %g', xrcut);
        yuse    = xrat <= xrcut;

        i1      = find(yuse);

        sxs     = sort(xsamp(:,i1),2);

% descriptive properties

        N       = length(i1);
        nset    = length(iset);

        effx    = prod(xsamp(:,i1),1).^(1/nset);

        lN      = 1 - [1 : N] .* (1/N);
        seffx   = sort(effx);

        Cfit    = 1e-1;
        xfit    = interp1(lN, seffx, Cfit);
        L       = -xfit / log(Cfit);

        xt      = 2;
        Cr      = exp(-xt/L);
        Crt     = interp1(seffx, lN, xt);
        C0      = Crt / Cr;

        feffx   = C0 .* exp(-seffx./L);

% plot

        hp      = loglog(seffx, [lN; feffx]);
        set(hp, 'linew', 1.5, 'color', cord(it1,:));
        set(hp(end), 'linest', ':');

% label

        hp      = text(xi, yi, ztext, 'units', 'norm');
        set(hp, 'fontw', 'bo', 'fonts', 10, 'color', cord(it1,:));
        yi      = yi + dy;

        hold on
end
set(gca,'xlim',[1e-0 1e4], 'ylim', [1e-2 1]);

pretty_plot('Effective Dimension [mm]', 'Cumulative Probability (x_i > x)');
if (ypr)
```

```
        pr_or_pause([zname '_log'], 1, 0, 1, 'epsc');

        set(gca,'ysc','li','ylim',[0 1]);
        pr_or_pause([zname '_lin'], 1, 0, 1, 'epsc');
end


%>>>>>>>
function show_maxrat_cdf(c, zname, ypr)
% show the maximum/minimum separation ratio cdfs

figure(1)
clf

% get colors for each set

cord    = get_pap('cord');

xran    = [Inf -Inf];
for it1 = 1:size(c,1)

        hp      = semilogx(c{it1,1}, c{it1,2});
        xran(1) = min(xran(1), c{it1,1}(1));
        xran(2) = max(xran(2), c{it1,1}(end));
%       hp      = plot(c{it1,1}, c{it1,2});
        set(hp, 'linew', 1.5, 'color', cord(it1,:));
        hold on;
end
set(gca, 'xlim', xran);

% label curves

xi      = 0.65; yi      = 0.06; dy      = 0.06;
for it1 = size(c,1):-1:1
        hp      = text(xi, yi, c{it1,3}, 'units', 'norm');
        set(hp, 'fontw', 'bo', 'fonts', 10, 'color', cord(it1,:));
        yi      = yi + dy;
end

pretty_plot('Maximum / Minimum Separation Ratio', 'Cumulative Frequency');
if (ypr)
```

```
        set(gca, 'xsc', 'li');
        pr_or_pause([zname '_lin'], 1, 0, 1, 'epsc');

        set(gca, 'xsc', 'lo');
        pr_or_pause([zname '_log'], 1, 0, 1, 'epsc');
end

```

RL 7/7/2010

## Code listing appendix for Seepage Workshop

### 12/28/05 show_seepage_stats.m.

SAS

The following *Matlab* program is used to create figures for the seepage workshop. The analysis using this program is reported in the entry dated 07/25/07.

RL 7/7/2010

```
function show_seepage_stats
% show seepage stats from fractures

ypr     = ~0;

zxlsfile        = 'fracture_spacing.xls';
zsheet_mn       = 'ECRB-Tptpmn';
zsheet_ll       = 'ECRB-Tptpll';

Lwp     = 5.2;
Ls      = 0.1;
Lt      = Lwp + Ls;
Af      = [0.18 0.27];

Lwp     = 5.2;
Ldw     = 0.1;
Ltw     = Lwp + Ldw;
Faf     = [0.18 0.27];

uvec    = linspace(-4, 4, 100);
ucdf    = normcdf(uvec);

% get Tptpmn information

[N,T]   = xlsread(zxlsfile, zsheet_mn);

chead   = T(3,:);
sta     = N(:,strmatch('Station', chead, 'exact'));
S.sep_mn        = diff(sta);
S.srt_mn        = sort(S.sep_mn);
n       = length(S.sep_mn);
S.cdf_mn        = linspace(0.5/n, 1-0.5/n, n)';
S.sawf_mn       = sort(Lwp ./ max(1e-3,S.sep_mn));
S.sawf_mn       = S.sawf_mn(:,[1 1]) .* Af(ones([n 1]),:);
S.lsep_mn       = log(max(0.5*min(S.sep_mn(S.sep_mn > 0)), S.sep_mn));

% get Tptpll information

[N,T]   = xlsread(zxlsfile, zsheet_ll);

chead   = T(3,:);
```

```
sta     = N(:,strmatch('Station', chead, 'exact'));
S.sep_ll        = diff(sta);
S.srt_ll        = sort(S.sep_ll);
n       = length(S.sep_ll);
S.cdf_ll        = linspace(0.5/n, 1-0.5/n, n)';
S.sawf_ll       = sort(Lwp ./ max(1e-3,S.sep_ll));
S.sawf_ll       = S.sawf_ll(:,[1 1]) .* Af(ones([n 1]),:);
S.lsep_ll       = log(max(0.5*min(S.sep_ll(S.sep_ll > 0)), S.sep_ll));

fprintf('mean mn separation = %g\n', mean(S.sep_mn));
fprintf('median mn separation = %g\n', median(S.sep_mn));
fprintf('std mn separation = %g\n', std(S.sep_mn));
fprintf('mean mn log-separation = %g\n', mean(S.lsep_mn));
fprintf('std mn log-separation = %g\n', std(S.lsep_mn));

fprintf('mean ll separation = %g\n', mean(S.sep_ll));
fprintf('median ll separation = %g\n', median(S.sep_ll));
fprintf('std ll separation = %g\n', std(S.sep_ll));
fprintf('mean ll log-separation = %g\n', mean(S.lsep_ll));
fprintf('std ll log-separation = %g\n', std(S.lsep_ll));

% set up plots

drive_plot('store_ypap', ~0);

cord    = drive_plot('get_pap', 'cord');
linw    = drive_plot('get_pap', 'linw');
fonts   = drive_plot('get_pap', 'fonts');

% begin plotting cumulative distributions

if (1)

        figure(gcf);
        clf;

        ax1     = drive_plot('init_axis', 'zlside', 'ltb');

        plot(Lwp .* [1 1], [-1 10], 'color', cord(4,:), 'linew', linw);
        hold on

        text(Lwp*1.2, 0.16, 'Package Length', ...
                'color', cord(4,:), ...
                'fontw', 'bo', 'fonts', fonts, 'fonta', 'oblique');

        umn     = exp(mean(S.lsep_mn) + std(S.lsep_mn).*uvec);
        ull     = exp(mean(S.lsep_ll) + std(S.lsep_ll).*uvec);
        plot([umn ; ull], ucdf, 'k', 'linew', linw);

        plot(S.srt_mn, S.cdf_mn, S.srt_ll, S.cdf_ll, 'linew', linw*1.5);
        set(gca, 'xsc', 'lo', 'ylim', [-0.05 1.09]);

% label the plot

        drive_plot('pretty_plot', 'Separation (m)', ...
                        'Cumulative Distribution');

% create dual-scale axes

        drive_plot('dual_axis', ax1, ...
                'xsc', 1/0.3048, ...
                'xlabel', 'Separation (ft)');

        drive_plot('set_paper_size', 'halfpagetop');
%       drive_plot('set_paper_size', 'fullpage');
        drive_plot('set_screen_to_paper_size');

% create normalized axis for annotations

        drive_plot('legend_axis', 'make');

        xl      = 0.85;
        yl      = 0.64;
        dy      = -0.06;
        c       = {
                'Tptpmn'        {'color' cord(1,:)}
                'Tptpll'        {'color' cord(2,:)}
        };
        for it1 = 1:size(c,1)
                text(xl, yl, c{it1,1}, c{it1,2}{:}, 'fontw', 'bo');
                yl      = yl + dy;
        end
        text(0.05, 0.94, 'Minimum Trace Length = 1 m', ...
                'horiz', 'le', ...
                'fontw', 'bo', 'fonts', fonts+2, 'fonta', 'oblique');

        drive_plot('after_plot', ypr, 'CDF_dx');
end

% begin plotting cumulative distributions

if (1)

        figure(gcf);
        clf;

        ax1     = drive_plot('init_axis', 'zlside', 'lb');

% zones

%       fill([1 1e8 1e8 1], [-1 -1 10 10], [0.9 1 1], ...
%               'edgecolor', 'c', 'linew', linw);
%       line([1 1e8 1e8 1], [-1 -1 10 10], ...
%               'color', 'c', 'linew', linw);

        plot([1 1], [-1 10], 'color', cord(4,:), 'linew', linw);
        hold on

% mn

        vx      = [S.sawf_mn(:,1); flipud(S.sawf_mn(:,2))];
        vy      = [S.cdf_mn; flipud(S.cdf_mn)];

        fill(vx, vy, 1 - (1 - cord(1,:)).*0.2, ...
                'linew', linw, 'edgecolor', cord(1,:));
        hold on

% ll

        vx      = [S.sawf_ll(:,1); flipud(S.sawf_ll(:,2))];
        vy      = [S.cdf_ll; flipud(S.cdf_ll)];

        fill(vx, vy, 1 - (1 - cord(2,:)).*0.2, ...
                'linew', linw, 'edgecolor', cord(2,:));
%       plot(S.sawf_mn, S.cdf_mn, S.sawf_ll, S.cdf_ll, 'linew', linw);
%       plot(S.sawf_mn, S.cdf_mn, S.sawf_ll, S.cdf_ll, 'linew', linw);

        set(gca, 'xsc', 'lo', 'ylim', [-0.05 1.09], 'xlim', [1e-2 1e3]);

% label the plot

        drive_plot('pretty_plot', 'L_{WP} / (x / F_{act})', ...
                        'Cumulative Distribution');

        drive_plot('set_paper_size', 'halfpagetop');
%       drive_plot('set_paper_size', 'fullpage');
        drive_plot('set_screen_to_paper_size');

% create normalized axis for annotations

        drive_plot('legend_axis', 'make');

        xl      = 0.05;
        yl      = 0.94;
        dy      = -0.06;
        c       = {
                'Tptpmn'        {'color' cord(1,:)}
                'Tptpll'        {'color' cord(2,:)}
        };
        for it1 = 1:size(c,1)
                text(xl, yl, c{it1,1}, c{it1,2}{:}, 'fontw', 'bo');
                yl      = yl + dy;
        end
        text(0.95, 0.12, sprintf('Some Packages\nWetted Multiple Times'), ...
                'horiz', 'ri', 'color', cord(4,:), ...
                'fontw', 'bo', 'fonts', fonts+2, 'fonta', 'oblique');
        text(0.05, 0.6, sprintf('Some Packages\nNot Wetted'), ...
                'horiz', 'le', 'color', cord(3,:), ...
                'fontw', 'bo', 'fonts', fonts+2, 'fonta', 'oblique');

        drive_plot('after_plot', ypr, 'CDF_SAWF');
end


```

```
if (1)

        nFaf    = 30;
%       nFaf    = 2;
        lFaf    = logspace(-2, 0, nFaf);
%       lFaf    = linspace(1e-3, 1, nFaf);

        nx      = 1e5;
        rx      = randn([nx 1]);

        lmy     = [mean(S.lsep_mn) mean(S.lsep_ll)];
        lsy     = [std(S.lsep_mn) std(S.lsep_ll)];
        [lSAWF,lWPmf]   = deal(zeros([length(lmy) nFaf]));

        wform   = [0.15 0.85];

        for it2 = 1:length(lmy)

                xc      = cumsum([0; exp(lmy(it2) + lsy(it2) .* rx)]);
%               xc      = cumsum([0; x.*(lmx(it2)/mx)]);
                nwp     = floor(xc(end) / Ltw);
                xend    = nwp * Ltw;
                xc(xc > xend)   = [];

% winnow out according to active fractures

                nxc     = length(xc);
                rx      = rand([nxc 1]);

                for it1 = 1:nFaf
                        xc1     = xc(rx <= lFaf(it1));
                        dx      = [diff(xc1(1:2));
                                0.5.*(diff(xc1(1:end-1)) + diff(xc1(2:end)));
                                diff(xc1(end+[-1 0]))
                                ] ./ Lwp;
                        w       = xc1 ./ Ltw;
                        i1      = find(rem(w, 1) > (Lwp/Ltw));
                        if (~isempty(i1))
                                dx(i1)  = [];
                                w(i1)   = [];
                        end

                        [uw,i1,i2]      = unique(floor(w));
                        lWPmf(it2,it1)  = sum(dx) / length(uw);
                        lSAWF(it2,it1)  = length(uw) / nwp;
                end
        end

%       lSAWF(end+1,:)  = [lSAWF' * wform']';
%       lWPmf(end+1,:)  = exp([log(lWPmf)' * wform']');

        if (1)
                figure(gcf)
                clf
                ylim    = [-0.05 1.08];
                v       = Faf([1:end end]);     v(end)  = NaN;
                plot(v([1 1],:), ylim, 'color', cord(6,:));
                hold on
                hp      = plot(lFaf, lSAWF, 'linew', 1.5);
                hold off
                set(gca, 'xsc', 'lo', 'ylim', ylim);
                set(gca, 'xsc', 'li', 'ylim', ylim);

% label the plot

                drive_plot('pretty_plot', 'Seeping Fracture Fraction', ...
                                'Subarea Wet Fraction');

                drive_plot('set_paper_size', 'halfpagetop');
%               drive_plot('set_paper_size', 'fullpage');
                drive_plot('set_screen_to_paper_size');

% create normalized axis for annotations

                drive_plot('legend_axis', 'make');

                xl      = 0.85;
                yl      = 0.64;
                dy      = -0.06;
                c       = {
                        'Tptpmn'        {'color' cord(1,:)}
                        'Tptpll'        {'color' cord(4,:)}
%                       'Weighted'      {'color' cord(3,:)}
                };
                for it1 = 1:size(c,1)
                        text(xl, yl, c{it1,1}, c{it1,2}{:}, 'fontw', 'bo');
                        set(hp(it1), c{it1,2}{:});
                        yl      = yl + dy;
                end
%               text(0.95, 0.12, sprintf('Some Packages\nWetted Multiple Times'), ...
%                       'horiz', 'ri', 'color', cord(4,:), ...
%                       'fontw', 'bo', 'fonts', fonts+2, 'fonta', 'oblique');
%               text(0.05, 0.6, sprintf('Some Packages\nNot Wetted'), ...
%                       'horiz', 'le', 'color', cord(3,:), ...
%                       'fontw', 'bo', 'fonts', fonts+2, 'fonta', 'oblique');

                drive_plot('after_plot', ypr, 'Faf_SAWF');
        end

        if (1)
                figure(gcf)
                clf
                v       = Faf([1:end end]);     v(end)  = NaN;
                plot(v([1 1],:), [1 1e8], 'color', cord(6,:));
                hold on
%               ylim    = [-0.05 1.08];
%               fill(Faf([1 2 2 1]), ylim([1 1 2 2]), [1 0.8 0.8], ...
%                       'edgecolor', [0.3 0 0]);
%               hold on
                hp      = plot(lFaf, lWPmf, 'linew', 1.5);
                hold off
%               set(gca, 'xsc', 'lo', 'ylim', ylim);

                ylim    = [1 10^ceil(log10(max(lWPmf(:))))];
                set(gca, 'xsc', 'li', 'ysc', 'lo', 'ylim', ylim);

% label the plot

                drive_plot('pretty_plot', 'Seeping Fracture Fraction', ...
                                'Waste Package Flow Multiplication Factor');

                drive_plot('set_paper_size', 'halfpagetop');
%               drive_plot('set_paper_size', 'fullpage');
```

```
                drive_plot('set_screen_to_paper_size');

% create normalized axis for annotations

                drive_plot('legend_axis', 'make');

                xl      = 0.85;
                yl      = 0.64;
                dy      = -0.06;
                c       = {
                        'Tptpmn'        {'color' cord(1,:)}
                        'Tptpll'        {'color' cord(4,:)}
%                       'Weighted'      {'color' cord(3,:)}
                };
                for it1 = 1:size(c,1)
                        text(xl, yl, c{it1,1}, c{it1,2}{:}, 'fontw', 'bo');
                        set(hp(it1), c{it1,2}{:});
                        yl      = yl + dy;
                end

                drive_plot('after_plot', ypr, 'Faf_WPFMF');
        end

        if (1)
                figure(gcf)
                clf
                v1      = logspace(-2,0,100);
                v2      = logspace(2,0,100);
%               ylim    = [-0.05 1.08];
%               fill(Faf([1 2 2 1]), ylim([1 1 2 2]), [1 0.8 0.8], ...
%                       'edgecolor', [0.3 0 0]);
                plot(v1, v2, 'k', 'linew', linw*1.5);
                hold on
                plot(lSAWF(1:2,:)', lWPmf', 'o', 'linew', 1.5);
                hold off
%               set(gca, 'xsc', 'lo', 'ylim', ylim);
                set(gca, 'xsc', 'lo', 'ysc', 'lo');

% label the plot

                drive_plot('pretty_plot', 'Subarea Wet Fraction', ...
                'Waste Package Flow Multiplication Factor');

        drive_plot('set_paper_size', 'halfpagetop');
%       drive_plot('set_paper_size', 'fullpage');
        drive_plot('set_screen_to_paper_size');

% create normalized axis for annotations

        drive_plot('legend_axis', 'make');

        xl      = 0.85;
        yl      = 0.94;
        dy      = -0.06;
        c       = {
                'Tptpmn'        {'color' cord(1,:)}
                'Tptpll'        {'color' cord(2,:)}
        };
        for it1 = 1:size(c,1)
                text(xl, yl, c{it1,1}, c{it1,2}{:}, 'fontw', 'bo');
                yl      = yl + dy;
        end

        drive_plot('after_plot', ypr, 'SAWF_WPFMF');
    end
end

```

RL 7/7/2010

# Final QA Information

Entries into Scientific NoteBook 714E for the period May 10, 2005, to July 1, 2010, have been made by Stuart Stothoff (SAS; July 1, 2010).

No original text entered into this Scientific Notebook has been removed (SAS; July 1, 2010).

The final entry date for this Scientific Notebook is July 26, 2007, and the notebook was closed on July 1, 2010 (SAS; July 1, 2010).

RL 7/7/2010

# ADDITIONAL INFORMATION FOR SCIENTIFIC NOTEBOOK NO. 714E

| | |
|---|---|
| **Document Date:** | 05/10/2005 |
| **Availability:** | Southwest Research Institute®<br>Center for Nuclear Waste Regulatory Analyses<br>6220 Culebra Road<br>San Antonio, Texas 78228 |
| **Contact:** | Southwest Research Institute®<br>Center for Nuclear Waste Regulatory Analyses<br>6220 Culebra Road<br>San Antonio, TX 78228-5166<br>Attn.: Director of Administration<br>210.522.5054 |
| **Data Sensitivity:** | ■“Non-Sensitive” □ Sensitive<br>□“Non-Sensitive - Copyright” □ Sensitive - Copyright |
| **Date Generated:** | 12/2005 |
| **Operating System:**<br>(including version number) | Windows |
| **Application Used:**<br>(including version number) | |
| **Media Type:**<br>(CDs, 3 ½, 5 1/4 disks, etc.) | 2 CD |
| **File Types:**<br>(.exe, .bat, .zip, etc.) | bbl, log, tex, aux, eps, xls |
| **Remarks:**<br>(computer runs, etc.) | Notebook supplemental material |